ICJ

THE INDIAN CONCRETE JOURNAL

Published by ACC Limited

Volume 95 • Number 7 • July 2021 • Pages 60 • ₹ 175

WORLD'S FIRST 3D PRINTED SCHOOL OPENS IN MALAWI

BUILDING A NEW AND STRONG INDIA

1800 1033 444

CEMENT ▪ READY MIX CONCRETE ▪ BUILDING MATERIALS

ACC
Cementing Relationships

ICJ
THE INDIAN CONCRETE JOURNAL
Volume 95 • Number 7 • July 2021 • Pages 60

ISSN (Digital) : 0019-4565

Founded in 1927

Published by ACC Limited, L. B. Shastri Road, Near Teen Haath Naka, Thane (West) 400 604. Maharashtra, INDIA.

This is a Scopus® indexed journal.

Cover
14Trees, a LafargeHolcim joint venture with CDC Group, the UK's publicly owned impact investor, is deploying 3D printing technology at scale to build affordable and low-carbon housing and schools in Africa, starting in Malawi. Cover image is the first application of 3D printing technology at scale for schools in Africa, starting in Malawi

Cover image source:
14Trees / Homeline Media

CIRCULATION OFFICE: The Indian Concrete Journal, ACC Limited. L. B. Shastri Road, Near Teen Haath Naka, Next to Eternity Mall, Thane (West) 400 604, Maharashtra, INDIA.
Website: http://www.icjonline.com; e-mail: info@icjonline.com, editor@icjonline.com

Dear Readers,

The Indian Concrete Journal (ICJ) is pleased to issue this current edition to all readers. With the growing demands of improving sustainability in concrete construction, the development of new innovative materials and design procedures are essential. Concrete being the widely used material, innovations in concrete technology for sustainable development in the 21st century should focus on today's challenges, emphasising environmental consciousness. In the current issue of the ICJ, six papers have been published covering both the material and structural aspects. This issue has interesting articles of high standards. They deal with novel developments in concrete technology and improved analysis approaches for developing sustainable and resilient infrastructure.

The first article in this issue explores the feasibility of using locally available sesame seeds (SS) as an alternative to synthetic foaming agents for foamed concrete production. The authors note that using such eco-friendly and abundantly available sesame seeds as a foaming agent can facilitate the wider use of foamed concrete. Also, the foam generated at the chosen surfactant production parameters can result in foam concrete with acceptable properties per ASTM standards.

The second article explores the use of fly ash in Roller Compacted Concrete (RCC) for pavement applications. The authors have explored the possibility of achieving higher strength in the Indian scenario. However, they noted that fly ash does uniformly not affect flexural strength. RCC pavement made with fly ash is economical than conventional concrete pavement. Furthermore, they noted that the RCC pavement could reduce CO_2 emissions significantly than conventional concrete pavement.

The third article focuses on an experimental study of the mechanical properties of fly ash (FA) and ground granular blast furnace slag (GGBFS) based on geo-polymer concrete (GPC) using glass fibres. They have observed fascinating results. The authors have explored mechanical properties like compressive strength, split tensile strength and flexural strength for different FA and GGBFS. They noted that though the increase of GGBFS content improves the strength, its workability decreased despite the addition of superplasticizer.

The fourth article shows a novel approach that micro-organisms like bacteria can be used to self-healing cracks in concrete. Bacteria they have explored generally of Bacillus species. The effectiveness of healer bacteria depends on the crack location. The effectiveness of healing depends on crack is located on the horizontal concrete surfaces like in slabs and floors or vertical as in columns and walls.

The fifth article focuses on developing specific design parameters for high-strength concretes between M65 and M110. The authors have developed expressions necessary for evaluating the P-M interaction curves using concrete stress block parameters given in IRC: 112 (2019) for high strength concretes. With the prevalent use of high strength concrete in building construction, the results of this study help compare the limitations of our code provisions. A comparative study of sectional capacities of rectangular RC sections using the different stress-block properties recommended in the design standards considered reveals that use of existing recommendations of IS: 456 (2000) for concrete of grades between M65 to M90 leads to an over-estimation of capacities with mean deviations ranging from 5 to 28%.

In the sixth and last article of this issue, the authors have proposed a new analytical bimodular elastic damage model for concrete. Salient aspects of the predicted mechanical behavior of concrete are discussed. They have restricted the scope of the new model in identifying the nonlinearity of damaged concrete. They have shown that Isotropically-damaged bimodular concrete belongs to the class of homogeneous mechanical systems.

We thank all the authors and reviewers for contributing to this issue. The ICJ is well-read by practicing engineers and decision-makers in the concrete industry, especially in India. Such a knowledgeable and wide readership (outside the academia and research community) can play a huge role in implementing the latest technologies in construction. We are glad to issue this edition of the ICJ dealing with innovative technologies that could help realise our infrastructure resilience objective. The topics covered in this edition are of great significance and will be helpful for concrete material and structural engineers to make a more sustainable society.

Thank you.

Prof. S. Suriya Prakash,
Editorial Board Member

ICJ
THE INDIAN CONCRETE JOURNAL

CALL FOR PAPERS

January 2022 Themed Issue of ICJ

Construction and Demolition Waste in Construction

Concrete is the favoured material of choice in the construction industry worldwide for applications in various forms, often under demanding conditions and increasingly specified with several durability performance parameters. The ingredients to make concrete are in huge demand and especially aggregates with essential characteristics fit for use are in short supply. This entails not only increase in cost of construction as more and more countries must import them but also depletes the finite good quality natural resources available on this planet. Nevertheless, these are inherent challenges that need to be addressed by a holistic approach both via research and practice, leading to responsible informed choices for construction to become even more sustainable. In this thematic issue, we invite papers relating to recycling and reuse of construction and demolition waste in concrete with focus both on research and application. Case studies are particularly welcome as we intend to make this issue a ready reference for researchers and practitioners alike. All the manuscripts will be subjected to double blind peer review process and the areas of contribution are indicated as follows:

- Use of recycled concrete aggregates for precast structural concrete;
- Application of recycled concrete aggregates in HPC/FRC/UHPC;
- Recycled construction and demolition waste for geopolymer binders and concrete;
- Recycled concrete aggregates for self-compacting concrete;
- 3D printing of concrete using recycled concrete aggregate;
- Use of recycled concrete aggregates for marine concretes;
- Processing technologies for manufacturing high quality recycled aggregates;
- CO_2 treatment of coarse and fine recycled concrete aggregates;
- Exemplar projects constructed using recycled aggregates;
- Architectural perspectives on recycled aggregates in the built environment;
- Guidelines for valorisation of recycled aggregates in concrete;
- Effective characterisation of recycled aggregates towards use in concrete;
- Recycled construction and demolition waste for sustainable pavement materials;
- Policy enablers for wider use of recycled aggregates.

Guest Editor : Dr Sivakumar Kandasami
Deputy General Manager, L&T Construction, Chennai, India.

Co-Guest Editor : Prof. Dr-Ing. Jiabin Li
Research Group RecyCon, Materials and Constructions, Bruges Campus, KU Leuven, Belgium.

Submission deadline : 30 September 2021

Submission guidelines : https://icjonline.com/downloads/contributors-guidelines-2019.pdf

Review Process : Double-blind peer review

Submit your paper : https://icjonline.com/be_an_author or email: info@icjonline.com

RILEM UPDATE

The International Union of Laboratories and Experts in Construction Materials, Systems and Structures

New RILEM State-of-the-Art Report

Reinforcement of existing timber elements and structures, state-of-the-art report of the RILEM Technical Committee 245-RTE; edited by Jorge Branco, Philipp Dietsch, Thomas Tannert. You can purchase the hardcopy or e-book on the Springer website bit.ly/33HG8sG. RILEM members are entitled to enjoy a 20% discount when they purchase all Springer e-books, including RILEM STARs. An unedited electronic version of this STAR is also available on bit.ly/3fiIwLS.

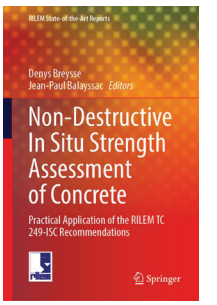

Online PhD courses at the 75th RILEM Annual Week

Five online PhD courses will take place during the two weeks prior the 75th RILEM Annual Week. If you are a PhD student or a post-doc, you can register up to a maximum of 4 courses and also attend the full conference event for 190 USD. It is also possible to register up to 3 courses (the cost per course will be 50 USD for PhD students and post-docs, 120 USD for industry professionals), without having to register for the conference. You can check course programs, schedules and teachers here: http://rilemweek2021.uanl.mx/phd-courses/.

2020 Outstanding M&S papers now Open Access

2020 Outstanding Papers are now OPEN ACCESS

The 2020 outstanding papers published on the flagship journal of RILEM *Materials and Structures* are now OPEN ACCESS and available to be downloaded here: bit.ly/316Xm2n. These papers cover all fields of RILEM activities and exemplify the highest standards in our scientific community.

ROC&TOK webinars

Have you missed the last RILEM ROC&TOK webinars? You can watch them all FOR FREE on our YouTube Channel here: bit.ly/3qweacj.

- May webinar: *Rheo-physics and shaping of fresh cement-based materials* – Dr Nicolas Roussel, Navier Laboratory, Gustave Eiffel University, France.
- June webinar: *Alkali-Silica reaction: research needs and the link to practice*. Prof. Jason H. Ideker, Oregon State University, USA.
- July webinar: *Digital concrete: dream or reality? New green or ecological monster?* Prof. Robert J. Flatt, Institute of Building Materials, ETH Zurich, Switzerland.

DEVELOPMENT OF NATURAL BASED FOAMING AGENT FOR THE POTENTIAL USE IN FOAM CONCRETE

SELIJA KHWAIRAKPAM,
INDU SIVA RANJANI GANDHI*

Abstract

The feasibility of the use of locally available sesame seeds (SS) as an alternate to synthetic foaming agents for foamed concrete production has been assessed in this study. The use of such eco-friendly and abundantly available material as foaming agent can facilitate wider use of foamed concrete. The various parameters involved in the extraction of surfactant from SS, such as SS concentration, duration of heating, heating temperature, sodium hydroxide concentration (alkali for hydrolysis), ammonium chloride concentration (for neutralization) and sodium fluoride concentration (antiseptic) are considered in the present study. Also, the foam generated at the chosen surfactant production parameters is observed to result in foam concrete with acceptable properties as per ASTM standards.

Keywords: Density, Foam concrete, Hydrolysis, Natural surfactant, Sesame seed, Temperature.

1. INTRODUCTION

Foam concrete (FC), also regarded as lightweight concrete, is a cement paste or mortar with entrapped air voids by a suitable foaming agent [1]. The quality of FC products largely depends on the stability and dispersion of foam used in the manufacture. The quality of foam mainly relies on the type of surfactant used since it affects the surface tension and interfacial properties of liquid-gas. Therefore, the selection of surfactant has a substantial impact on concrete properties. Surfactants are classified into two based upon the sources, viz., (i) synthetic and (ii) natural surfactant. The continuous search for an alternate material for replacing the synthetic materials with an environmental friendly material has led to exploring more towards the potential natural foaming agent. A variety of biological sources are being identified these days for the development of naturally occurring foaming components and surface-active proteins with captivating structures and functions [2]. It is critical to comprehend the primary function of proteins in foams as it helps to decrease the tension in the interface, increase the viscous and elastic properties of the liquid phase, and also facilitates the formation of strong films around the air bubble in foam.

Generally, the natural-based surfactant can be derived from animal or vegetable sources, and most of the earlier literature had reported the use of animal protein in foam concrete [3-6]. Some examples of a commonly used source of animal protein are keratin, hoof and horn meal, cattle hooves, fish scales, casein, blood, bones of cows, pigs, and residues of animal carcasses [7]. It has been reported that many plant species are found abundantly in India, which are either rich in protein or saponin with potential foaming ability. Plant such as leguminous plants- lentils, beans, and soya, has also been reported to have an abundant amount of protein content [8]. The quality of protein-stabilized foams relies on the ingredient structure and the circumstances in the final product [9].

Comparative studies on the type of surfactant have established that the use of a protein-based surfactant has many advantages over synthetic based surfactants in terms of improvement of the microstructure of concrete, sustainability, and cost reduction [10]. Despite the advantages, the complications involved in the manufacturing process of natural surfactants have limited its wider use. Hence there is an essential need for identifying locally available natural foaming agents to facilitate more extensive use of FC in India. Furthermore, there is an arduous requirement for more studies on the foam, which is more essential to attain the desired properties of FC. Hence, the objective of the present study is to identify a potential source of natural surfactant and to optimize the method of preparation of surfactant from the source based on foam performance. Furthermore, assessments are made to find its suitability for using it in the production of FC.

Based on the review of literature, it is identified that sesame (*Sesamum indicum* L.) has a protein content of 20-25% [11] and hence has an excellent potential foamability. Further, India is one of the world's largest producer of Sesame Seeds (SS) [12] with 18.8% of the total world contribution. It is reported that the seeds are commonly used for oil extraction and the flour

*Corresponding author : Indu Siva Ranjani Gandhi, Email: gindu@iitg.ac.in

that remains after oil extraction also has higher protein content. Sesame seeds, as it is rich in protein content and available abundantly, has been chosen for the production of surfactant in this study. Based on the review it is identified that there are different stages involved in the preparation of protein-surfactant such as pre-treatment, hydrolysis, neutralization, treatment with preservative, homogenization and stabilization [13]. Also, it is to be noted that to date, the use of sesame seed surfactant in foam concrete production has not been reported in earlier studies.

Further it is to be noted that one of the major deterrents to the structural application of foam concrete is the high drying shrinkage. Shrinkage being cement paste related phenomenon, the shrinkage strain of foamed concrete which is basically a mortar is significantly greater than that of normal weight concrete. Based on the review, there are limited studies found on shrinkage mitigation of foam concrete through use of water reducing admixtures [14], mineral admixtures and fibres [15-17]. Similarly, the durability related performance has also been evaluated in few studies which includes behaviour of foam concrete in sulphate environment [18], sorption characteristics of foam concrete [19], studies on frost resistance and carbonation [20]. However still there is need for full-scale long-term studies in the above-mentioned areas to increase the structural applications of foam concrete.

2. MATERIALS AND METHODOLOGY OF PRODUCTION OF SESAME SURFACTANT

For the present study, the locally available SS (Figure 1a) are collected and subjected to pre-treatment which involves the physical processes such as grinding and boiling to facilitate easy hydrolysis [21]. After the pre-treatment processes, the hydrolysis of SS is carried out using sodium hydroxide (NaOH) solution. Then the next step is to do neutralization as the pH of solutions plays a significant role in stabilization and the foaming intensity of the protein foam [2]. In this context, few studies had established that as the dissociation degree of ionized groups of protein is dependent on the pH of the solution and hence it is not recommendable to choose a highly acidic or basic solution. Furthermore, it was reported in the earlier studies that a pH range from 8.5 to 9.5 were recommended for protein based on legumes pea plant [8]. Hence for the present study, the required pH level of the solution is fixed as 8±0.5 based on preliminary studies, which confirms good foamability. Neutralization is done with the help of ammonium chloride (NH_4Cl) until the pH level is reduced to 8±0.5. Since the protein surfactants are susceptible to degradation by the bacteria and microorganisms, it is highly recommended to carry out the treatment with preservatives. Sodium fluoride (NaF) has been chosen as a preservative for the present study. Further, from the review of literature, it is identified that few researchers had used ferrous sulfate as a stabilizer to enhance the stability of foam produced from leguminous plant surfactant [8]. However, such stabilization is not adopted for the present study as it is found from preliminary studies that ferrous sulfate is not compatible with the sesame foaming solution. Hence, in the present study, the parameters considered with respect to the method of preparation of surfactant are SS concentration, duration of heating, heating temperature, NaOH concentration (alkali for hydrolysis), NH_4Cl concentration (neutralization) and NaF concentration (antiseptic). Since many parameters are involved in the experimental programme, in order to simplify the experimental programme, as a first step in the preliminary studies, the SS concentration and NaF concentration are kept constant at 10% and 0.1%, respectively. The analysis of the above-mentioned surfactant extraction parameters is carried out based on the performance of foam evaluated through the measurement of initial foam density (IFD). The list of parameters and the range of parameters adopted for the present study are presented in Table 1.

(a) (b) (c)

Figure 1: (a) Sesame seed (b) Sesame seed surfactant (c) Foam produced with sesame seed surfactant

Table 1: Parameters considered for the production of protein-based surfactant

PARAMETER	LEVELS OF PARAMETERS
SS concentration	10%
Heating duration	4 to 8 hours
Heating temperature	50 -100°C
NaOH concentration (alkali for hydrolysis)	6 - 25%
NH_4Cl concentration (neutralization)	6-25%
NaF concentration (antiseptic)	0.1%

3. METHOD OF FOAM AND FOAM CONCRETE PRODUCTION

The production of foam is done by aerating the produced sesame surfactant solution (Figure 1b) by means of a high-speed stirrer based on the mechanical method. An electronic stirrer capable of varying frequency from 2800 to 3600 rpm is used for thorough mixing of the surfactant solution. It is reported in the literature that the mixing speed is a significant parameter which controls the nature of produced foam with a stirrer [22]. Thus, as an initial step, the assessment is made on the basis of the impact of the rotation speed of the stirrer on IFD. Subsequent to fixing the rotational speed of stirrer, as a next step, the evaluation of different surfactant production parameters is carried out based on single-factor experiments.

The preparation of FC consists of first preparation of homogeneous base mix of cement and sand slurry of w/c ratio of 0.58 and then addition of preformed foam made from SS surfactant to the base mix. The mixing is done till the foam is uniformly blended into the slurry.

4. RESULTS AND DISCUSSIONS

4.1 Effect of the rotational speed of the stirrer

By varying the stirrer mixing speed from 2800 to 3600 rpm, its influence on IFD is studied, as represented in Figure 2. To eliminate the influence of the variability of other parameters on initial foam density, the parameters such as the SS concentration, heating temperature, heating duration, and NaOH concentration are fixed as 10%, 60°C, 6 hours, and 10%, respectively. It is observed from experimental studies that with the increase in stirrer speed, there is a substantial reduction in IFD. For instance, a 67.80% reduction in IFD is observed when the speed of the stirrer is increased to 3600 rpm. This reduction in foam density is due to the improvement in the foam quality as a result of a decrease in the amount of liquid fraction. This is in agreement with the findings of earlier researchers who have proved that the higher speed of stirrer is needed for the

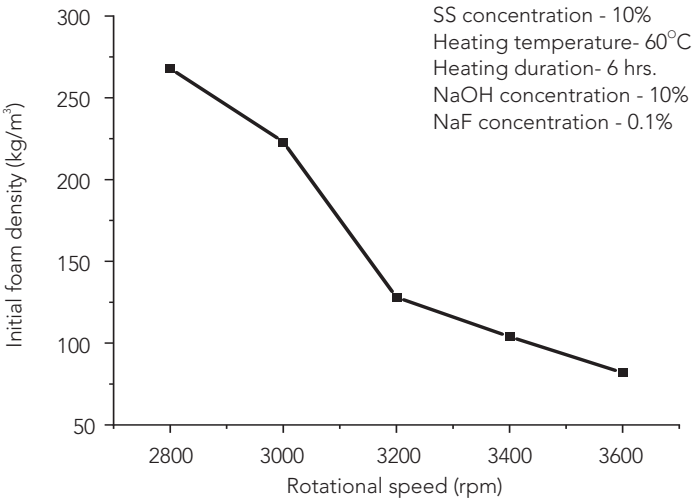

Figure 2: Effect of the rotational speed of the stirrer on IFD

production of good quality of foam with more amount of air and smaller bubble size [23]. Hence, it is evident that the maximum speed of stirrer is needed for thorough mixing of liquid and air for good quality foam production with a comparatively lesser IFD. Thus, recommended speed for the stirrer used in the present study is 3600 rpm, and this speed will be adopted for all the further experimental studies with sesame surfactant.

4.2 Effect of heating temperature and heating duration

As the process of hydrolysis of protein is very much dependent on the heating temperature and duration, it is necessary to optimize the heating process based on the performance of the foam. Preliminary trials indicate that the surfactant solution prepared at a temperature of less than 50°C does not result in sufficient foam production. Further, most of the literature had reported an upper limit of the temperature of less than 100°C for studies on hydrolysis. Hence for the present study, in order to analyse the influence of temperature of heating, the range of temperature is fixed at 50 to 100°C, and the duration of heating and SS concentration are fixed as 6 hours and 10%, respectively. It is evident from the experimental results that by increasing the heating temperature of the surfactant solution, the foam quality is improved significantly in terms of reduction in foam density (Figure 3). This can be attributed that the degree of hydrolysis increases with the temperature of heating. For example, a significant decline of about 63% in IFD is achieved for an increase in heating temperature from 50 to 70°C as shown in Figure 3. However, heating beyond 70°C does not further improve in the quality of foam in terms of the reduction of IFD. Hence it can be concluded that for heating duration of 6 hours, 70°C is the optimal temperature required for the sesame surfactant solution extraction that can yield better foam quality with the comparatively less liquid fraction.

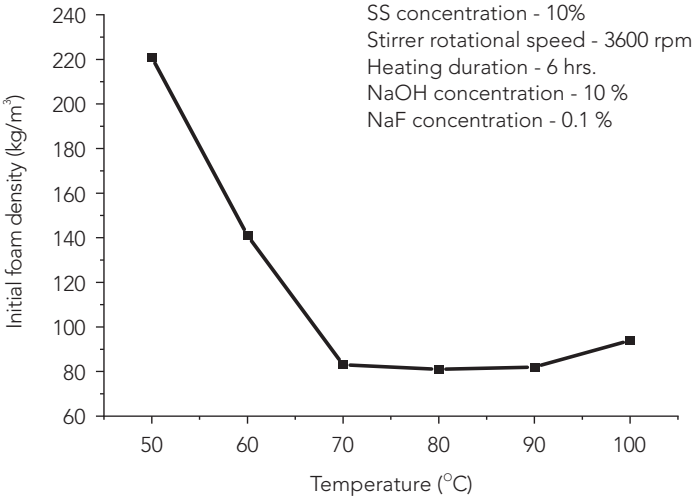

Figure 3: Effect of heating temperature of surfactant preparation solution on IFD

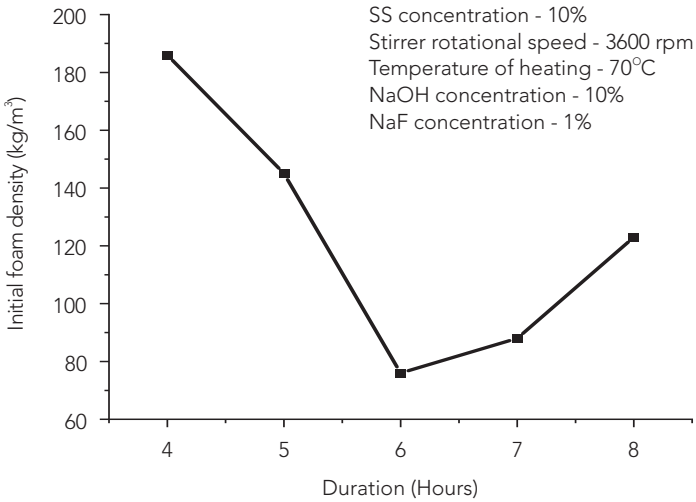

Figure 4: Effect of heating duration of surfactant preparation solution on IFD

Having optimized the heating temperature as 70°C for 6 hours of heating duration, in the subsequent step, the influence on changing the heating duration of surfactant preparation solution on IFD is studied, as shown in Figure 4. From the preliminary studies, it is observed that the surfactant solution prepared by heating for a duration of less than 4 hours exhibits poor foamability. Hence for the present study, the range of duration of heating is varied from 4 to 8 hours. From Figure 4, it can be observed that at a constant temperature of 70°C, as the duration of heating is increased from 4 to 6 hours, a substantial reduction of 187% in IFD is observed. This improvement in the foam quality can be ascribed to the improvement in the degree of hydrolysis of protein achieved due to an increase in the duration of heating. However, a further increase in heating duration beyond 6 hours results in an increase in IFD. Hence, in line with observations of earlier studies, there is an optimum level of hydrolysis for the protein for maximum foamability [9]. On the basis of the experimental observations, it can be inferred that at 70°C, the optimum duration required to achieve foam with the comparatively lesser liquid fraction is 6 hours, and it must be noted that the duration of heating needed will vary with the temperature of heating [24].

4.3 Effect of NaOH concentration

It is reported in earlier studies that hydrolyzed proteins have a much higher foaming capacity than the proteins themselves, and furthermore, the foaming properties depend on the degree of hydrolysis [25]. Hence the addition of alkali such as NaOH can promote the degree of hydrolysis by breaking down complex protein into the simpler element. For the present study, the optimum concentration of NaOH needed for hydrolysis is determined through studies on IFD, as shown in Figure 5. In order to eliminate the influence of other parameters on IFD, SS concentration, heating temperature, and heating duration are fixed as 10%, 70°C, and 6 hours, respectively. Experimental studies show that an increase in NaOH concentration from 5 to 15% results in a substantial reduction of 66% in IFD, which can be ascribed to the improved quality of foam achieved through hydrolysis of protein-surfactant. At the dosage of 15% NaOH concentration, the amount of NH_4Cl needed for neutralization to bring the pH level to 8±0.5 is 25%. Furthermore, it is inferred from the graph that the adoption of NaOH concentration beyond 15% results in an increase in IFD. The reason for the reduction in quality of foam (increase in the liquid fraction of foam) beyond 15% NaOH concentration is due to the increase in demand for NH_4Cl solution for neutralization. Few researchers have reported in earlier studies that usage of a higher dosage of NH_4Cl solution can reduce the viscosity of a surfactant solution, which in turn can affect the quality of foam. Hence for the present study, the optimum dosage of NaOH is recommended as 15%, considering the amount of neutralization also required as one of the criteria for good foamability.

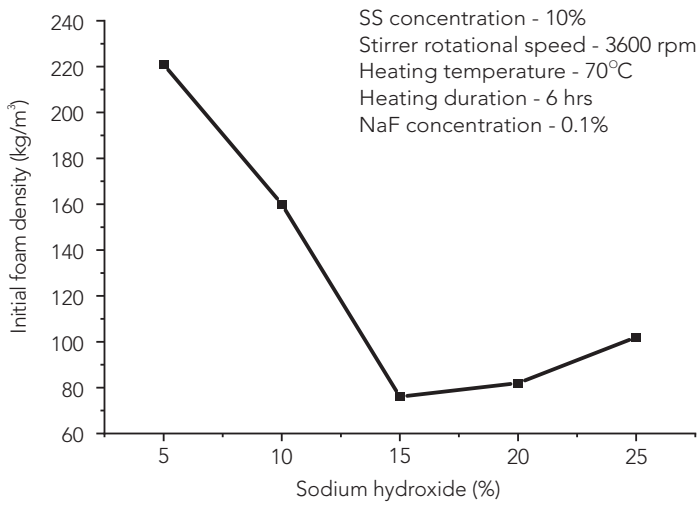

Figure 5: Effect of NaOH concentration on IFD

4.4 Check for suitability of SS foam in foam concrete

With the completion of the process of evaluation of parameters involved in the production of surfactant and foam, as a next step, the potential of foam produced for use in production of FC is required to be verified. A constant cement-sand ratio (river sand passing through 300 microns) of 1:2 by weight is used for preparing FC with three different target densities, as tabulated in Table 2. The volume of foam required for producing FC with particular target densities is determined from the guidelines of ASTM C 796 [26]. FC is produced by mixing the preformed foam made from sesame surfactant adopting selected surfactant extraction parameters viz., SS concentration-10%, heating temperature- 70°C, heating duration - 6 hours, NaF concentration- 0.1%, NaOH concentration-15% for hydrolysis and NH_4Cl -25% for neutralization and cement-sand mortar with w/c ratio of 0.58.

The stability of test mixes is evaluated by relating the actual (Act) and estimated (Est) quantities of foam needed to achieve fresh density within ±50 kg/m^3 of the target (Figure 6). The foam stability is found to be satisfactory for foam concrete production as the actual-estimated foam ratio is found to be one indicating that an additional amount of foam is not needed to compensate for foam that had collapsed. Also, the actual plastic density of concrete for all design densities is found to be within ±50 kg/m^3 of target density, satisfying the requirements of ASTM C869 [27] (Table 2). Hence the derived values of surfactant production parameters are satisfactory to produce a stable FC mix.

Further, water absorption test was conducted as per ASTM C 642 [28] with 6 number of 50 mm size cubes after water curing for 28 days and then test for compressive strength was conducted as per ASTM C495 [29] with another 6 no. of 50 mm size cubes. It is seen from the experiment outcomes that density is a direct function of compressive strength and decreases significantly with decrease in density. Many researchers had also reported that the strength of foam concrete is primarily a function of entrained air voids. Also, it is observed from Table 2 that the foam concrete produced meets the requirements of strength and water absorption as prescribed in IS: 1077 [30] and IS: 2185 [31] for brick masonry and concrete masonry units. Hence it can be recommended as an alternative for brick and concrete masonry units for different applications because of its unique attributes such as lighter weight, higher construction productivity, better thermal, and sound insulation.

Table 2: Experimental results of FC

PROPERTIES OF FC		
Target density (kg/m^3)	1000	1500
Fresh density (kg/m^3)	967	1521
Dry density (kg/m^3)	840	1350
Water-solids ratio	0.58	0.58
Compressive strength (MPa)	3.8	12.2
Water absorption (% by weight)	15	16
Actual/Estimated foam ratio	1	1

Based on cost analysis, it is observed that the cost of sesame seed surfactant production at the optimized foam production parameters for one cubic meter of FC production (target density 1500 kg/m^3), amounts to ₹ 540. However, the cost can be further reduced through use of compressed air method of foam production which can result in production of drier foam (with lesser liquid fraction) which will eventually result in reduction in requirement of amount of foam needed for foam concrete production. Further the amount of chemicals needed for sesame seed surfactant extraction is likely to be reduced if the foam generator (based on compressed air method) is adopted for foam production. Hence the sesame seed surfactant can be a sustainable material when compared to the costlier synthetic foaming agents for the application of foam concrete.

(a) (b)

Figure 6: (a) Stability test of foam concrete (b) Water curing of prepared foam concrete mix

5. CONCLUSIONS

Sesame seed surfactant is found to be a promising sustainable alternative to synthetic surfactants for the application of foam concrete. As there are different stages involved in the preparation of sesame surfactant which is protein-based, the following parameters such as SS concentration, duration of heating, heating temperature, NaOH concentration (alkali for hydrolysis), NH_4Cl concentration (neutralization) and NaF concentration (antiseptic) are identified to be significant in the preparation of sesame surfactant. Among the various parameters studied, the heating process of a surfactant solution is found to influence the IFD significantly as it affects the degree of hydrolysis of proteins. From the experimental outcome, it is noted that the rise in temperature of the surfactant solution results in substantial improvement in foam quality through a reduction in IFD. Further, at a heating temperature of 70°C, the optimum duration of heating needed to produce foam with comparatively lesser liquid fraction is found to be 6 hours. Adding to the above, the addition of alkali, such as NaOH can promote the degree of hydrolysis and eventually improve the performance of foam through the reduction of IFD. However, it is to be noted that the addition of a higher dosage of NaOH demands a more significant amount of NH_4Cl for neutralization, which in turn can reduce the viscosity of surfactant solution and thereby affects foam quality. Hence the alkali concentration needed for hydrolysis needs to be also optimized from the point of neutralization required, and for the present study it is fixed as 15%.

The foam produced from a sesame surfactant solution with a stirrer with the selected surfactant production parameters is observed to result in adequately stable FC mixes satisfying the requirements of ASTM C 869 [27]. As the water absorption and compressive strength of produced foam concrete mixes are satisfactory, and hence it can be recommended as an alternative for bricks and concrete masonry units for different applications.

6. SCOPE OF FUTURE WORK

As the results of the preliminary studies on suitability of sesame seed surfactant for use in foam concrete production are found to be encouraging, further studies on improvement of foam quality with compressed air method of foam production need to be carried out. Further long-term studies on dimensional stability and durability of foam concrete are necessitated to enhance the structural applications of foam concrete.

REFERENCES

[1] Ramamurthy, K., Nambiar, E. K. K., and Ranjani, G. I. S. (2009). "A classification of studies on properties of foam concrete", *Cement and Concrete Composites*, Vol. 31, pp. 388-396.

[2] Amankeldi, F., Ospanova, Z., and Musabekov, K. (2018). "Composite foaming agents on the basis of high-molecular natural surfactants", *Colloids and Interfaces*, Vol. 2, No. 2, pp. 1-8.

[3] Chen, B., and Liu, N. (2013). "A novel lightweight concrete-fabrication and its thermal and mechanical properties", *Construction and Building Materials*, Vol. 44, pp. 691-698.

[4] Jiang, J., Lu, Z., Niu, Y., Li, J., and Zhang, Y. (2016). "Study on the preparation and properties of high-porosity foamed concretes based on ordinary Portland cement", *Materials and Design*, Vol. 92, pp. 949-959.

[5] Remadnia, A., Dheilly, R., Laidoudi, B., and Quéneudec, M. (2009). "Use of animal proteins as foaming agent in cementitious concrete composites manufactured with recycled PET aggregates", *Construction and Building Materials*, Vol. 23, No. 10, pp. 3118-3123.

[6] Tian, T., Yan, Y., Hu, Z., Xu, Y., Chen,Y., and Shi, J. (2016). "Utilization of original phosphogypsum for the preparation of foam concrete", *Construction and Building Materials*, Vol. 115, pp. 143-152.

[7] Valore, R. C. (1954). "Cellular concretes Part 1: composition and methods of preparation", Proceedings of Journal of the American Concrete Institute, Vol. 50, No. 5, pp. 773-796.

[8] Fedorovich, D.N., Viktorovich, U. V., and Valer'evna, K. T. (2009). "Method for production of foaming agent and foaming agent produced by this method", *Russian Federation, Federal service for intellectual property, Patents and Trademarks, Patent Number - RU 2368582 C2*, Retrieved from http://www.freepatent.ru/patents/2368582.

[9] Wierenga, P., and Gruppen, H. (2010). "New views on foams from protein solutions", *Current Opinion in Colloid & Interface Science*, Vol. 15, pp. 365-373.

[10] Panesar, D. K. (2013). "Cellular concrete properties and the effect of synthetic and protein foaming agents", *Construction and Building Materials*, Vol. 44, pp. 575-584.

[11] Singharaj, S., and Onsaard, E. (2015). "Production and characteristic of sesame proteins", *Journal of Food Science and Agricultural Technology*, Vol. 1, No. 1, pp. 188-192.

[12] Kanu, P. J. (2011). "Biochemical analysis of black and white sesame seeds from China", *American Journal of Biochemistry and Molecular Biology*, Vol. 1, No. 2, pp. 145-157.

[13] Sahu, S. S., Gandhi, I. S. R., and Khwairakpam, S. (2018). "State-of-the-art review on the characteristics of surfactants and foam from foam concrete perspective", *Journal of The Institution of Engineers (India): Series A*, Vol. 99, No. 2, pp. 391-405.

[14] Steshenko, A., Kudyakov, A., Konusheva, V., and Syrkin, O. (2017). "Structure formation control of foam concrete". Proceedings on Youth, Science, Solutions: Ideas and Prospects (YSSIP-2016), AIP Publishing.

[15] Chindaprasirt, P., and Rattanasak, U. (2011). "Shrinkage behavior of structural foam lightweight concrete containing glycol compounds and fly ash", *Materials and Design*, Vol. 32, No. 2, pp. 723-727.

[16] Giannakou, A., and Jones, M. R. (2002). "Potential of foamed concrete to enhance the thermal performance of low-rise dwellings", Proceedings of the International Conference on Innovations and Developments In Concrete Materials And Construction held at the University of Dundee, Scotland, UK, Thomas Telford Publishing, pp. 533-544.

[17] Jones, M. R., and McCarthy, A. (2002). "Preliminary views on the potential of foamed concrete as a structural material", *Magazine of Concrete Research*, Vol. 57, No.1, pp. 21-31.

[18] Ranjani, G. I. S., and Ramamurthy, K. (2012). "Behaviour of foam concrete under sulphate environments", *Cement and Concrete composites*, Vol. 34, No. 7, pp. 825-834.

[19] Nambiar, E. K. K., and Ramamurthy, K. (2007). "Sorption characteristics of foam concrete", *Cement and concrete research*, Vol. 37, No. 9, pp. 1341-1347.

[20] Namsone, E., Genadij, S., and Aleksandrs, K. (2017). "Durability properties of high performance foamed concrete", *Procedia Engineering*, Vol. 172, pp. 760-767.

[21] Brodeur, G., Yau, E., Badal, K., Collier, J., Ramachandran, K., and Ramakrishnan, S. (2011). "Chemical and physicochemical pre-treatment of lignocellulosic biomass: a review", *Enzyme Research*, pp. 1-17.

[22] Delvigne, F., and Lecomte, J. P. (2009). "Foam formation and control in bioreactors", *Encyclopedia of Industrial Biotechnology: Bioprocess, Bioseparation, and Cell Technology*, pp. 1-13.

[23] Indrawati, L., Wang, Z., Narsimhan, G., and Gonzalez, J. (2008). "Effect of processing parameters on foam formation using a continuous system with a mechanical whipper", *Journal of Food Engineering*, Vol. 88, pp. 65-74.

[24] Siva, M., Ramamurthy, K., and Dhamodharan, R. (2017). "Development of a green foaming agent and its performance evaluation", *Cement and Concrete Composites*, Vol. 80, pp. 245-257.

[25] Zeng, M., Adhikari, B., He, Z., Qin, F., Huang, X., and Chen, J. (2013). "Improving the foaming properties of soy protein isolate through partial enzymatic hydrolysis", *Drying Technology*, Vol. 31, pp. 1545-1552.

[26] ASTM C 796-97 (2019). "Standard test method for foaming agents for use in producing cellular concrete using preformed foam", West Conshohocken, (Pennsylvania): ASTM International. doi: 10.1520/C0796_C0796M-19.

[27] ASTM C 869-11 (2016). "Standard specification for foaming agents used in making preformed foam for cellular concrete", West Conshohocken, (Pennsylvania): ASTM International. doi:10.1520/C0869_C0869M-11R16.

[28] ASTM C 642-13 (2013). "Standard test method for density, absorption, and voids in hardened concrete", West Conshohocken, (Pennsylvania): ASTM International. doi:10.1520/C0642-13.

[29] ASTM C 495-12 (2019). "Standard test method for compressive strength of lightweight insulating concrete", West Conshohocken, (Pennsylvania): ASTM International. doi: 10.1520/C0495_C0495M-12R19.

[30] IS: 1077 (1992). "Indian standard code of practice for common burnt clay building bricks -specification", New Delhi: Bureau of Indian Standards.

[31] IS: 2185 (Part 1) (2005). "Indian standard code of practice for concrete masonry units — specification Part 1 Hollow and solid concrete blocks", New Delhi: Bureau of Indian Standards.

KHWAIRAKPAM SELIJA holds a B.Tech. Degree in Civil Engineering from Kalasalingam University, Tamil Nadu, & M.Tech. Degree in Structural Engineering from Vellore Institute of Technology, Tamil Nadu, and is pursuing her Ph.D. Degree at Infrastructure Engineering and Management, Department of Civil Engineering, Indian Institute of Technology (IIT) Guwahati. Her research interest includes foam concrete, lightweight concrete, special concretes, sustainability and durability of concrete. Email: k.selija@iitg.ac.in

G. INDU SIVA RANJANI holds a Ph.D. Degree in Civil Engineering (Building Technology and Construction Management) from Indian Institute of Technology Madras, India. Presently she is working as Assistant Professor at Indian Institute of technology Guwahati, India. She has also proposed new materials for the production of foamed concrete. Also she is incessantly exploring several promising possibilities to incorporate sustainability aspect in concrete. She has contributed in development of new mix design methods of concrete using particle packing concept. Her work has been published in peer reviewed journals and cited more than 800 times in leading scientific journals throughout the world. Email: gindu@iitg.ac.in

Cite this article: Khwairakpam, S. and Gandhi, I. S. R. (2021). "Development of natural based foaming agent for the potential use in foam concrete", *The Indian Concrete Journal*, Vol. 95, No. 7, pp. 7-13.

ROLLER COMPACTED CONCRETE USED IN PAVEMENT

S. KAR*, S. K. DEB,
B. BHATTACHARJEE

Abstract

The use of fly ash in roller compacted concrete (RCC) is an avenue for fly ash utilization. This study focuses on investigating the possibility of achieving higher strength, investigating the use of fly ash in RCC, and economic analysis of RCC in the Indian scenario. In this study, cementitious material contents are varied from 15% to 25%, and fly ash contents are used as the replacement of cement in a proportion of 25% and 30%. It is found that the compressive strength of RCC increases with the increase of cementitious material content and fly ash content within the limits of investigations. It is also found that the flexural strength of RCC increases with the increase of cementitious material content. But, the fly ash does not affect flexural strength uniformly.

Keywords: Soil compaction approach, power chart curve, optimum moisture content, vebe consistency, zero-slump concrete.

1. INTRODUCTION

Roller compacted concrete (RCC) has been drawing attention worldwide. RCC is a zero-slump concrete. For constructing the pavement, RCC is placed by an asphalt paver and compacted by a vibrating roller [1-2]. Higher volumes of fine and coarse aggregates are usually used in RCC mix (75% to 80%) than in conventional concrete mix (65% to 75%). Use of less water content and dry mixing reduces the shrinkage and bleed water in RCC compared to conventional concrete [3-4]. Due to the well grading of aggregate and compaction using a vibratory roller, RCC causes less permeability, leads to high strength, and provides excellent durability. However, salt scaling is a common problem with RCC. This may appear due to saline solution such as de-icing salt. Pozzolana and air entraining agent can be used in RCC to deal with this issue [5]. However, the effect of de-icing salt is not an issue in tropical countries like India. RCC sample has low abrasion resistance at an early age, whereas it increases significantly at later age. Fly ash can increase abrasion resistance of RCC [6]. Further, modulus of elasticity of RCC is generally similar or higher compared to the normal concrete with the same amount of cement [5].

The mix proportioning of roller compacted concrete should be such that it has sufficient paste to coat the aggregates and fill the voids of the compacted mix. The aggregate plays a dominant role in the concrete. Fine and coarse aggregate is proportioned to produce a well graded combined aggregate. To produce well graded aggregate, 0.45 power chart curve is used [3]. 0.45 power chart has been widely used to develop uniform gradations for cement concrete mixture design. Past studies revealed that the mixture incorporating the 0.45 power chart gradations gave the highest strength when compared to other power charts and the control concrete [7]. Power chart curve is obtained by the following equation:

$$P = \left(\frac{d}{D}\right)^{0.45} \quad [1]$$

where, d represents a given particle size, D represents the maximum aggregate size, and P represents the percent of the aggregate that is finer than d.

Soil compaction approach may be used for mix proportion of RCC as specified in ACI 211.3R [8-9]. This approach involves establishing a relationship between the dry density and moisture content of the RCC. Optimum moisture content is determined using the procedure described in ASTM D1557 [10]. Consistency of RCC is measured by Vebe time in a modified Vebe consistometer conforming to ASTM C1170 [11]. Cylindrical mold of RCC is cast under a surcharge weight of 9 kg for compressive strength test as described in ASTM C1176 [12]. Beam shaped mold of RCC is cast under a surcharge pressure of 5.1 kPa for flexural strength test [13].

The materials for the roller compacted concrete are mixed in a pug mill or rotary drum mixer such that it can produce a homogeneous mixture. RCC is placed in the paver and is compacted with the vibratory roller without any delay [14]. Typically, RCC is compacted within one hour of mixing the concrete at the plant to achieve the maximum density of 96%-98%. Curing is an extremely important factor in the ultimate strength and durability of RCC. Because RCC has no bleed water, evaporation immediately begins removing water from the paste, which can lead to shrinkage cracking and micro-cracks. This will result in surface deterioration. Therefore, to prevent evaporation of mix water, effective curing treatments for RCC must be applied as soon as possible after final compaction. To prevent roller compacted concrete pavement from drying, the surface is kept moist for a minimum period of 3 to 10 days [15-16]. RCC is particularly appropriate for pavements at industrial

*Corresponding author : Santu Kar, Email: santu.iitd.11@gmail.com

facilities such as intermodal shipping yards, port, and container terminals because construction cost of RCC pavement is low. RCC is also used in bulk material storage, truck parks, low volume urban and rural roads, composite slabs, and pre-casting yards.

No formwork and no conventional finishing are required for RCC pavement construction. Such type of pavement needs no dowels or reinforcing steel. So, RCC pavement is an economical choice compared to conventional rigid pavement. Incorporating fly ash into RCC can further reduce the cost and enhance the performance. Fly ash is used as the replacement of cement because of its pozzolanic nature. The inclusion of fly ash increases the total binder contents that make the RCC easier to compact. Moreover, its inclusion also potentially reduces the heat of hydration. Cao *et al*. (2000) studied the influence of fly ash on early age and later age compressive strength of RCC. They identified that compressive strength decreased at 3 days curing with the increase of fly ash addition up to 45%, while, at 28 days age compressive strength exhibited an increase with the increase in fly ash content up to 45%. However, with the further increase in fly ash content, the trend reversed exhibiting the decrease in strength with the increase of fly ash content up to 95% [17]. Mardani-Aghabaglou and Ramyar (2013) investigated on mechanical properties of high volume fly ash roller compacted concrete. The researchers replaced a part of aggregates by fly ash and found that increasing the fly ash content increased the strength of RCC mixture at all ages. On the other hand, when cement was replaced by 20%, 40%, and 60% of fly ash, the researchers identified that compressive strength, as well as flexural strength, reduced with increased fly ash content up to even 180 days [18]. The results obtained from the above two studies contradict each other. Hence, the influence of fly ash on the mechanical properties of RCC is still unclear. Thus, more study is required to identify the influence of fly ash on the compressive and flexural strength of RCC.

Several past studies were conducted on RCC using waste aggregate, silica fume, granulated blast furnace slag, natural pozzolans such as khash pozzolan and pars pumice pozzolan, chemical admixture [13, 19-22]. However, characteristic of RCC using fly ash has been less addressed experimentally in literature. Two such studies described earlier, where fly ash was used, contradict each other and failed to provide a clear conclusion on the effect of fly ash on the mechanical properties of RCC [17,18]. Over 112 million tons of fly ash are being generated annually in thermal power plants in India [23]. The use of fly ash in RCC gives an avenue for fly ash utilization. Moreover, the compressive strength of RCC using fly ash has been achieved up to 20-25 MPa in the past [24,25]. So, the objective of this research is to investigate the possibility for achieving the compressive strength of RCC up to 35-40 MPa using the ingredients available around the Delhi region, also to investigate the use of fly ash content up to 30%-35% by mass of cementitious material, to determine the flexural strength, and also look into the resulting economy.

By investigating the possibility of achieving the higher strength of RCC to use it in pavement and identifying the influence of fly ash on compressive and flexural strength of RCC, this study bridges an important gap in the existing knowledge. Further, this study illustrates that the fly ash incorporated RCC can be effectively used in pavement and making it economical as well as reducing carbon footprints.

2. RCC MIX PROPORTIONING

Mix proportioning of RCC specimens was carried out in soil compaction approach. The mix proportioning steps of RCC are as follows:

In step 1, coarse and fine aggregate were combined to produce a well graded curve. In step 2, cementitious materials content was selected for trial mixes for modified Proctor compaction test. The moisture content and dry density of the RCC mixes were determined using the combined aggregate and the selected cementitious materials content conducting the compaction test in accordance with ASTM D1557 in step 3. Four samples were prepared with varying added water content and used for compaction test. Water content was varied by increasing 1% of the total solid in each successive batch. In step 4, dry density versus respective moisture content was plotted to determine the optimum moisture content for maximum dry density as described in ASTM D1557. Finally, in step 5, the absolute volumes and masses of the materials per unit volume of concrete were calculated using the optimum moisture content, the selected cementitious materials content, and well graded aggregate proportions. An entrapped air content of 2.0% was assumed in the mix proportion.

3. EXPERIMENTAL PROGRAMME

The Vebe consistometer, available in the lab, conforms to EN 12350-3 which has no surcharge load. So, the apparatus was fabricated to satisfy the criteria for measuring consistency as mentioned in ASTM C1170. The apparatus was also fabricated to meet the requirement as per ASTM C1176 for preparing a cylindrical mold (150 mm diameter and 300 mm height) for compressive strength test. To cast the beam shaped mold (100 mm × 100 mm × 500 mm) for flexural strength test, a surcharge load was fabricated that generated a required pressure of 5.1 kPa. Figure 1 shows the fabrication of the apparatus.

Cement used for the study was ordinary Portland cement (OPC) of 43 grade with a specific gravity of 3.14. 20 mm and 10 mm nominal sizes of coarse aggregate (CA) with a specific gravity

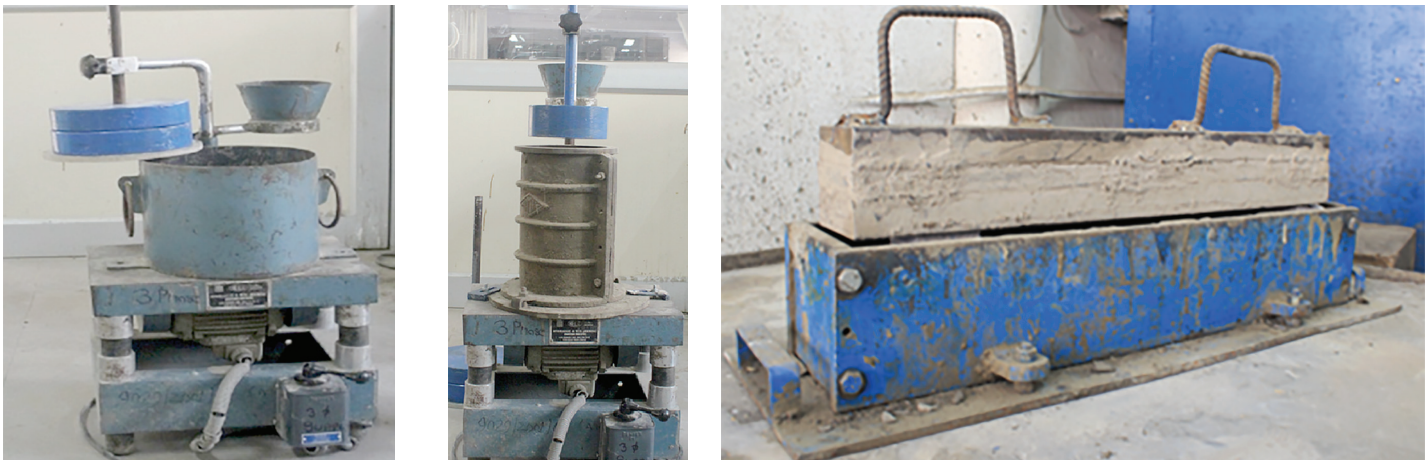

(a) (b) (c)

Figure 1: Fabrication of apparatus (a) set up for Vebe consistency measurement (b) set up for cylindrical mold preparation for compressive strength test (c) set up for beam shaped mold preparation for flexural strength test

of 2.93 were used for the study. Locally available sand with a specific gravity of 2.62 was used for the experiment. Fly ash (FA) having 2.2 specific gravity was used in the study and brought from the Badarpur thermal power plant in India.

Sieve analysis was carried out for 20 mm and 10 mm coarse aggregate, and sand. After sieve analysis, it was found that available sand was complying with the grading zone II. Data obtained from sieve analysis was analyzed to get the combined gradation of aggregates. Percentage of aggregates was varied so that the combined gradation curve matches with the 0.45 power chart curve. Power chart curve results in the well graded aggregate so, it was attempted to match the combined gradation curve with the power chart curve by changing the aggregate proportions in different trials. After several trials, the final proportion of aggregates were obtained as 19% 20 mm CA, 30% 10 mm CA, and 51% sand. The resulted combined gradation curve matched with the power chart curve which ensured the dense grading of aggregates as shown in Figure 2(a). This aggregate proportion was used in the concrete mix proportions. The resulted gradation curve was also verified with the ACI recommended gradation limit by plotting a graph as shown in Figure 2(b). From Figure 2(b), it can be observed that the combined aggregate gradation is almost within the ACI recommended limit. Only at the lower portion of the curves just lies below the ACI lower limit curve which could be incorporated by adding high volume fly ash to the mix proportions.

Three levels of cementitious materials were used as 15%, 20%, and 25%. Two combination of cementitious material were taken: (i) 75% OPC + 25% FA, and (ii) 70% OPC + 30% FA. Four samples with water content 5, 6, 7, and 8% were used for each mix

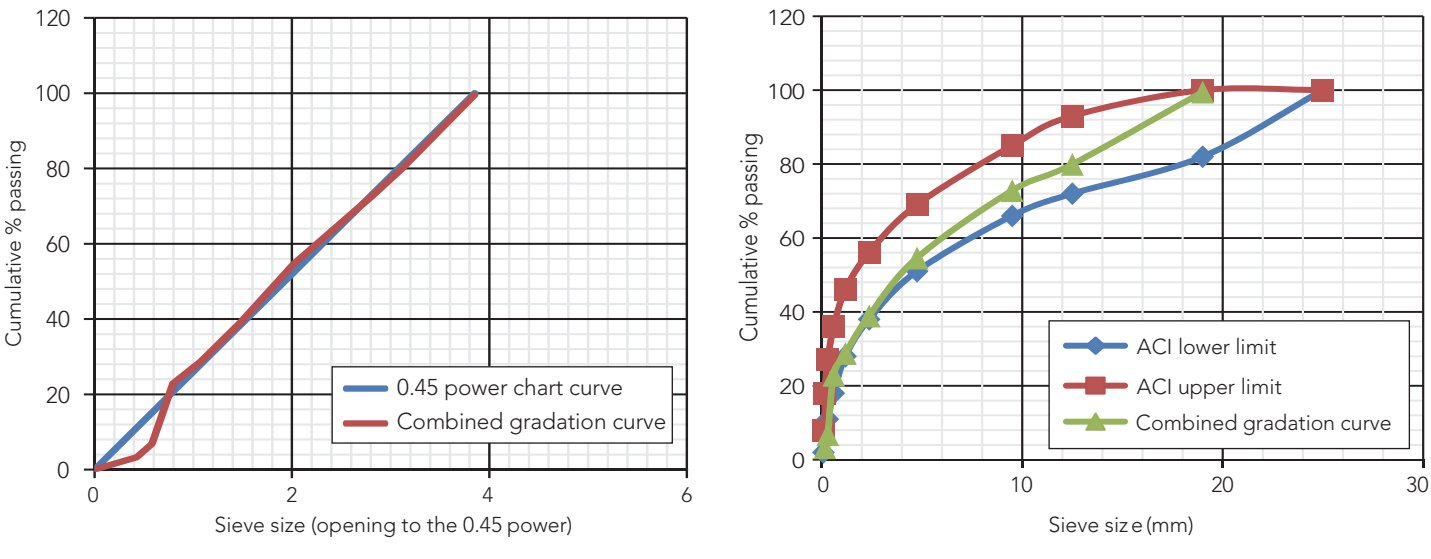

Figure 2: Combined aggregate gradation curve (a) Comparison of combined aggregate gradation curve with power chart curve (b) Comparison of combined aggregate gradation with ACI limits.

Table 1: Optimum water content and maximum dry density of different mix proportions

MIXTURE DESIGNATION	DESCRIPTION	OPTIMUM WATER CONTENT (% OF TOTAL SOLID)	MAXIMUM DRY DENSITY (kg/cu·m)
CM15FA25	15% CM (.75 OPC + .25 FA)	6.2	2500
CM15FA30	15% CM (.70 OPC + .30 FA)	5.7	2460
CM20FA25	20% CM (.75 OPC + .25 FA)	6.4	2548
CM20FA30	20% CM (.70 OPC + .30 FA)	6.95	2516
CM25FA25	25% CM (.75 OPC + .25 FA)	5.7	2346
CM25FA30	25% CM (.70 OPC + .30 FA)	6.8	2508

Table 2: Material quantities per unit volume of concrete

MIXTURE DESIGNATION	DESCRIPTION	CEMENTITIOUS MATERIALS (kg/cu·m)		WATER (kg/cum)	W/(C+F)	SAND (kg/cu·m)	AGGREGATE (kg/cu·m)	
		OPC	FLY ASH				20 mm CA	10 mm CA
CM15FA25	15% CM (.75 OPC + .25 FA)	227	75	144	0.47	1028	383	605
CM15FA30	15% CM (.70 OPC + .30 FA)	214	92	133	0.43	1039	387	611
CM20FA25	20% CM (.75 OPC + .25 FA)	289	96	148	0.38	982	366	577
CM20FA30	20% CM (.70 OPC + .30 FA)	261	112	156	0.41	990	355	560
CM25FA25	25% CM (.75 OPC + .25 FA)	352	118	134	0.28	959	357	564
CM25FA30	25% CM (.70 OPC + .30 FA)	315	135	153	0.33	955	342	540

proportion. A compaction curve was plotted between water content and dry unit weight to determine the optimum water content. The water content was used in the final mix proportion of RCC as given in Table 1. The material quantities of different RCC mixes were calculated as given in Table 2.

Vebe consistency was required to be more than 20 seconds to meet the criteria for zero-slump concrete in procedure A or B as per ASTM C1170. Measured Vebe consistency and Vebe density are provided in Table 3. Vebe consistencies of the mixes were more than 20 seconds that confirmed the zero slump of RCC.

4. RESULTS AND ANALYSIS

4.1. Compressive strength and flexural strength of different mix proportions

Cylindrical RCC specimens of 150 mm diameter and 300 mm length were tested for compressive strength in the compression testing machine after 3, 7, 28 days, curing in submerged condition under water. Cementitious material contents and fly ash contents were varied to observe their effect on strength. The beam shaped RCC specimens were tested for flexural strength by third-point loading system as per ASTM C78 after 28 days

Table 3: Measured Vebe consistency and Vebe density of different mix proportions

MIXTURE DESIGNATION	DESCRIPTION	VEBE DENSITY (kg/cu·m)	VEBE CONSISTENCY (s)	COMMENT
CM15FA25	15% CM (.75 OPC + .25 FA)	2438.3	28	Zero slump
CM15FA30	15% CM (.70 OPC + .30 FA)	2499.12	23	Zero slump
CM20FA25	20% CM (.75 OPC + .25 FA)	2525.65	28	Zero slump
CM20FA30	20% CM (.70 OPC + .30 FA)	2580.95	39	Zero slump
CM25FA25	25% CM (.75 OPC + .25 FA)	2493.59	45	Zero slump
CM25FA30	25% CM (.70 OPC + .30 FA)	2527.87	40	Zero slump

Table 4: Results of compressive strength test and flexural strength

MIXTURE DESIGNATION	DESCRIPTION	CYLINDER COMPRESSIVE STRENGTH (MPa)			FLEXURAL STRENGTH (MPa) IN 28 DAYS
		3 DAYS	7 DAYS	28 DAYS	
CM15FA25	15% CM (.75 OPC + .25 FA)	10.177	13.97	24.79	5.1
CM15FA30	15% CM (.70 OPC + .30 FA)	5.82	9.44	27.14	5.22
CM20FA25	20% CM (.75 OPC + .25 FA)	10.409	12.49	26.09	5.69
CM20FA30	20% CM (.70 OPC + .30 FA)	6.94	11.66	29.99	4.6
CM25FA25	25% CM (.75 OPC + .25 FA)	6.66	12.76	29.16	5.8
CM25FA30	25% CM (.70 OPC + .30 FA)	5.82	13.88	35.27	6

curing [26]. Results of the compressive strength test and flexural strength test are provided in Table 4. For compressive strength test as well as flexural strength test, six mix proportions were used in this study namely CM15FA25, CM15FA30, CM20FA25, CM20FA30, CM25FA25, and CM25FA30, as shown in Table 2. Three cylindrical specimens were tested for compressive strength for every 3, 7, and 28 days for each mix proportion which resulted in the testing of nine cylindrical specimens for each proportion. Besides, three beam shaped specimens were tested for 28 days flexural strength for each mix proportion.

The 28 days strength results are represented in Figure 3 to see the effect of variation in cementitious material content and the effect of fly ash content in RCC. Error bars are also shown in this figure. The maximum variation was within ±5% from the mean.

Figure 3 shows that the increase in the percentage of cementitious material content increases the 28 days cylinder compressive strength. Figure 3 also shows that compressive strength increases as the percentage of fly ash content increases. Maximum compressive strength among the six mix proportions used in this study was 35.27 MPa as 28 days cylinder compressive strength.

The reaction of fly ash with $Ca(OH)_2$ also known as the pozzolanic reaction that results in the production of more hydrated gel which is responsible for the strength of concrete. The depletion of lime begins only after 10 - 14 days indicating initiation of the pozzolanic reaction. Refer to Table 1; it can be seen that optimum moisture content does not vary in a systematic and significant manner with cementitious material content. Neither does it vary significantly with change in fly ash content. However, it can be seen that densities are more or less similar, implying similar plastic density and hence similar initial porosity. As hydration progress, the pozzolanic reaction takes place and leads to the formation of denser microstructure of the hydrated cementitious phase resulting in improved strength compared to 3 and 7 days. It may be mentioned here that the maximum percentage of fly ash was 30% which is below the limit prescribed in IS: 456 (2000) for structural concrete. Hence it is likely that most of the silica and alumina system can react with lime liberated from cement in the long run without leaving any unreacted active pozzolana. Therefore, the inclusion of fly ash lowers the early age compressive strength of RCC, whereas it increases the long-term strength. Hence the results obtained from this study are also theoretically justified.

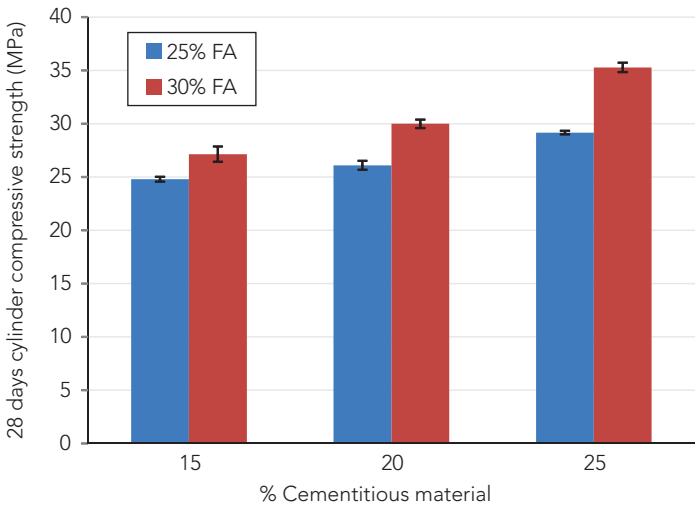

Figure 3: Effect of cementitious material content on compressive strength

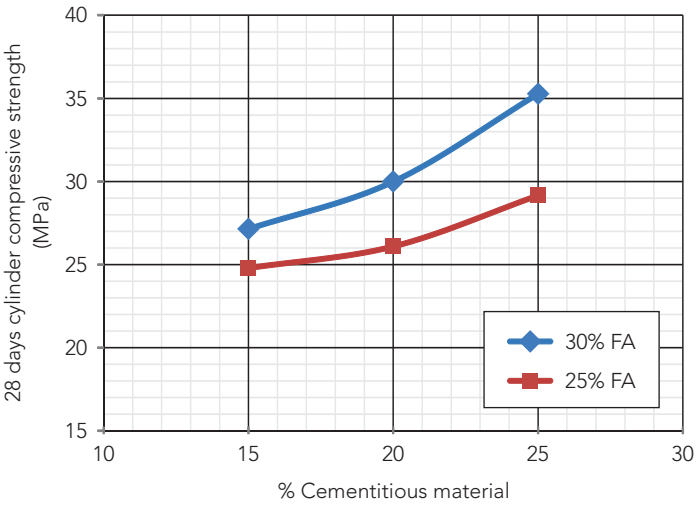

Figure 4: Cylinder compressive strength vs. % cementitious material

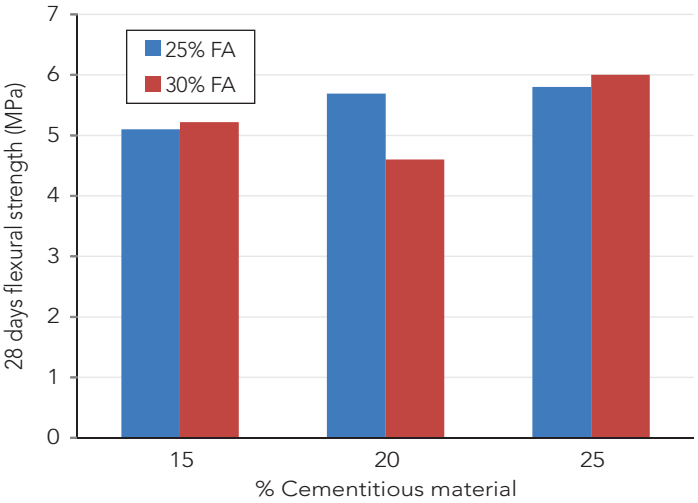

Figure 5: Effect of cementitious material content on flexural strength

The results are also plotted to get the curve in between cylinder compressive strength and cementitious material content. The curve shown in Figure 4 could be used to suggest the required cementitious material content for any specific compressive strength of RCC in the Indian scenario. Results from the flexural strength are represented in Figure 5 to see the effect of different mix proportions.

Figure 5 shows that flexural strength of RCC increases with the increase in cementitious material content. Figure 5 also shows that use of fly ash does not affect the flexural strength uniformly.

4.2. Economic analysis and sustainability assessment of the RCC pavement

Economic analysis was carried out considering the CM20FA30 RCC mix having cylinder compressive strength of 29.99 MPa and flexural strength of 4.6 MPa at 28 days curing. The cost of RCC pavement was compared with the cost of conventional concrete pavement of M25A20 mix which was used in Subansiri Lower Hydro Electric project located on Subansiri river, which is on the border of Arunachal Pradesh and Assam. In the cost comparison, the cost of materials, plant and equipment, and labor were included based on the rates imposed by Arunachal Pradesh Public Works Department [27], as shown in Table 5.

Table 5: Cost of RCC pavement for mixture CM20FA30 and of conventional concrete pavement for mixture M25A20

ITEM	UNIT	QUANTITY		RATE (Rs)	AMOUNT (Rs)	
		RCC	CONVENTIONAL CONCRETE		RCC	CONVENTIONAL CONCRETE
(A) Material						
OPC	kg/cu·m	261	320	10231/tonne	2670	3274
Fly ash	kg/cu·m	112	0	1200/tonne	134	0
Sand	kg/cu·m	990	860	260/tonne	257	224
Aggregate (20 mm, 10 mm)	kg/cu·m	915	1025	699/tonne	640	716
16 mm diameter tie bars	kg/cu·m	0	1.11	67600/tonne	0	75
32 mm diameter dowel bars	kg/cu·m	0	9	67600/tonne	0	608
(B) Plant and equipment						
Front end loader 1 cu·m bucket capacity	hour	0.013	0	1580/hour	21	0
Cement concrete batch mix plant @ 75 cu·m/hour	hour	0.013	0.013	5336/hour	69	69
Paver @ 75 cu·m/hour	hour	0.013	0	3683/hour	48	0
Vibrator	day	0	0.07	370/day	0	26
Vibratory roller 8-10 tonne capacity	hour	0.018	0	829/hour	15	0
(C) Labor						
Unskilled labor	day	0.05	0.23	350/day	18	81
Skilled labor	day	0.01	0.35	500/day	5	175
Total					3877	5248
Water charges @1%					39	52
Total					3916	5301
Add 15% contractor's profit and overhead					587	795
Total cost for 1 cu·m of compacted volume of concrete pavement					4503	6096

Table 6: CO_2 emission from construction RCC pavement and conventional concrete pavement

MATERIALS	UNIT	QUANTITY		CO_2 kg/kg OF MATERIALS	CO_2 EMISSION (kg/cu·m)	
		RCC	CONVENTIONAL CONCRETE		RCC	CONVENTIONAL CONCRETE
OPC	kg/cu·m	261	320	0.825	215.3	264.0
Fly ash	kg/cu·m	112	0	0.019	2.1	0.0
Sand	kg/cu·m	990	860	0.0026	2.6	2.2
Aggregate (20 mm, 10 mm)	kg/cu·m	915	1025	0.0075	6.9	7.7
Production of fresh concrete	kg/cu·m	2278	2205	0.0077	17.5	17.0
Total CO_2 emission from the construction of 1 cu·m of concrete pavement					244.4	290.9

However, the transportation cost of concrete was not included because it depends on the distance from the batch mix plant to the location of pavement. In RCC pavement, fewer joints are sawed that are spaced farther apart (4.6 to 9.1 m transversely) and the load is transferred through aggregate interlock provided by dense graded aggregates [3,4]. So, RCC pavement does not require any dowels bar and tie bars. Table 5 shows that cost of RCC pavement is lesser by 35% than conventional concrete pavement. Thus, RCC pavement is economical than conventional concrete pavement.

Furthermore, the use of fly ash in RCC pavement would help in reducing the burden on landfills as well as reducing the CO_2 emissions. Table 6 shows that RCC pavement resulted in a reduction of CO_2 emission by 19% than conventional concrete pavement. The comparison of CO_2 emissions included the CO_2 emissions from the production of fresh concrete and raw materials such as cement, fly ash, sand, and aggregates, as obtained from [28]. However, the CO_2 emissions from material transportation were not accounted for in this comparison. The economic analysis and sustainability assessment reveal that pavement made by RCC incorporated with fly ash would not only lower the cost of pavement but would also lead to environmental benefits such as disposal of fly ash and reduction in carbon footprints. The findings of this study would enhance the awareness amongst academicians and practitioners on the potential utilization of RCC incorporated with fly ash in pavement construction.

5. CONCLUSIONS

This study reveals that the fly ash content up to 30% and cementitious material content up to 25% can be effectively used in RCC to enhance the long-term strength. It has been demonstrated to this study that it is possible to produce RCC with incorporating fly ash up to cylinder compressive strength of 35.27 MPa (equivalent cube compressive strength of 44.08 MPa) and flexural strength up to 6 MPa at 28 days curing using soil compaction approach. An economic analysis has been made which shows that RCC pavement is economical than conventional concrete pavement. Furthermore, the comparison of CO_2 emissions shows that RCC pavement can reduce CO_2 emissions significantly than conventional concrete pavement. Thus, the fly ash incorporated RCC can be effectively used in pavement construction and making it economical as well as reducing carbon footprints.

In the future study, abrasion resistance of RCC could be investigated, test on durability properties of RCC might be carried out, and thermal behavior and shrinkage of RCC in the tropical region could be investigated.

REFERENCES

[1] Halsted, G. E. (2009). "Roller-compacted concrete pavements for highways and streets", Portland Cement Association, Annual Conference of the Transportation Association of Canada, British Columbia, pp. 1-15.

[2] Mehata, P. K., and Monterio, P. J. M. (2006). "Concrete: microstructure, properties, and materials", Third edition, Tata Mcgraw-Hill Publishing Company, pp. 544-549.

[3] Harrington, D., Adbo, F., and Adaska, W. (2010). "Guide for roller compacted concrete pavements", Portland Cement Association, pp. 40-50.

[4] Mueller, P. E. (1990). "Roller compacted concrete pavement", Arizona Department of Transportation, Report No. FHWA-AZ88-832, pp. 7-22.

[5] Calis, G., and Sadık, A. Y. (2019). "Investigation of roller compacted concrete: literature review", *Challenge Journal of Concrete Research Letters*, Vol. 10, No. 3, pp. 63-74.

[6] Won, J. P., Jang, C., Lee, S. W., and Kim, W. Y. (2009). "Durability performance of roller compacted concrete using fly ash", *Brittle Matrix Composites*, pp. 161-167.

[7] Panchalan, R. K., and Ramakrishnan, V. (2007). "Validity of 0.45 power chart in obtaining the optimized aggregate gradation for improving the strength aspects of high-performance concrete", *ACI Special Publications*, No. 243, pp. 99 -108.

[8] Boyle, M. J. (2002). "Guide for selecting proportions for no-slump concrete", American Concrete Institute, ACI 211.3R-02, pp. 6-26.

[9] Atis, C. D. (2005). "Strength properties of high-volume fly ash roller compacted and workable concrete, and influence of curing condition", *Cement and Concrete Research*, pp. 1113-1120.

[10] ASTM D1557-12. (2012). "Standard test methods for laboratory compaction characteristics of soil using modified effort", ASTM International.

[11] ASTM C1170/C1176M-08. (2008). "Standard test method for determining consistency and density of roller-compacted concrete using a vibrating table", ASTM International.

[12] ASTM C1176/C1176M-08. (2008). "Standard practice for making roller-compacted concrete in cylinder molds using a vibrating table", ASTM International.

[13] Vahedifard, F., Nili, M., and Meehan, C. L. (2010). "Assessing the effects of supplementary cementitious materials on performance of low-cement roller compacted concrete pavement", *Construction and Building Materials*, Vol. 24, pp. 2528-2534.

[14] Shoenberger, J. E. (1994). "Roller compacted concrete pavement", US army Center for Public Works, Report No. FEAP-UG-94/03, pp. 1-13.

[15] Kalantari, B., Mafian, S., and HuatBujan, B. K. (2009). "RC concrete versus conventional concrete", *Contemporary Engineering Sciences*, Vol. 2, No. 3, pp. 139 -148.

[16] Brotman, I., Crist, M., and Gaul J. (2007). "Roller compacted concrete pavement: properties, design, and construction", *Soil and Material Inputs for Mechanistic-Empirical Pavement Design*, pp. 2-10.

[17] Cao, C., Sun, W., and Qin, H. (2000). "The analysis on strength and fly ash effect of roller-compacted concrete with high volume fly ash", *Cement and Concrete Research*, Vol. 30, No. 1, pp. 71-75.

[18] Mardani-Aghabaglou, A., and Ramyar, K. (2013). "Mechanical properties of high-volume fly ash roller compacted concrete designed by maximum density method", *Construction and Building Materials*, Vol. 38, pp. 356-364.

[19] Tavakoli, D., Dehkordi, R. S., Divandari, H., and Brito, J. (2020). "Properties of roller-compacted concrete pavement containing waste aggregates and nano SiO_2", *Construction and Building Materials,* No. 249, pp. 118747.

[20] Saluja, S., Goyal, S., and Bhattacharjee, B. (2019). "Strength and abrasion resistance of roller compacted concrete incorporating GGBS and two types of coarse aggregates", *Advances in Concrete Construction,* Vol. 8, No. 2, pp. 127-37.

[21] Pourkhorshidi, A. R., and Ramezanianpour, A. A. (2020). "Roller compacted concrete pavement using natural pozzolan: experimental investigation and salt-scaling durability model", *International Journal of Pavement Engineering*, Vol. 8.

[22] Nero, M. A., and Haldenbilen, S. (2020). "Determining the effects of chemical admixtures on roller compacted concrete (RCC)", *American Journal of Engineering and Technology Management*, Vol. 5, No. 1, pp. 27-34.

[23] Dhadse, S., Kumari, P., and Bhagia, L. J. (2008). "Fly ash characterization, utilization and government initiatives in India – a review", *Journal of Scientific & Industrial Research*, Vol. 67, pp. 11-18.

[24] Ganapati, N. P., Kumar, B. J., and Satayanarayana, P. V. V. (2012). "A study on strength properties of roller compacted concrete with 30% replacement of OPC 53 grade cement by fly ash", *International Journal of Computational Engineering Research*, Vol. 2, No. 3, pp. 912-918.

[25] Chhorn, C., Seong, J. H., and Seung, W. L. (2018). "Relationship between compressive and tensile strengths of roller-compacted concrete", *Journal of Traffic and Transportation Engineering,* Vol. 5, No. 3, pp. 215-223.

[26] ASTM C78/C78M-10. (2010). "Standard test method for flexural strength of concrete (using simple beam with third point loading)", ASTM International.

[27] Public Works Department Arunachal Pradesh (2018). *Analysis of rates for road and bridge works*, pp. 173-177.

[28] Debbarma, S., Ransinchung, G. D., Singh, S., and Sahdeo, S. K. (2020). "Utilization of industrial and agricultural wastes for productions of sustainable roller compacted concrete pavement mixes containing reclaimed asphalt pavement aggregates", *Resources, Conservation and Recycling*, Vol. 152, pp.104504.

SANTU KAR is an Early Doctorate fellow at the Department of Civil Engineering, Indian Institute of Technology Delhi, New Delhi (India). He started his career with Larsen and Toubro Ltd and worked with this prestigious organization for more than five years. He completed his Ph.D. and M.Tech. from the Department of Civil Engineering, Indian Institute of Technology Delhi. His research interests pertain to the area of material management, sustainable construction, automation in construction, optimization, risk management, and concrete technology. He has published in these areas in reputed national and international journals. Email: santu.iitd.11@gmail.com

S. K. DEB is a retired faculty from the Department of Civil Engineering, Indian Institute of Technology Delhi, New Delhi (India). His research interests pertain to transportation engineering, urban engineering, fuzzy system modeling and airways, sustainable city and its sub-system. Email: skdeb@civil.iitd.ac.in

BISHWAJIT BHATTACHARJEE is emeritus professor at the Department of Civil Engineering, Indian Institute of Technology Delhi, New Delhi (India). His research interests pertain to the domains of cement and concrete technology, building science, sustainable construction, and health monitoring of structures. His publications in these areas are well cited. He is also a recipient of the Indian Concrete Institute's Life Time Achievement Award. Email: bishwa@civil.iitd.ac.in

Cite this article: Kar, S., Deb, S. K., and Bhattacharjee, B. (2021). "Roller compacted concrete used in pavement", *The Indian Concrete Journal*, Vol. 95, No. 7, pp. 14-22.

AN EXPERIMENTAL INVESTIGATION ON THE MECHANICAL PROPERTIES OF GLASS FIBRE REINFORCED GEOPOLYMER CONCRETE

KALLEMPUDI MURALI,
T. MEENA*

Abstract

This article focuses on an experimental study of the mechanical properties of fly ash (FA) and ground granular blast furnace slag (GGBFS) based geo polymer concrete (GPC) using glass fibres. In this study, an 8-molarity concentration of NaOH with an alkaline liquid ratio of 2.5 was used. Mechanical properties like compressive strength, split Tensile strength and flexural strength of GPC20, GPC40 and GPC60 grades of concrete with FA and GGBFS have been found out. Five different volume fractions, viz., 0.1, 0.2, 0.3, 0.4 and 0.5% of 13 mm length glass fibres were considered in this study. The parameters considered in this research work were different proportions of fly ash and GGBFS, i.e., 70:30, 60:40 and 50:50, at ambient curing conditions. Based on the test results, it is observed that gradual addition of glass fibres improved both split tensile strength and flexural strength of fibre-based geopolymer concrete. The optimum dosage of glass fibre was found tobe 0.3% by volume of concrete.

Keywords: Fly ash, Glass fibre reinforced geo polymer concrete, Ground granular blast furnace slag.

1. INTRODUCTION

Usage of concrete is second only to water in the world [5]. Conventionally, ordinary Portland cement (OPC) is being used as the primary binding material in the making of concrete due to adequate availability of the raw materials [15]. The application of concrete in transportation, infrastructure and habitation has greatly promoted the development of civilization, stability and quality of life. Now-a-days, with the advent of high-performance concrete (HPC), the durability and strength characteristics of concrete have been improved largely [6]. There are many environmental issues associated with the production of OPC; for every ton of OPC produced, an equivalent quantity of CO_2 gets released [34, 35]. Moreover, the amount of energy required for the manufacture of OPC is next only to that for aluminium and steel [36]. In addition to that, there is an abundant availability of fly ash and GGBFS as by-products in steel industries, which can be put to potential use as a partial substitute for OPC in the making of cement concrete elements [24].

Various efforts have been made by researchers to find an alternate binder material to cement; geopolymer concrete (GPC) is a primary solution in this direction. In order to produce GPC, low calcium fly ash, a source material, needs to be activated by an alkaline solution to produce polymeric Si-O-Al bonds. The alkaline solution is the combination of sodium hydroxide (NaOH) and sodium silicate (Na_2SiO_3) [9]. This alkaline solution reacts with SiO_2 and Al_2O_3 in fly ash to form N-A-S-H gel; and calcium in GGBS to form C-S-H gel. The curing conditions, especially temperature significantly enhances the polymerization process [8].

Purdon [23] was probably the first researcher to investigate the alkaline-activated slags. Subsequently, many other researchers conducted further studies on alkaline-activated slags, thereby giving rise to an alternate to OPC, namely GPC. It was first introduced by Joseph Devodovit based on the development of fly ash-based geopolymer in the year 1979 to eliminate the cement content during the manufacturing process of concrete. Fly ash, which is obtained from the burning of coal in thermal power plants, is a by-product. Both high-calcium and low- calcium fly ash having high contents of SiO_2 and Al_2O_3 are suitable for GPC [20, 10] have suggested that geopolymer concrete moulds cured at 65, 70 and 80°C for 24 hours showed an enhancement of the mechanical properties and it played a significant role in geopolymerization for fly ash-based geopolymer.

Use of low-calcium fly ash would result in reduced strength and the process of curing would consume longer [16]. In order to mitigate this issue, GGBFS - a residue from the iron and steel industry - can be utilised as a binding material, which has the potential to develop high-strength geopolymer under contiguous curing conditions. GGBFS particles have a glassy texture which enables them easier to activate than fly ash, whereas fly ash contains enormous amount of crystalline phase, which stipulates a temperature range of 40°C to 85°C to stimulate the reaction [21]. Due to the high content of Al_2O_3, SiO_2

*Corresponding author : T. Meena, Email: meena.t@vit.ac.in

and CaO in glassy state, GGBFS has been used as an exclusive binding material in this research work. GGBFS possesses better binding properties with low heat of hydration, high mechanical properties and excellent resistance to aggressive chemicals [15]. In GGBFS, the C-S-H gels formed due to the presence of CaO, has the potential to increase the strength [26]. C-A-S-H and/or C-S-H gels are formed during the activation of GGBFS similar to that of OPC [11].

According to Davidovits [4], the following 3 types of structures are formed: poly (sialate) (–Si–O–Al–O–), poly (sialate-siloxo) (Si–O–Al–O–Si–O) and poly (sialate- disiloxo) (Si–O–Al–O–Si–O–Si–O). Polycondensation of hydrated silicate and aluminate species are responsible for setting or hardening of geopolymer. Dissolution, hydrolysis and condensation reactions with varying Si/Al ratios in alkaline medium have been discussed [28].

Reactions involving dissolution and hydrolysis are:

$$Al_2O_3+3H_2O+2OH^- \rightarrow 2(Al(OH)_4)^- \quad (1)$$

$$SiO_2+2OH^- \rightarrow (SiO_2(OH)_2)^{2-} \quad (2)$$

$$SiO_2+H_2O+OH^- \rightarrow (SiO(OH)_3)^- \quad (3)$$

The raw aluminate materials, due to either dissolution or hydrolysis, result in silicate $(SiO(OH)_3)^-$ and aluminate $(Al(OH)_4)^-$ species. These dissolved species reshuffle and compress among themselves, thus forming Si-O-Si and Si-O-Al framework [7]. This contraction occurs either between silicate and aluminate species or between silicate species themselves depending upon Si concentration.

Djobo *et al.* [7] have reported that the geopolymer system contains C-S-H, (N, C)-A-S-C-(N)-A-S-H, N-(C)-A-S-H gels depending on the Si, Al, Ca and Na contents, whereas (N, C)-A-S-H is a hybrid gel with chemical composition between C-(N)-A-S-H and N-(C)-A-S-H gels. Thus, GGBFS-based geopolymer concrete gives improved mechanical properties than those based on fly ash. Compared to potassium-based activator, sodium-based activators are relatively cheaper. Alkaline solution made with the combination of Na_2SiO_3 and NaOH are suitable for the preparation of GPC. Any changes in the ratios of fly ash and GGBFS, NaOH molarity, Na_2SiO_3/NaOH solution ratio, type of curing influence the mechanical properties of concrete [3] they have further suggested that the required compressive strength could be achieved if NaOH molarity is in between 8-12M and the ratio of Na_2SiO_3/NaOH solution is 2.5 [9, 24]. Curing too plays an important role in attaining the desired strength [33]. It was observed that compressive strength of fly ash-based geopolymer specimens cured in oven was higher than the ambient cured specimens [1]. During the process of polymerization, silicon oxide and aluminium oxide present in fly ash react with the alkaline solution, which configures the cementitious material. Partial replacement of fly ash with GGBFS was not only found to be beneficial in avoiding oven-curing stage but also in improving the mechanical properties of GPC [24].

Fly ash-based geopolymer concrete requires oven-curing so as to improve the mechanical properties of concrete; however, this is not possible in practice, under in-situ conditions. Consequently, it acts as an impediment for the up-scaling of this material to the industrial levels, while GGBFS-based geopolymer concrete averts the need for external energy source (oven curing) and attains the required strength at outdoor curing itself [24].

Based on various research works in the past, it could tacitly be understood that adding fibres to the concrete mix results in an enhancement of its mechanical properties and controls propagation of cracks. Choi and Yuan [2] have reported the effect of addition of glass and polypropylene fibres on hardened properties of cement concrete. Compressive and split tensile properties of fibre-reinforced concrete at 7, 28 and 90 days were determined. They observed that addition of glass and polypropylene fibres improved the split tensile strength by 20-50%.

Vijai *et al.* [30] studied the effect of inclusion of glass fibres on fresh and hardened properties of fly ash-based geopolymer concrete and the results indicated that with an increase of fibres, the split and flexural strength of GPC also increases. But the drawback is that workability decreases with increase in the fibre content. Vijai *et al.* [30] have reported that the glass fibre reinforced GPC composites containing 90% of fly ash and 10% of OPC. Replacement of 10% of fly ash in OPC in GPC mix eliminates the two limitations of GPC mix such as delay in setting time and necessity of heat curing to gain strength. There were 3 different volume fractions, viz., 0.01, 0.02 and 0.03% of glass fibres in this study and the results had shown an increase in compressive, flexural and split tensile strength of GPC with an increase in fibre content.

1.1 Research significance

GGBFS and fly ash-based geopolymer concrete is attractive since it is a cement-free concrete. A scholarly review of the literature reveals that while there are many studies on GPC based on fly ash, not much of research has been carried out on GGBFS-based GPC. Therefore, it has been concluded that GPC has comparable mechanical properties to that of OPC concrete, but not much literature is available on the study of modulus of elasticity of GPC under ambient curing. This study aims at experimentally determining the mechanical properties namely compressive strength, split tensile strength and flexural strength of GPC20, GPC40 and GPC60 with fly ash and GGBFS as binders along with glass fibre under ambient curing.

2. MATERIALS

2.1 Binder used

GGBFS procured from Toshali Cements, Vishakapatnam, India and fly ash purchased from the Ramagundam Thermal Power Plant of National Thermal Power Corporation (NTPC) Limited, India, were used in this research work. The chemical compositions of fly ash and GGBFS are shown in Table 1. GGBFS and fly ash have the specific gravity of 2.9 and 2.17 respectively.

2.2 Aggregates

Fine aggregate used in this research is river sand having a specific gravity of 2.62 with bulk density of 1600 kg/m^3 and corresponding to Zone-II as per IS: 383 [12]. Crushed rock having a specific gravity of 2.7 and sizes 10 mm and 12.5 mm combination was used as the coarse aggregate.

2.3. Alkaline activator solution

The alkaline activator solution is a combination of sodium hydroxide and sodium silicate [32]. NaOH in the pellet form and Na_2SiO_3 in the liquid form were used. The sodium hydroxide pellets used in the present study had 98% purity; sodium silicate used in the liquid form had a chemical composition of 65% of H_2O, 26.5% of SiO_2 and 8.5% of Na_2O by mass.

2.4 Preparation of alkaline solution

Initially, the required molarity of sodium hydroxide (NaOH) pellets were dissolved in water. Depending upon the concentration of the NaOH solution, the mass of NaOH pellets will vary. In this research work, 8-molarity of NaOH was employed [19, 22]. The molecular weight of NaOH is 40. A total weight of 320 grams, i.e., 8 × 40, of NaOH pellets are dissolved in 1 litre of potable water. Then, the calculated quantity of sodium silicate solution is added to the NaOH solution. Na_2SiO_3/NaOH taken as 2.5 [29]. For proper mixing and to reduce the heat due to hydration, the solution was prepared one day prior to the casting of the specimens.

Table 1: Chemical composition of fly ash and GGBFS

Composition	SiO_2	Al_2O_3	Cao	Fe_2O_3	SO_3	MgO	Na_2O	LOI
FA	60.11	26.52	4.1	4.28	0.37	1.21	0.2	0.2
GGBFS	34.08	20.3	32.4	0.7	0.8	7.93	NIL	NIL

2.5 Superplasticizer (SP)

High water content reduced sulphonated naphthalene based conplast SP-430 was used, which was bought at Fosroc Chemicals Limited, India. The dosage of superplasticizer was used with respect to weight of the binder (fly ash and GGBFS) so that there is an improvement in the workability of concrete [31].

3. EXPERIMENTAL PROGRAM

The objective of this experimental program is to determine the fresh and hardened properties of fly ash and GGBFS based geopolymer concrete under ambient curing conditions [27]. Mechanical properties of GPC20, GPC40 and GPC60 grades of concrete were determined. The specimens were cast in cube moulds of dimension 150 mm for determining compressive strength and cylinders of 150 mm diameter and 300 mm height for determining split tensile strength and modulus of elasticity and prisms of dimension 100 × 100 × 500 mm for determining flexural strength of concrete. Glass fibre of size 13 mm was used [17]. The mix proportions for GPC20, GPC40 and GPC60 are illustrated in Table 2. The mix proportions were adopted from the literature [25].

3.1 Preparation of the geopolymer concrete specimens

The raw materials were weighed and batched in accordance with the mix proportions given in Table 2. First, the fine aggregate

Figure 1: Ambient curing of specimens

Figure 2: Preparation of NaOH solution

Table 2: Mix proportions of geopolymer concrete

MIX	FLY ASH (kg/m³)	GGBFS (kg/m³)	FINE AGGREGATE (kg/m³)	COARSE AGGREGATE (kg/m³)	ALKALINE SOLUTION (kg/m³)	Na_2SiO_3 (kg/m³)	NaOH (kg/m³)	GLASS FIBRE (%)	SP (%)
GPC20	252	108	774	1098.8	198	141.42	56.57	0	4.0
GPC20	252	108	774	1098.8	198	141.42	56.57	0.1	4.0
GPC20	252	108	774	1098.8	198	141.42	56.57	0.2	4.5
GPC20	252	108	774	1098.8	198	141.42	56.57	0.3	5.0
GPC20	252	108	774	1098.8	198	141.42	56.57	0.4	5.5
GPC20	252	108	774	1098.8	286	204.28	56.57	0.5	6.0
GPC40	270	180	760	972	248	177.15	70.85	0	4.0
GPC40	270	180	760	972	248	177.15	70.85	0.1	4.0
GPC40	270	180	760	972	248	177.15	70.85	0.2	4.5
GPC40	270	180	760	972	248	177.15	70.85	0.3	5.0
GPC40	270	180	760	972	248	177.15	70.85	0.4	5.5
GPC40	270	180	760	972	248	177.15	70.85	0.5	6.0
GPC60	260	260	717.6	915.2	286	204.28	81.72	0	4.0
GPC60	260	260	717.6	915.2	286	204.28	81.72	0.1	4.0
GPC60	260	260	717.6	915.2	286	204.28	81.72	0.2	4.5
GPC60	260	260	717.6	915.2	286	204.28	81.72	0.3	5.0
GPC60	260	260	717.6	915.2	286	204.28	81.72	0.4	5.5
GPC60	260	260	717.6	915.2	286	204.28	81.72	0.5	6.0

and coarse aggregate were mixed in an electrically- operated rotating drum for 3 to 4 minutes; then, the binders- both fly ash and GGBFS –followed by glass fibre, were added to this proportion and thoroughly mixed for about 3 more minutes [18]. Thereafter, the prepared alkaline activator was added to the superplasticizer. The mixing was continued for 5 minutes until a homogeneous mix was obtained. Then the workability of the fresh concrete was measured with the help of the slump cone. Concrete was then placed in the respective moulds, i.e., cubes, cylinders and prisms, in 3 layers by tamping each layer by 25 blows using the tamping rod. Then, the moulds were shifted into the electrically-operated vibrating table for approximately 2 minutes to expel air voids. The specimens were demoulded after one day of casting and placed in ambient curing.

3.2 Testing of geopolymer concrete specimens

According to IS: 516 (1959), compressive strength of cubes and split tensile strength of cylinders were determined using the compression testing machine (CTM) with a capacity of 2000 kN [13]. The flexural strength of prisms was determined with the help of the flexural testing machine with a capacity of 1000 kN. The experimental setup for compressive, split and flexural tensile tests are shown in Figure 3.

Figure 3: Testing of cylinders

4. RESULTS AND DISCUSSION

4.1 Workability of GPC

The workability of different mix proportions of GPC is shown in Table 3.

From Table 3, it is clearly observed that, for all the grades of GPC, as the content of GGBFS is increased, there is a decrease in the workability of the concrete mixes consistently. This might be due to the rapid polymerization which takes place with an

Table 3: Workability of GPC

GPC MIX	MIX PROPORTION (BINDER : FA : CA : ALKALINE SOLUTION)	FIBRE (%)	SLUMP (mm)
GPC20	1 : 2.15 : 3.05 : 0.55	0	115
GPC20	1 : 2.15 : 3.05 : 0.55	0.1	95
GPC20	1 : 2.15 : 3.05 : 0.55	0.2	83
GPC20	1 : 2.15 : 3.05 : 0.55	0.3	71
GPC20	1 : 2.15 : 3.05 : 0.55	0.4	55
GPC20	1 : 2.15 : 3.05 : 0.55	0.5	20
GPC40	1 : 1.69 : 2.16 : 0.5	0	93
GPC40	1 : 1.69 : 2.16 : 0.5	0.1	81
GPC40	1 : 1.69 : 2.16 : 0.5	0.2	65
GPC40	1 : 1.69 : 2.16 : 0.5	0.3	50
GPC40	1 : 1.69 : 2.16 : 0.5	0.4	35
GPC40	1 : 1.69 : 2.16 : 0.5	0.5	0
GPC60	1 : 1.38 : 1.76 : 0.5	0	73
GPC60	1 : 1.38 : 1.76 : 0.5	0.1	50
GPC60	1 : 1.38 : 1.76 : 0.5	0.2	38
GPC60	1 : 1.38 : 1.76 : 0.5	0.3	0
GPC60	1 : 1.38 : 1.76 : 0.5	0.4	0
GPC60	1 : 1.38 : 1.76 : 0.5	0.5	0

increase in the content of GGBFS, which results in a decreased workability inspite of adding superplasticizer.

4.2 Mechanical properties of GPC

The compressive, split [14] and flexural characteristics of the different GPC specimens were determined after 28 days of ambient curingand the values are listed in Table 4.

Table 4 : Mechanical properties of GPC

MIX	BINDER CONTENT (kg/m^3)	FIBRE (%)	COMPRESSIVE STRENGTH (MPa)	SPLIT TENSILE STRENGTH (MPa)	FLEXURAL STRENGTH (MPa)
GPC20	360	0	27.1	2.2	2.3
GPC20	360	0.1	27.5	2.6	2.6
GPC20	360	0.2	27.4	2.8	2.9
GPC20	360	0.3	27.8	3.1	3.4
GPC20	360	0.4	27.8	3.0	2.8
GPC20	360	0.5	27.5	3.0	2.7
GPC40	450	0	43.8	4.1	4.1
GPC40	450	0.1	43.8	4.4	4.3
GPC40	450	0.2	43.4	4.8	4.6
GPC40	450	0.3	44.1	5.3	5.5
GPC40	450	0.4	44.7	4.5	4.7
GPC40	450	0.5	44.9	4.3	4.5
GPC60	520	0	62.3	5.8	6.0
GPC60	520	0.1	63.5	6.1	6.3
GPC60	520	0.2	63.8	6.7	6.5
GPC60	520	0.3	64.1	7.2	7.3
GPC60	520	0.4	64.6	6.3	6.7
GPC60	520	0.5	64.2	6.2	6.6

A comparative visualization of compressive, split tensile and flexural strengths of the various GPC specimens with the varying quantities of fibre content is presented in Figures 4, 5 and 6 respectively.

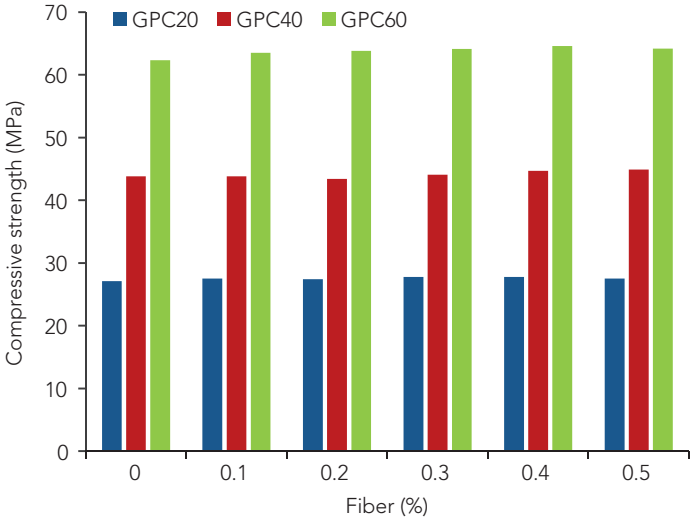

Figure 4: Compressive strength vs Fibre content

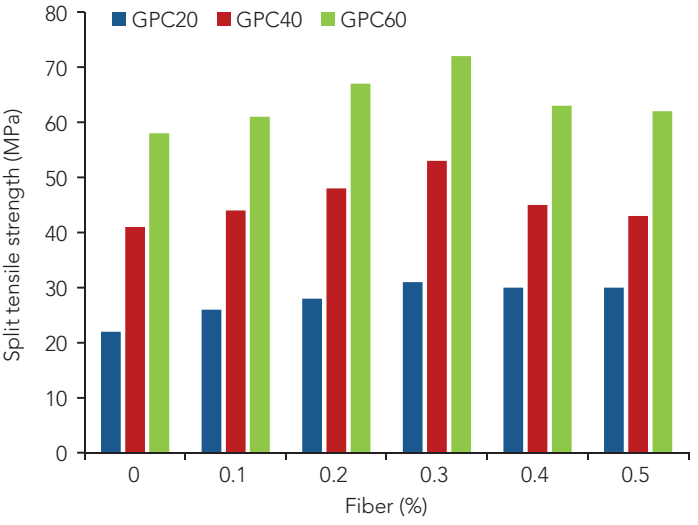

Figure 5: Split tensile strength vs Fibre content

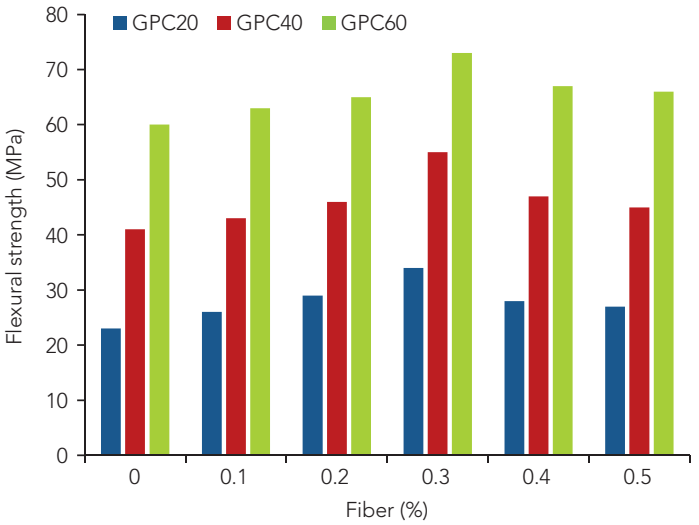

Figure 6: Compressive Strength vs Fibre Content

From the above graphs, it is observed that with an increase in GGBFS binder content, compressive strength also increases. The ratio of fly ash to GGBFS used for the different grades of GPC, namely, GPC20, GPC40 and GPC60 are 70:30, 60:40 and 50:50 respectively. At higher binder content levels, a large quantity of alkaline solution is available for polymerization, which results in an increased strength. As the GGBFS content is increased, more calcium is available for polymerization, which results in the formation of additional C-A-S-H gel along with N-A-S-H gel, consequently enhancing its strength.

To find the tensile strength of concrete, tests on split and flexural strength were carried out. From the results, it is concluded that, with an increased slag content, split and flexural tensile strength also get increased. By the addition of increased quantities of glass fibres to the mix, split and flexural strength values were found to be increased whereas as not much of a change was observed in the case of compressive strength.

5. CONCLUSIONS

Based on the experimental work, the following conclusions are drawn:

1. An increase in the percentage of GGBFS content in a mix correspondingly increases the compressive, split and flexural strengths, implying that GGBFS addition improves the strength of GPC.
2. Though increase of GGBFS content improves the strength, its workability is decreased inspite of superplasticizer addition.
3. By the addition of glass fibre, compressive strength is marginally increased by 2-5%, whereas the split and flexural strength get increased by 20-30% for each grade of GPC. The presence of fibre and its content positively influence both the split tensile and flexural strengths in GPC, inhibiting crack formation as well as propagation.
4. The optimum dosage of glass fibre was found to be 0.3% (by volume of concrete) in improving the tensile and flexural properties of the three grades of GPC viz. GPC20, GPC30 and GPC40.
5. The replacement of fly ash with GGBFS is found to be more suitedto ambient curing compared to steam curing that increases the cost.

REFERENCES

[1] Al Bakri, A. M., Kamarudin, H., Bnhussain, M., Nizar, I. K., Rafiza, and A. R., Zarina, Y. (2011). *"Microstructure of different NaOH molarity of fly ash-based green polymeric cement"*, J. Eng. Technol. Res., Vol. 3, No. 2, pp. 44-49.

[2] Chindaprasirt, P., De Silva, P., Sagoe-Crentsil, K., and Hanjitsuwan, S., (2012). *"Effect of SiO_2 and Al_2O_3 on the setting and hardening of high calcium fly ash-based geopolymer systems"*. J Mater Sci, Vol.47, pp. 4876-4883.

[3] Choi, Y. and Yuan, R. L. (2005). *"Experimental relationship between splitting tensile strength and compressive strength of GFRC and PFRC"*, Cement Concrete Res., Vol. 35, No. 8, pp.1587-1591.

[4] Davidovits, J. (1978). *"Synthetic Mineral Polymer Compound of the Silicoaluminate Family and Preparation Process"*, US Patent, 4472199.

[5] Davidovits, J. (1994). *"Properties of geopolymer cements. Alkaline CemConcr"*, Kiev, Ukraine, pp. 131-149

[6] Davidovits, J., Comrie, DC., Paterson, J. H., Ritcey, D. J. (1990). *"Geopolymeric concretes for environmental protection"*. ACI Concr Int, Vol. 12, No.7, pp. 30-40

[7] Djobo, J. N., Tchakoute´, H. K., Ranjbar, N., Elimbi, A., Tchadjie´, L.N., and Njopwouo, D. (2016). *"Gel composition and strength properties of alkali-activated oyster shell-volcanic ash: effect of synthesis conditions"*. J Am Ceram Soc, Vol. 99, No. 9, pp. 3159-3166.

[8] Rao, G. M., and Rao, T. D. G. (2018). "A quantitative method of approach in designing the mix proportions of fly ash and GGBS-based geopolymerConcrete", Australian Journal of Civil Engineering, 2018, Vol. 16, No. 1, pp. 53-63,

[9] Hardjito, D., Wallah, S.E., Sumajouw, D.M.J. and Rangan, B.V. (2004). *"On the development of fly ash-based geopolymer concrete"*, ACI Mater. J., Vol. 101, No. 6, pp. 467-472.

[10] Hardjito, D., Cheak, CC., and Ing, CHL. (2008). *"Strength and setting times of low calcium fly ash-based geopolymer mortar"*. Mod Appl Sci, Vol.2, No.4, pp. 3-11

[11] Ismail, I., Bernal, SA., Provis, JL., San Nicolas R., Hamdan, S., and Van Deventer, JSJ. (2014). *"Modification of phase evolution in alkali activated blast furnace slag by the incorporation of fly ash"*.CemConcr Compos, Vol. 45, pp. 125-135.

[12] IS: 383 (2016), *"Indian Standard Specification for Coarse and Fine Aggregates from Natural Sources for Concrete"*, Bureau of Indian Standards, New Delhi, India.

[13] IS: 516 (2018), *"Indian Standard Methods of Tests for Strength of Concrete"*, Bureau of Indian Standards, New Delhi, India.

[14] IS: 5816 (1999), "Splitting *Tensile Strength of Concrete-Method of Test*", Bureau of Indian Standards, New Delhi, India.

[15] Kroehong, W., Sinsiri, T., Jaturapitakkul, C., and Chindaprasirt, P. (2011). *"Effect of palm oil fuel ash fineness on the microstructure of blended cement paste"*. Constr. Build. Mater., Vol. 25, No.11, pp. 4095-4104

[16] Kumar, S., Kumar, R., and Mehrotra, SP. (2010). *"Influence of granulated blast furnace slag on the reaction, structure and properties of fly ash-based geopolymer"*. J Mater. Sci., Vol. 45, No. 3, pp. 607-615.

[17] Lv, Y., Cheng, H.M. and Ma, Z. G. (2012). *"Fatigue performances of glass fibre reinforced concrete in flexure"*, Procedia Eng., Vol. 31, pp. 550-556.

[18] M.S Midhun, Rao, T.G. and Thunuguntla, C (2018) *"Mechanical and fracture properties of glass fibre reinforced geopolymer concrete"*, Adv. Concrete Constr., Vol. 6, No.1, pp. 29-45.

[19] Puertas, F., Martínez-Ramírez, S., Alonso, S. and Vázquez, T., (2004). *"Alkali activated fly ash/slag cement strength behavior and hydration products"*, Cement Concrete Res., Vol. 30, pp. 1625-1632.

[20] Phoo-ngernkham, T., Chindaprasirt, P., Sata, V., Pangdaeng, S., and Sinsiri, T. (2013) *"Properties of high calcium fly ash geopolymer pastes co, ntaining Portland cement as additive"*. Int J Miner Metall Mater, Vol. 20, No.2, pp. 214-220

[21] Puertas, F., Martınez-Ramırez, S., Alonso, S., Vazquez, T., (2000), *"Alkaliactivated fly ash/slag cements: strength behaviour and hydration products"*. Cem. Concr. Res, Vol. 30, No. 10, pp. 1625-1632.

[22] Puertas, F., Mart nez-Ram rez, S., Alonso, S. and V zquez, T., (2000), *"Alkali-activated fly ash/slag cements: strength behaviour and hydration products"*, Cement Concrete Res., Vol. 30, No. 10, pp. 1625-1632.

[23] Rao, G. M. and Rao, T. D. (2016). *"Sulphuric acid and nitric acid attack on fly ash and GGBS based geopolymer concrete"*, Proceedings of the International Conference on Trends and Recent Advances in Civil Engineering.

[24] Rao, G. M. and Rao, T. G., (2015). *"Final setting time and compressive strength of fly ash and GGBS-based geopolymer paste and mortar"*, Arab. J. Sci. Eng., Vol. 40, No. 11, pp. 3067-3074.

[25] Rao, G.M., Rao, T. D., Seshu, D. R. and Venkatesh, A., (2016). *"Mix proportioning of geopolymer concrete"*, Cement WapnoBeton, Vol. 21, No. 4, pp. 285.

[26] Ravikumar, D., Peethamparan, S., and Neithalath, N. (2010). *"Structure and strength of NaOH activated concretes containing fly ash or GGBFS as the sole binder"*. Cement Concr. Compos., Vol. 32, No. 6, pp. 399-410.

[27] Rao, G. M. and Rao, T. G. (2017). *"Effect of fly ash and GGBS combination on mechanical and durability properties of GPC"*, Adv. Concrete Constr., Vol.5, No. 4, pp. 313-330.

[28] Swaddle. T. W., (2001). *"Silicate complexes of aluminium (III) in aqueous systems"*. Coord Chem Rev, Vol. 219, pp. 665-686.

[29] Thunuguntla, C., and Gunneswara Rao, T., (2018). *"Appraisal on Strength Characteristics of Alkali-Activated GGBFS with Low Concentrations of Sodium Hydroxide"*. *Iran J Sci Technol Trans CivEng,* Vol. 42, pp. 231-243.

[30] Vijai, K., Kumutha, R., and Vishnuram, B.G. (2012). *"Properties of glass fibre reinforced geo-polymer concrete composites"*, Asian J. Civil Eng., Vol. 13, No. 4, pp. 511-520.

[31] Venu, M., and Gunneswara Rao, T. D., (2008), "An Experimental Investigation of the Stress-Strain Behaviour of Geopolymer Concrete", Slovak Journal of Civil Engineering, Vol. 26, No. 2, pp. 30-34.

[32] Wallah, S. E., and Rangan, B. V. (2006). "Low-calcium fly ash-based geopolymer concrete: long-term properties", Dissertation, Curtin University, Australia, pp.76-80

[33] Xu, H., and Van Deventer, JSJ. (2009). "*The geopolymerisation of aluminosilicate minerals*". Int J Miner Process, 2000, Vol. 59, pp. 247-266.

[34] Teja, K. V., and Meena, T. (2019). An insight into temperature characteristics of ternary blended concrete with perlite powder. *Asian Journal of Civil Engineering*. Vol. 21, No. 1, pp. 41-48.

[35] Teja, K. V., and Meena, T. (2019). Exploration of Perlite Concrete Under Elevated Temperatures. *Indian Concrete journal*, Vol. 93 No. 10, pp. 27-33.

[36] Teja, K. V., and Meena, T. (2020). Performance of Ternary Blended Concrete and Binary Concrete Made with Perlite Powder at Elevated Temperatures. *Jordan Journal of Civil Engineering*, Vol. 14 No. 2, pp. 198-209.

KALLEMPUDI MURALI holds a B.Tech. Degree from GMR Institute of Technology, Jawaharlal Nehru Technological University, Kakinada (JNTUK), a Master's Degree in Structural Engineering from Andhra University, Visakhapatnam, and currently pursuing his Ph.D. from Vellore Institute of Technology (VIT), Vellore. His research area is on geopolymer concrete with hybrid fibers.
Email: kallempudi.murali2016@vitstudent.ac.in

T. MEENA acquired her B.E. Degree in Civil Engineering from Govternment College of Engineering, Tirunelveli, Master's degree in Structural Engineering from Thiagarajar College of Engineering, Madurai and Ph.D. Degree from Anna University, Chennai. She has 22 years of teaching experience in various technical institution and is currently working as an Associate Professor in the Department of Structural and Geo-technical Engineering, School of Civil Engineering, Vellore Institute of Technology, Vellore. She has published 35 articles in reputed International journals apart from National and International conferences. Her research areas include self compacting concrete, fibre reinforced concrete, nano-silica concrete, concrete under elevated temperatures, geopolymer concrete and study of carbonation, sustainability and durability of concrete. Email: meena.t@vit.ac.in

Cite this article: Kallempudi, M., and T., M. (2021). "An experimental investigation on the mechanical properties of glass fibre reinforced geopolymer concrete", *The Indian Concrete Journal*, Vol. 95, No. 7, pp. 23-30.

AN EXPERIMENTAL STUDY ON BIO-COMPOSITES BY THE METHODS OF BACTERIAL IMMERSION AND INJECTION

GIRISH S.*, SOUMYA T.,
ANANYA GIRISH

Abstract

The recent researches have shown that micro-organisms can be helpful material to self-repair of cracks in concrete by using bacteria, generally of Bacillus species as a novel approach of "Bacterial Concrete". The method of application of healer bacteria to the cracks in concrete structures also needs a focus on whether the location of crack is on horizontal concrete surfaces like slabs and floors or vertical as columns and walls. Immersion method suits horizontal concrete surfaces and the injection method suits vertical concrete surfaces. The present study concentrates on the effectiveness of using bacteria on crack healing and the effective methods such as immersion method and injection method of application of bacteria into the concrete. The experimental study on Bacillus species under different methods of application through compressive strength and UPV tests reveals that Bacillus sphaericus in combination with phosphate buffer solution suits through immersion method for horizontal cracked surfaces and with calcium lactate through injection method for vertical cracked surfaces is a best-suited combination.

Key Words: *Bacterial concrete, Bacterial immersion, Bacterial injection, Crack remediation, Self-healing.*

1. INTRODUCTION

Concrete being a massively used construction material world-over bears the responsibility of being collapse resistant and effectively serviceable during its intended lifetime. Many researches focus mainly on concrete being collapse resistant where the performance of the concrete structures encompasses both its capacity to sustain the load and maintain its serviceability without major repairs and also increment in its durability properties [1]. Concrete due to unreacted cement can undergo autogenous healing [2] which fits to be a fundamental platform for the idea of bio concrete. Among many repair methods, self-healing concept is an ideal solution since it is a real time sustainable repair method [3]. Among various self -healing concepts and robustness described by Victor and Emily [4] and Richard P Wool [5], bio concrete proves to be a promising, innovative and effective approach for self-healing of cracks in distressed condition.

The novelty of bacterial concrete research, when compared to other repair methods, lies in the fact that majority of the self-healing mechanism such as using healer chemicals, mineral admixtures etc., [6] involves materials which may not address the multiple crack events repetitively on the same location. Very importantly, bio concrete can address effectively the repair issues under such conditions, repetitively, without human intervention. The species of bacteria being aerobic and alkaliphilic and when supplied with sufficient nutrient medium can get activated in concrete in the presence of oxygen and clog the cracks by generating calcium carbonate crystals besides enhances the compressive strength of concrete. Bio concrete is formed by blending this kind of bacteria with concrete materials using many methods. But the basic method is by direct addition of this alkaliphilic bacteria as an ingredient in solution form to the concrete components which hold the responsibility of uniformly dispersing throughout the concrete matrix and addresses the micro cracks in any location of the structure [7,8]. The bacteria so chosen are alkaliphilic and can survive in a pH of 12 to 13. It is also observed from the research carried out by Wictor. V that the practical application of bio engineered spray or injection into the cracks exhibits effective healing [9].

Many investigations are undertaken in the research field on selection of specific bacteria among many and each of them has its limitations for practical adaptability in bacterial concrete. Choosing a beneficial bacterium is also a challenge and a necessity.

However, Bacillus species with its long-life span, alkaliphilic nature, calcium carbonate crystal-forming capacity and aerobic nature is best suited for enacting as a component in bacterial concrete for its self-healing and strength enhancement capacity. The bacillus species which can precipitate copious amount of calcium carbonate crystals in the presence of calcium based nutrient medium is ideally suited as an ingredient in bacterial concrete even in the high alkaline environment [10].

*Corresponding author : Girish S., Email: girish.civ@bmsce.ac.in

Bacillus sphaericus which is an alkaliphilic, spore forming, ureolytic bacteria inherent the ability to produce calcite crystals suits in enhancement of strength and durability of cement composites. It is a Gram-positive bacterium and also non-pathogenic. It is a soil bacterium and can form resistant endospore that is tolerant to high temperatures, chemicals and can remain viable for long periods of time. Any bacteria which come under the category of endospore forming are resistant to unfavorable conditions. These bacteria during tough environment instead of death they move back to a spore state which germinates once favorable conditions reboot back. Especially the endospores of bacillus species are liable to years together in spore state also called deactivated state or dormant state. It's the general micro biological feature of this species and are already standardized. Hence bacteria *Bacillus sphaericus* can be an ideal bio healer due to its effectiveness in performance. Since cement is a prominent ingredient to promote alkalinity to the concrete medium, this study focuses on the incorporation of bacteria into the cement mortar medium to check their performance under high alkaline condition which can inline assure the performance of bacteria in concrete medium also. With respect to practical applicability of this bio concrete through immersion method and injection method the study has been conducted on mortar specimens in the laboratory condition. The real time concrete cracks in RC column of a college building were also examined by bacterial injection method.

2. MATERIAL CHARACTERIZATION

2.1 Characterization of Mortar Ingredients

Ordinary Portland cement (53 grade) conforming to the requirements of Indian standard [IS: 12269 (2013)] [11] was used in the study. The required quantity of cement used was from a single source, stored in a nearly air tight container. The specific gravity of cement was 3.15 and fineness 394 m^2/kg by air blain's permeability test. Locally available river sand free from all deleterious materials was used as fine aggregates taking care to sieve through 4.75 mm sieve to remove pebbles and coarse materials. The grading of fine aggregates conforms to Zone II with specific gravity 2.63 and water absorption 1.5%.

2.2 Characterization of Bacterial Source

The bacteria used are of genus bacillus species which has potential to resist high alkalinity and the role of direct addition of alkaliphilic bacteria in concrete medium is been described by Senot Sangadji [12] in his research work**.** There are various bacteria that satisfy this condition such as *Bacillus flexus* [13], *Bacillus pasteurii* [14], *Bacillus subtilis, Bacillus sphaericus*, etc. out of which bacillus sphaericus is applied because of its suitability in concrete environment for strength enhancement and self-healing ability [15]. The requirement of bacteria to be thermal resistant is also been proved by the performance of *Bacillus sphaericus* [16]. The bacterial strains of *Bacillus sphaericus* procured from the Microbial Type Culture Collection and Gene Bank (MTCC), Chandigarh are in a freeze-dried condition. The bacterial sample is subjected to the fundamental microbial testing and is as follows:

2.2.1 *Gram Staining*

Gram staining test aims at determining the gram reaction and morphological characteristics of bacteria.

Bacterial smear was prepared and fixed, by heating it on a glass slide. First two to three drops of crystal violet are poured on bacterial smear and kept for 1 minute, and then it was washed with distilled water. Next the iodine was poured on the bacterial smear for 12 seconds and then the smear was gently washed with distilled water. De-colorization of the smear was performed with ethanol for 8 to 12 seconds and again it was washed with distilled water. Safranin staining was done for 15 seconds and washed with water. The prepared sample of bacterial smear slide is visualized under an optical microscope to study morphology and Gram reaction of the bacterial smear.

Gram-positive bacteria consist of thick peptidoglycan in their cells due to which crystal violet do not decolorizes and hence appear purple. Whereas Gram negative bacteria consist of thin peptidoglycan and large amount of lipid content in the cell wall due to which it appears pink. The test reveals that the bacteria *Bacillus sphaericus* was found to be gram positive and was having a rod-shaped morphology. The bacteria are nonpathogenic.

2.2.2 *Calcium Carbonate Estimation*

Before the application of bacteria in to mortar mix, its calcite precipitating ability was studied under standard conditions. This test was conducted to determine the amount of calcium carbonate precipitated by bacteria as it is required to quantify the amount of calcite required to clog the cracks in the concrete medium. The procedure involves an acid -base test conducted, in which 4 mL of bacterial solution was injected into the calcite precipitating media solution A (urea: 20 g/L. and calcium chloride: 49 g/L.), in separate conical flasks and it was incubated at 37°C in an incubator and studied for amount of calcite precipitated at regular intervals. Standard solution was prepared by taking accurately weighed 0.5 g of standard calcium carbonate, taken in a 250 mL standard flask in which salt crystals were dissolved by adding minimum quantity of dilute HCl until effervescence ceases. The prepared solution was diluted well for uniform concentration and was marked as solution B.12 mL of standard $CaCo_3$ solution with 2 mL dilute HCl was titrated with standard NaOH solution. The titration readings were tabulated. After 2 days 12 mL of solution from incubator containing bacteria, urea, calcium chloride was taken and 2 mL of HCl was

Table 1: Test results of kinetic studies on amount of $CaCo_3$ precipitation

NO OF DAYS	CALCIUM CARBONATE g/L
Day 2	0.61
Day 4	3.8
Day 6	4.7

added to it, to dissolve $CaCo_3$ precipitate in that solution. Then it was titrated with standard NaOH solution and the results were tabulated. The results were interpreted as quantity of $CaCo_3$ precipitation which is achieved by the difference in NaOH consumption to neutralize the solution is as shown in Table 1.

The interpretation of the above results says that at day 6 bacteria is able to precipitate 4.7 grams of calcite crystals per liter.

2.2.3 *Survival Test*

In this concept, a trial has been made to bio-mimic the suitable survival media of alkaliphilic bacteria in the laboratory and tested for its survival in it [17]. This test has been conducted since it is required to check the survival of bacteria in concrete medium that is a high alkaline medium. To achieve this, a predefined alkaline environment with known pH was created and investigated. As per the concept the bacteria in high alkaline environment liberates spores and become inactive and remain intact for years waiting for the right environment to come back into active state. The right environment is with the combination of optimum pH i.e., around 7 to 9, food, water and oxygen. To mimic this concept in laboratory two solutions were prepared: one is a solution of sodium hydroxide having the pH same as that of concrete around 13 and the other is a tablet solution which is having a pH of 9.4 as it is a predefined reference solution which is specifically used in the regular experimentation of survival tests on microorganisms. Then the bacterium with nutrient media is mixed in the above said two solutions into which the bacteria is injected and kept in rotary shaker for 24 hours for uniform growth. Optical density test was conducted using colorimeter and the absorbance was checked before and after keeping the solution in rotary shaker as expected there was no growth due to high pH or alkaline environment.

Then after 1 week, a solution media was prepared same as that of subculture media, in which nutrient broth is mixed in distilled water, which has a pH around 7 to 8 which also contains food, water and oxygen which is the right environment for bacteria to get activated. The composition of the nutrient broth provides nutrients, water and also it is kept exposed to air hence provide oxygen. All these three factors are the fundamental germinating environment for any microorganisms, especially aerobic bacteria. From the two solutions one is sodium hydroxide and the other is tablet solution in which due to high pH bacteria went to dormant state, a sample of 15 mL was taken from these

Table 2: Test results of colorimeter for survival test

	COLORIMETER READINGS	
State of bacteria	Bacteria in dormant state	Bacteria in activation state
Solution	Before dilution and absorbance	After dilution and absorbance
NaOH [pH-13]	0.000	0.019
Tablet [pH-9.4]	0.000	0.036

solutions and was injected into the prepared nutrient broth and were kept in rotary shaker for 24 hours for growth and checked for results by colorimeter for survival test which are as shown in Table 2. Colorimeter measures the transmittance and also the absorbance. The value obtained is in mg/L or ppm which are calculated from measured values.

In concrete when the cracks get initiated the entry of water and oxygen dilutes the alkalinity of the location of crack which in turn drops the pH favoring the activation of bacteria [18]. In the above solution similar environment has been created by decreasing the pH of range 13-9.4 to 7-8 as that required for the activation of bacteria. The results obtained in Table 3 clearly indicate the activation of bacteria by exhibiting 0.019 and 0.036 absorbance for alkaline and standard solutions respectively.

2.2.4 *Bacterial Growth Test*

Bacterial growth was confirmed by the appearance of turbidity overnight, and by optical density test in colorimeter. The standard absorbance was fixed to 595 nm, then the turbidity was checked prior and after culturing in colorimeter and there was an increase in absorbance by that sample after culturing. The colorimeter readings also show that the initial readings indicated as 0.000 conforms that there was no bacterial contamination prior to culturing.

2.2.5 *Optical Density Test*

Optical density is the process of transmission of light or other electromagnetic radiation through matter. The process of emission and absorption depends on the radiation's wavelength, which includes the interaction between fundamental particles like electrons, atoms, ions etc. When a beam of light is interacted with absorbing atoms then the absorption takes place. It is depended on the sample's thickness and the concentration of the absorbing atoms. Optical density of the bacterial solution is measured using photoelectric calorimeter. The cell count for the entire research was maintained as 10^6/mL throughout as it is found to give optimum results based on the article by Ghosh and Mandal [15]. The optical density test is used to obtain the cell concentration by indirectly correlating the optical density with cell concentrations using the below given

formula. The Correlation equation between optical density and concentration of cells/mL is adopted from reference article [16].

$$Y = 8.59 \times 10^7 X^{1.3627}$$

where, X = OD reading at 600 nm

Y = concentration of cells/mL

3. METHODOLOGY

3.1 Methodology of Culturing Bacteria

The bacteria *Bacillus sphaericus* was procured in a sealed tube in lyophilized form. The growth media for *Bacillus sphaericus* was prepared by using the composition as specified by MTCC for preparing a nutrient broth (beef extract [1 g/l], yeast extract [2 g/l], peptone [5 g/l], NaCl [5 g/l]). The nutrient broth media for 2 main cultures for *Bacillus sphaericus* were prepared in a standard 250 mL conical flask and are sterilized in an autoclave at 121°C for 15 minutes. A small amount of the culture was inoculated in the 2 sterilized nutrient broth media in UV chamber and named as main culture 1 and 2. These samples are kept in a rotary shaker for 24 hours overnight at 30°C for promoting uniform distribution of fermentation of bacteria. The appearance of turbidity overnight, confirmed bacterial growth and applied for the experimental work.

The bacteria so chosen are Gram positive, nonpathogenic and are available as soil bacterium which is harmless to human health. Even beyond that care has been taken by sanitizing hands with ethanol before and after working with any bacteria with proper safety measures during experimentation.

3.2 Crack Remediation

Crack remediation in concrete components is a vital area in rehabilitation of concrete structures. The traditional methods of crack remediation pose their own limitations in providing a long-term service to maintain durability of concrete structure. Here an effective method of crack remediation by bacteria as a crack healer has been investigated and can be conducted by two methods, i.e., by immersion method and injection method.

3.3 Crack remediation by immersion method

In immersion method the distress or artificially cracked horizontal surface of cement mortar is submerged in bacterial solution of 10^6 cells/mL concentration to allow complete ingress of bio healing agent into the concrete which may be effective in horizontal members such as slabs and floors where ponding of bacterial healer solution is possible. The activity of microorganisms and its precipitation is at micro level. If the cracks are attended and clogged initially itself at micro level, then there will be less chances of macro cracks. In view of this micro cracks of 0.1 to 0.2 mm are focused in the study.

3.3.1 *Methodology*

Standard Mortar cube specimens of size 100 × 100 × 100 mm were cast for testing. Artificial cracks are formed by inserting a 0.2 mm thick copper sheet while casting so that the crack healing can be studied more precisely. Mortar cubes are prepared by mixing 200 g of cement and 600 g of standard sand in the proportion 1:3 by weight with water, the quantity of water used was (p/4+3) % of combined weight of cement and sand, P is the % of water required to produce a paste of standard consistency and the value was 28%. The mortar was mixed in standard manner and after thorough mixing the sample was placed in cube and compacted. Before completely filling the mortar in the cubes or before finishing, copper plates of 2 mm thick were inserted into the fresh mortar up to a depth of 20 mm, which form an artificial crack by which the healing can be monitored precisely. The specimens were demoulded after 24 hrs and kept for curing. Artificial induced cracks in demoulded cubes are shown in Figure 1.

After de-molding, the mortar cubes were subjected to curing in water for 21 day, and then the specimens were kept in freshly prepared bacterial solution for 48 hrs and 5 days in different nutrient solutions. The first 48 hours are the complete germination duration for bacillus sphaericus as per the standards provided by MTCC and a trial period of 5 days' immersion is extra supplement of nutrients in solution form was checked for its feasibility. And it's a trial period.

The nutrients suitability plays a major role in deciding the quantum of healing by bacteria which was studied by Tziviloglou *et al.* [19]. The research work by Bang *et al.* [14] has quoted the nutrients for solution A, B, C. The compositions used for the food source are as shown in table 3. The bacterially immersed cubes were immersed in these Nutrient solutions for a period of 5 days.

Figure 1: Artificially cracked specimen

Table 3: Composition of nutrient solutions

SOLUTION A	SOLUTION B	SOLUTION C
• Sodium gluconate [109 g/l] • Calcium nitrate [118 g/l] • Urea [20 g/l] • Yeast extract [1 g/l]	• Calcium chloride [50 g/l] • Urea [20 g/l] • Yeast extracts [1 g/l]	• Mono potassium phosphate [21.75 g/l] • Di potassium phosphate [8.5 g/l] • Sodium hydrogen phosphate [33.5 g/l] • Ammonium chloride [1.7 g/l]

3.3.2 *Tests on Hardened Properties*

100 mm mortar cubes were cast and cured for 21 days of water curing and 7days by bacterial immersion totally 28 days. Control specimens were continued to cure for 28 days in water.

Compression test was conducted using universal testing machine for the demoulded specimens. Control specimens were also cast and cured in water for 28 days and tested for the same parameters and results were analyzed. Ultrasonic pulse velocity test was conducted to analyze the micro structure of the bio-mortar by transmitting the ultrasonic pulse through it. From the test the resistance to the transmission of pulse waves was interpreted to be the cracks, air gaps, honey combing or the presence of micro pores. The specimen was subjected to curing for 28 days and was air dried. The specimens were cast and treated under the room temperature without any control environment to check their practical suitability. UPV reading was taken Prior to the cracking and later after cracking and was recorded. The bacterial concrete specimens were again subjected to observation after healing of cracks and the results were analyzed. The mortar specimens are so chosen for the entire study in order to study the performance of bacteria in high alkaline medium. The UPV results depicts the variations in micro seconds and it is liable as the activities of microorganisms in micro level to clog the micro cracks can be observed through the minor variations in UPV provided the test needs to be conducted with utmost care and sensitivity.

3.4 Crack Remediation by Injection Method

For the distress at the vertical face of the structure the immersion method may not be suitable because of not been able to pond the solution of healing agent on vertical cracked surface where injection method may be a suitable solution. In injection method the bacterial solution is injected through the micro cracks and will be sprayed by nutrient solution at regular interval to assure accelerated healing.

3.4.1 *Methodology*

The experimental program for injection was so chosen as to include crack remediation of a micro cracked concrete column in a college building and also for mortar cubes the cracks were induced by applying minimum load for distress using CTM. The micro cracked concrete column was marked and surface of the cracked column is roughly cleaned. Simultaneously the healer bacterial solution at the concentration of 10^6 cells/mL was prepared using colorimeter under the optical density test. The required optical density is 0.206 for 10^6 cells/mL. In continuation the nutrient required for bacteria Bacillus sphaericus is achieved by using Slope Formula, $y - y_0 = [(y_1 - y_0) / (x_1 - x_0)] * (x - x_0)$. By taking the bacterial Solution of 280 mL, concentration of 10^6 cells/mL was achieved by diluting the bacterial sample with nutrient broth as shown in Table 4.

In table 4 the bacterial solution by one part[x] is diluted with nutrient broth of one part hence the bacterial dilution ratio in the total solution is 0.5. In next iteration the sample is diluted further by adding 2 parts of nutrient broth and the dilution ratio of bacteria obtained is 0.25. Similarly, by continuing the iterations up to 16 parts of nutrient broth to one part of bacteria it has arrived at bacterial dilution ratio of 0.03125. The bacterial ratio required for attaining 10^6 cells/mL count is 0.0381 by optical density test. Hence the interpolation between the nutrient broth values [y] and the bacterial dilution ratio arrives at bacteria: Nutrient broth = 1: 14.25, which is by adding 14.25 parts of nutrient broth for one part of bacterial solution it is arrived at 10^6 cells/mL.

Calcium lactate being an additional precursor compound accelerates the $CaCo_3$ precipitation. It is taken with the concentration of 70 g for 1 liter solution. The required amount of calcium lactate is added to the bacteria and the solution is mixed uniformly.

3.4.2 *Hardened Property Tests*

In this method of remediation the healer injected mortar specimen was subjected to ultrasonic pulse velocity test an ultrasonic pulse velocity test is an in-situ, non-destructive test to check the quality of concrete and natural rocks. In this test,

Table 4: Correlation table for dilution of nutrient broth to achieve the required cell count of bacteria

BACTERIA	NUTRIENT BROTH [y]	DILUTION RATIO [x]	OPTICAL DENSITY
1	1	0.5	
1	2	0.25	
1	4	0.125	
1	8 [y0]	0.0625 [x0]	x = 0.0381
1	16 [y1]	0.03125 [x1]	

the strength and quality of concrete is assessed by measuring the velocity of an ultrasonic pulse passing through a concrete structure. UPV test on bio concrete is to study the variation in velocity of ultrasonic waves influenced by densification of microstructure by calcite precipitation. The healing of cracks was examined at 7, 14 and 21 days by digital microscope at 2 locations of crack. The morphology of the microstructure after bacterial injection was studied under scanning electron microscopy to locate the calcite precipitation. The SEM image are procured under the magnification of 10 kX.

4. RESULTS AND DISCUSSION

4.1 Experimental Observations

Initially characteristic study of bacteria was carried out to study its viability, i.e., whether it is in active or inactive state to process and whether Gram positive and rod-shaped cells which so as to indicate it has a thick cell wall which protects the bacteria in alkaline environment in dormant state. Results have shown that the bacterium are viable, Gram positive and has rod shaped cells. Calcium carbonate estimation which was performed before the application of bacteria into mortar specimens depicts the ability of bacteria to produce calcium carbonate in controlled environment and the results were promising by the day 6, 4.7g/L of calcium carbonate was precipitated by the bacteria. The selected bacteria *Bacillus sphaericus* will go to dormant State during high alkaline environment and get activate again at suitable environment by getting the supply of air, moisture and less alkalinity. In this test, positive results were found as the bacteria went in dormant state in sodium hydroxide solution and tablet solution and got activated back when subjected in nutrient media solutions by the survival test.

4.2 Remediation by Immersion Method

4.2.1 *Compressive Strength Test*

The test was conducted on bacterially treated and untreated cubes along with control cubes. The orientation of artificial crack is maintained to be perpendicular to the testing load. Figure 2 shows the results of compressive strength of cubes for solution A, B and C along with bacteria from which it may be observed that there is an increase in compressive strength in all the three nutrient sources and a slight decrease in bacterially treated cubes without nutrients when compared with control specimen. This may be because of the bacteria after being deactivated due to non-availability of nutrients for germination and calcite precipitation. This may act as an organic mass and create a minute weak zone which may affect the compressive strength of mortar cube. This decrement in compressive strength may be balanced when adopted for different grades of concrete by immobilization of bacteria by encapsulation technique, since it is deemed to have avoided the bacteria from creating a possible weak zone as an organic mass after deactivation. When

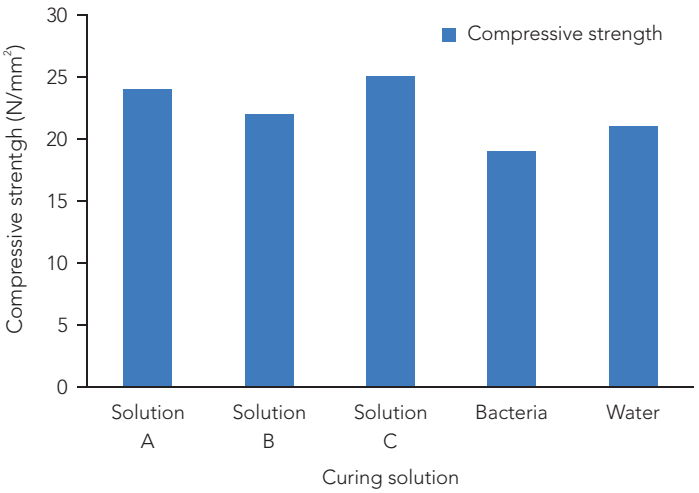

Figure 2: Graph depicting compressive strength v/s different nutrient medium

compared for compressive strength between different nutrient sources, cubes from Solution A and Solution C performed better than cubes from Solution B. The increase in compression strength when compared with control specimen is directly due to precipitation of calcite into the micro pores of the cube. The smaller variation in enhancing compressive strength paves the way for need of self-encapsulation of bacteria to perform with completely and effectively in self-healing and compressive strength enhancement. And also, the addition of bacteria to promote self-healing without compromising the compressive strength is the main objective of the study.

4.3.2 *UPV Test*

The bacterial and nutrient source treatment results in calcium carbonate precipitate on the surface as well as in the crack. The UPV test conducted showed an increase in velocity in all the bacteria with nutrient treated specimens indirectly indicating the precipitation of calcium carbonate. The UPV test was conducted on the 28 days' water cured cubes, and then the cubes were kept for bacterial treatment for 7 days along with Solution A, Solution B and Solution C defined as A + Bacteria, B + Bacteria and C + Bacteria. It was checked for calcite precipitation and healing.

The performance of cubes dipped in bacteria and phosphate buffer solutions indicate ultrasonic pulse velocity of waves as 4304.8 m/s which is greater value compared to other food sources as shown in Table 5. The minute variations in UPV indicate the variations in microstructure of concrete which plays crucial role in inhibiting micro crack propagation.

Table 5 containing zero values for A, B, C indicates that there is no role of nutrients in enhancing the UPV and compressive strength without the catalyzation of bacteria. Since it is significant to highlight the crucial role of bacteria in in performance enhancement these representations are made.

Table 5: UPV results on bio concrete specimen

SOLUTIONS	VELOCITY BEFORE	VELOCITY AFTER	% INCREASE	AVG % INCREASE
A + BACTERIA	3879.12	3944.13	1.676	2.395
	3836.96	3944.13	2.793	
	3735.45	3836.96	2.717	
B+ BACTERIA	4057.47	4107.47	1.232	1.718
	4057.47	4177.51	2.958	
	3944.13	3982.13	0.963	
C+ BACTERIA	4177.51	4304.88	3.049	2.655
	4304.88	4440.25	3.145	
	4177.51	4251.51	1.771	
BACT	4304.88	4304.88	0.000	0.000
	3944.13	3944.13	0.000	
	4304.88	4304.88	0.000	
WATER	4177.51	4177.51	0.000	1.558
	4304.88	4304.88	0.000	
	3151.79	3299.07	4.673	
A	3944.13	3944.13	0.000	0.000
B	3735.45	3735.45	0.000	0.000
C	4304.88	4304.88	0.000	0.000

4.3 Remediation by Injection Method

4.3.1 *Ultrasonic Pulse Velocity Test*

The test was conducted on mortar specimens of 100 mm size cast and cured for 28 days. The specimens were artificially cracked by applying a low rate of compressive loading. The cracks were injected with bio healer solution and kept under observation up to 21 days. The test set up for UPV was made and experimented.

The results of the UPV test shown in the graph plotted in Figure 3 convince that the mortar specimens subjected to UPV test at the before cracking stage takes less time of travel for ultrasonic pulse waves to pass through it because of the material continuity. At the after-cracking stage, it is observed that the time of travel has got increased due to the discontinuity of material by cracks. But the significant observation noticed is at healing stage where the bacterial activity has promoted the recovery of this cracked zone and again bridges the discontinuity to an extent that the time of travel of Ultrasonic pulse waves has come back to the values of before cracking stage. The increasing rate of time of travel of ultrasonic pulse indicates the densified micro structure by the calcite deposition through bacterial mediation. This clearly convinces that the role of bacteria is significant in the recovery of distress in concrete structures.

4.3.2 *Healing Observation*

The same specimens which were tested for UPV were also examined for crack healing using digital microscope. These mortar specimens injected with Bacillus sphaericus and were examined for a period of 3 weeks at 7 days' interval for assessing the rate of healing of cracks. The healing observation is carried out using 5X magnification digital microscope and the healing images after bacterial treatment are as shown in Figure 4

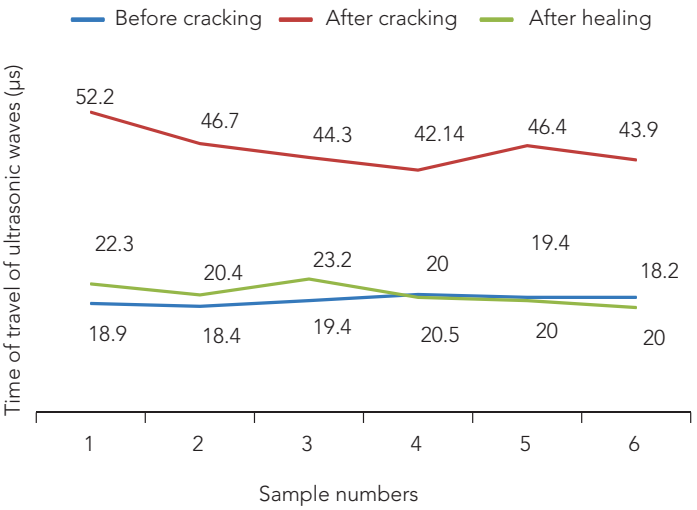

Figure 3: Crack healing observations by UPV test

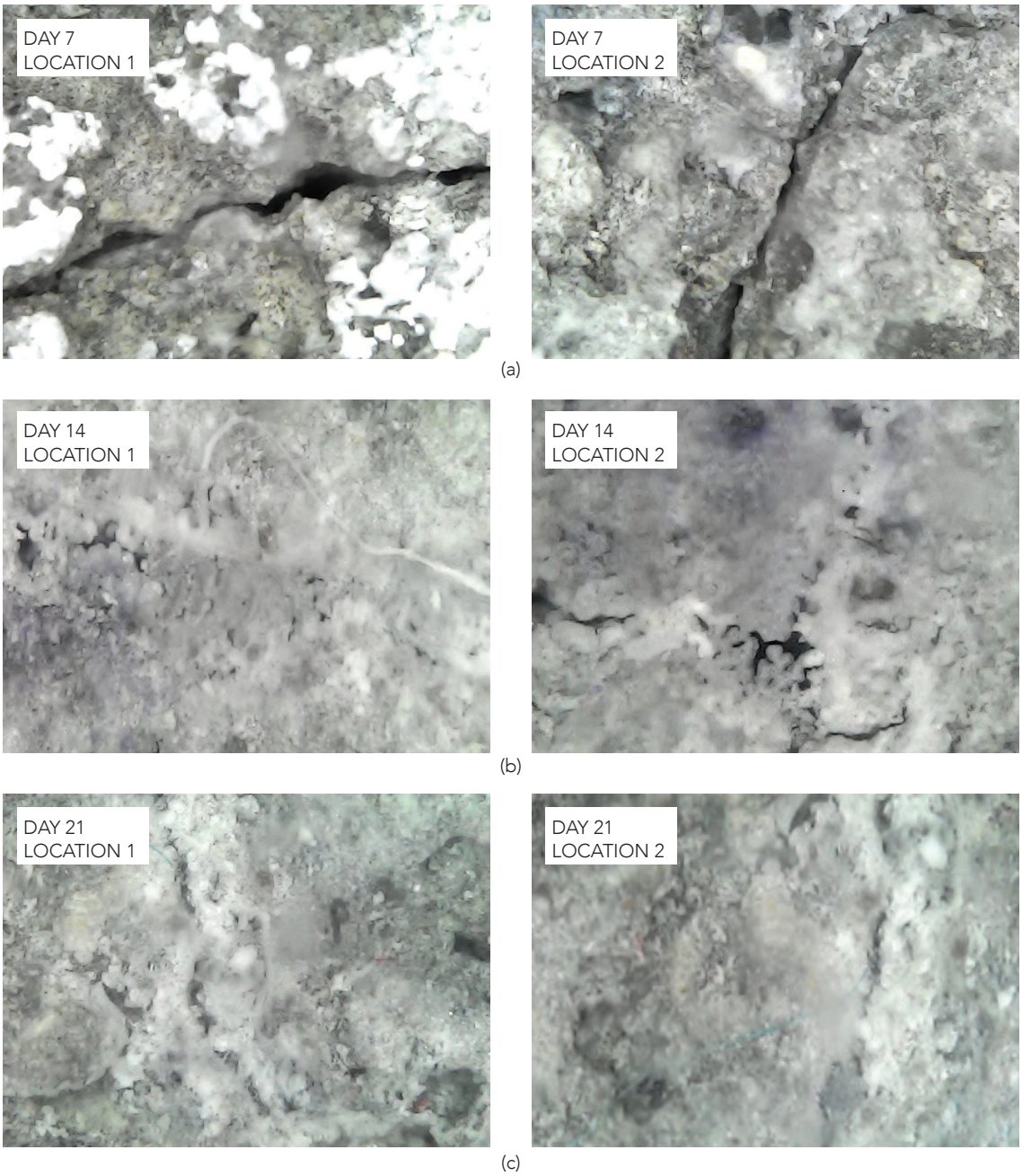

Figure 4: Healing observations at different intervals

The healing observations from Figure 4[a] show that at 7th day the activation of bacteria and germination has taken place. In continuity the precipitation of calcite crystals which possess the property of adhering to the internal cracked surface. This continuous deposition initiates the crack healing as observed by white patches in and around the crack.

In continuity at 14th day as shown in Figure 4[b] a thin layer of calcite crystal deposition is observed which depicts the continuity of precipitation promoting bridging of the crack. At 21st day as shown in Figure 4[c] the healing is observed by thick deposition of calcite in and around the cracks indicating the complete and compact healing of cracks. Healing observed was quicker, proving the role of catalyst activity of bacteria in bio deposition of stable calcite. *Bacillus sphaericus* proved better in achieving strength and also has faster healing ability which is indicated by fastest closure of crack injected with it.

4.3.3 *Scanning Electron Microscopy*

The SEM analysis of the cement mortar cubes with bacteria *Bacillus sphaericus* with nutrients depicts the abundance of calcite crystals deposition and in turn states the role of calcite in restoring the voids and cracks in the mortar specimen. This is evident in the scanning electron micrograph pictures as shown in Figure 8 where the marked area highlights the stable calcite precipitation by bacteria.

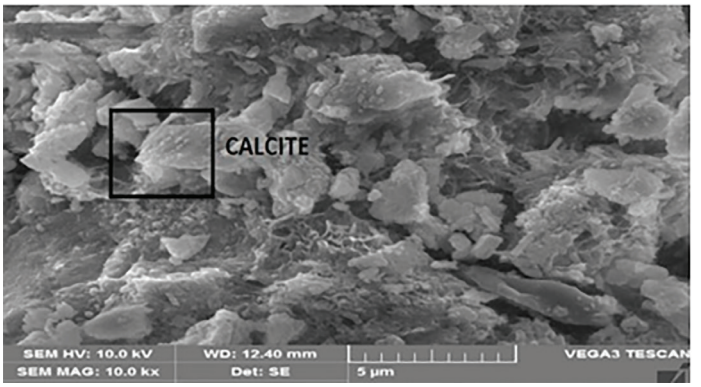

Figure 5: SEM of specimen (Immersed in food solution and Bacillus sphaericus bacterial solution together) after 28 days of curing and the calcite precipitation at 28 days

5. CONCLUDING REMARKS

This study has given an idea that the bacterially induced calcite precipitation [BICP] is effective in clogging the minor crack and improving the internal micro structure of the mortar thereby enhancing the strength properties.

The study on compressive strength enhancement through experimentation on bacterial concrete by immersion method indicates the marginal increase in compressive strength of mortar cubes with the optimized combination of bacteria, *Bacillus sphaericus* and nutrient, phosphate buffer solution. Here the role of nutrient medium in quantum of calcite precipitation through bacterial mediation has also been explored, which directly influences the compressive strength and crack healing capacity of bacteria.

The study on ultrasonic pulse velocity through the mortar medium treated with immersion into the Bacillus sphaericus bacteria and nutrient phosphate buffer solution clearly indicates effective crack remediation by immersion method. The method is simple and has practical significance especially in case of horizontal concrete members.

Similarly, the study on ultrasonic pulse velocity and microscopic kinetic observations clearly demonstrates the usefulness of injection method. The injection method can be advantageously used for vertical distressed members. Additionally, the solution combination of bacteria with nutrient medium acts as a bio healer spray which can be instantly applied on micro cracks of any concrete structures especially water retaining structures for their rejuvenation and restoration.

ACKNOWLEDGMENT

The authors wish to thank the management for extending the support during the research work and also appreciate and place on record the support given by concrete laboratory technical head and UG & PG students while carrying out the experimental work.

REFERENCES

[1] Erik Schlangen, Senot Sangadji. (2013). "Addressing infrastructure durability and sustainability by self-healing mechanisms - Recent advances in self-healing concrete and asphalt", Proceedings of the 2nd International Conference on Rehabilitation and Maintenance in Civil Engineering, 2013, Vol 54, pp 39-57. doi: 10.1016/j.proeng.2013.03.005

[2] Carola Edvardsen. (1999). "Water permeability and autogenous healing of cracks in concrete", ACI Materials journal, 96-M56, pp. 448-454.

[3] Seshagiri Rao. M. V, Srinivasa Reddy. V, M. Hafsa, Veena. P and Anusha. P. (2013). "Bioengineered concrete - A sustainable self-healing construction material", Research Journal of Engineering sciences, Vol. 2, No. 6, pp. 45-51.

[4] Victor C, Emily Herbert. (2012). "Robust self-healing concrete for sustainable infrastructure", Journal of advanced concrete technology, Vol 10, pp. 207-218. doi:10.3151/jact.10.207.

[5] Richard P. Wool. (2008). "Self-healing materials: a review", Soft Matter, Vol 4, pp. 400-418. doi: 10.1039/b711716g.

[6] Tae-Ho Ahnand Toshiharu Kishi. (2010). "Crack self-healing behaviour of cementitious composites incorporating various mineral admixtures", Journal of Advanced Concrete Technology, Japan Concrete Institute, Vol. 8, No. 2, pp. 171-186.

[7] Sierra Beltran. M. G and Jonkers. H. M. (2015). "Crack self-healing technology based on bacteria", Journal of Ceramic Processing Research, Vol. 16, pp. 33-39.

[8] Eirini Tziviloglou, Zichao Pan, Henk M Jonkers. Erik Schlangen. (2017). "Bio based self- healing mortar: an experimental and numerical study", Journal of Advanced Concrete Technology, Vol 15, pp. 536-543.

[9] Wiktor. V, Jonkers H. M, (2015). "Field performance of bacteria-based repair system: Pilot study in a parking garage", Case Studies in Construction Materials, Vol 2, pp.11–17. http://dx.doi.org/10.1016/j.cscm.2014.12.004

[10] Henk M. Jonkers and Erik Schlangen. (2009). "A two component bacteria-based self-healing concrete", Concrete Repair, Rehabilitation and Retrofitting II, pp. 215-220.

[11] IS: 12269. (2013). "Ordinary Portland cement, 53 Grade-Specifications", New Delhi (India): Bureau of Indian Standards.

[12] Senot Sangadji, Virginie Wiktor, Henk Jonkers, Erik Schlangen. (2016). "The use of alkaliphilic bacteria- based repair solution for porous network concrete healing

mechanism", Sustainable Civil Engineering Structures and Construction Materials, Procedia engineering, Elsevier, Vol 171, pp 606-613. doi: 10.1016/j.proeng.2017.01.387.

[13] Ravindranatha Rao, Udaya Kumar, Suhas Vokunnaya, Priyodip Paul, Ioannou Orestis. (2015). "Effect of *Bacillus flexus* in healing concrete structures", International Journal of Innovative Research in Science, Engineering and Technology, Vol. 4, No 8. pp. 7273-7280. doi:10.15680/IJIRSET.2015.0408106.

[14] Sookie S Bang, Johnna K, Galinat, V Ramakrishnan. (2001). "Calcite precipitation induced by polyurethane-immobilized *Bacillus pasteurii*", Enzyme and microbial technology, Vol 28, pp. 401-409.

[15] Ghosh, P. and Mandal. S. (2006). "Development of bio concrete material using an enrichment culture of novel thermophilic anaerobic bacteria", Indian Journal of Experimental Biology, Vol. 44, pp. 336-339.

[16] Santhosh, K., Ramachandran, V., Ramakrishnan, Sookle S Bang. (2001). "Remediation of concrete using Micro-Organisms", ACI Materials Journal, pp 3-9.

[17] Rajshekhar Rao. (2014). "Biomimicry in architecture", International Journal of Advanced Research in Civil, Structural, Environmental and Infrastructure Engineering and Developing, Vol 1, No. 3. pp. 101-107.

[18] Renee, M., Mors and Henk M. Jonkers. (2012). "Bacteria-based self-healing concrete – Introduction", Proceedings of 2nd International Conference on Micro structural-related Durability of Cementitious Composites, April 2012, The Netherlands, Amsterdam. pp. 1626-1633.

[19] Eirini Tziviloglou, Virginie Wiktor, Henk M Jonkers, Erik Schlangen. (2017). "Selection of nutrient used in biogenic healing agent for cementitious materials", Frontiers in materials, Vol 4. pp. 1-7. doi: 10.3389/fmats.2017.00015.

S. GIRISH has 34 years of experience in teaching, consultancy and research and is presently working as Professor in the Department of Civil Engineering, B.M.S. College of Engineering, Bangalore, India. He has worked on self- compacting concrete for his doctoral work and has published research papers in various National and International journals and conferences. He has presented papers abroad several times notably in RILEM Conferences in Ghent, Belgium (SCC 2007), Montreal, Canada (SCC 2010) and Paris, France (SCC 2013). He was the recipient of State Academic award from Karnataka State Council for Science and Technology for the best project in the year 2009, 2011, 2013 and 2015 and Institutional level award for innovative project in the year 2017and 2019. His research interests include self-compacting concrete, rheology of concrete, recycling of concrete waste, bacterial concrete, pervious concrete, self-healing concrete and geo-polymer concrete. Email: girish.civ@bmsce.ac.in

T. SOUMYA is a research scholar in the Department of Civil Engineering, B.M.S. College of Engineering, Bangalore, India. She is working in the area of bacterial concrete for her doctorate work. She has worked on self-sensing concrete for structural health monitoring and dynamic behavior of concrete structures and has published many papers. Her research interests are self-healing concrete, structural health monitoring, self-sensing concrete and foam concrete. Email: Soumya.civ@bmsce.ac.in

ANANYA GIRISH is presently working as house Surgeon at MVJ Medical College and Research Hospital, Bangalore. She has keen interest in research work and is currently working on five projects. The prestigious Indian Council of Medical Research (ICMR), Rajiv Gandhi University of Health Sciences and other agencies have recognized her work. She has participated in many activities at state level and national level and won awards in paper presentations and quizzes. Her areas of interest include public health and education, mental health to name a few and also on inter disciplinary research area like bacterial concrete. Email: anigirish24@gmail.com

Cite this article: Girish, S., Soumya, T., and Girish, A. (2021). "An experimental study on bio-composites by the methods of bacterial immersion and injection", *The Indian Concrete Journal*, Vol. 95, No. 7, pp. 31-40.

STUDIES ON *P-M* INTERACTION CURVES FOR UNIAXIAL BENDING OF HIGH STRENGTH CONCRETE RECTANGULAR SECTIONS

P. S. RAO,
M. N. SHARIFF*,
N. HARSHA

Abstract

High-strength concretes (of grades higher than M55) are now commonly used in the construction of high-rise buildings, industrial structures and long span bridges. However, IS: 456 (2000) restricts the applicability of the concrete design parameters given in the code only to concretes of grades up to M55. The IRC: 112 (2019) (also its 2011 version) and EN 1992 - 1 - 1 : 2004 + A1 : 2014 give grade-specific design parameters for concrete grades between M65 and M90 or M110. Expressions necessary for evaluating the *P-M* interaction curves have been developed in this paper using concrete stress block parameters given in IRC: 112 (2019) for high strength concretes. Results obtained for two numerical examples using the expressions derived have been presented. Closed form expressions proposed by the authors for the magnitude and line of action of the concrete compressive force, as per IRC: 112 guidelines, when the neutral axis lies outside the cross-section should enable the designers to develop their own design charts for uniaxial bending of rectangular sections.

Keywords: High-strength concrete, Interaction curve, Stress block.

1. INTRODUCTION

The inherent advantages of high-strength concrete (greater than M55 grade) make it a preferred choice in many critical structures such as tall buildings, industrial structures and bridges. However, IS: 456 (2000) [1] states in a footnote in Table 2 that "*for concretes of compressive strength greater than M55, design parameters given in the standard may not be applicable and the values may be obtained from specialised literature and experimental results*". The design concrete stress-block specified in IS: 456 (2000) [1] for design of uni-axial bending of cross-sections is the same as that in IS: 456 (1978) [2]. The design stress-block given in IS: 456 (1978) was itself adopted from the by then available codal specifications in early 1970s [3-5] of several European countries. With the formation of the European Union the same recommendations were continued in the successive Eurocodes issued starting from early 1990s [6-8]. These recommendations contained in all these various codes were based on extensive laboratory investigations [9,10] carried out in 1950s and 60s. It was quite well documented that these tests were carried out on specimens made of concrete of grades ranging between M20 and M55. This was the reason for inserting the cautionary footnote in IS: 456 (2000) mentioned above.

In the absence of data from IS: 456 (2000), designers preferring to use concretes of grades higher than M55 are required to look for other sources of information. The Eurocode EN 1992-1-1:2004 [6] is one of the earliest International codes to have explicitly specified design parameters for structural concrete of grades between M65 and M105, while retaining the old concrete stress-block parameters for concretes up to M60 grade. The IRC: 112 (2011) [11] is the first Indian code to have specified design parameters for concrete strengths between M65 and M90 and its recommendations are very much the same as those of the Eurocode. The latest revisions of the Eurocode EN 1992-1-1: 2004 + A1 : 2014 [8] and the IRC Code IRC: 112 (2019) [12] retain the same recommendations as in their earlier versions.

While the original source for the recommendations made in all the codes mentioned above for grades of concrete up to M60 could be clearly identified as [9] and [10], the authors were not able to lay their hands on the original source from which the recommendations contained in the codes for high strength concretes were drawn. But as they have become part of Nationally and Internationally accepted codes of practice, it is justified to assume that these recommendations have been made after thorough investigations on the topic.

Although the relevant specifications for high strength concretes are available in the codes mentioned above, the authors have not come across any literature so far giving design aids based on these specifications in Indian codes. Therefore the authors have taken up the task of developing a methodology for obtaining load-moment (*P-M*) interaction diagrams for rectangular RC sections using properties specified in IRC: 112 (2019) for higher concrete strengths. The results are presented in this paper.

*Corresponding author : M. N. Shariff, Email: mnshariff@alumni.iitm.ac.in

For designers accustomed to using design charts presented in SP 16 [13] based on the old IS: 456 (1978) [also valid for IS: 456 (2000)] specifications, it will be of considerable academic interest to know the magnitude of difference in the load carrying capacities of rectangular sections evaluated using the grade-independent concrete stress block given in IS: 456 (2000) and using the grade -dependent parameters given in IRC: 112 (2019). Therefore, results of such a comparative study on two numerical examples have also been presented in this paper.

2. DESIGN PROPERTIES FOR HIGH STRENGTH CONCRETES AS PER IRC: 112 (2019)

The necessary design data have been presented in the Code in the form of a Table [refer Table 6.5 of IRC: 112 (2019)] and also in the form of expressions which are functions of the characteristic cube strength (f_{ck}) of concrete. Figure 1 shows the schematic shape of the design stress block and the expressions for the important values are reproduced below:

$$\sigma_c = f_{cd}\left[1-\left(1-\frac{\varepsilon_c}{\varepsilon_{c2}}\right)^n\right] \text{ for } 0 \le \varepsilon_c \le \varepsilon_{c2}; \quad (1a)$$

$$\sigma_c = f_{cd} \text{ for } \varepsilon_{c2} \le \varepsilon_c \le \varepsilon_{cu2} \quad (1b)$$

where, ε_c is the strain in concrete, ε_{c2} is the strain corresponding to attainment of peak stress, ε_{cu2} is the ultimate strain in concrete (see Figure 1) and n is an empirically determined power term. The concrete design stress f_{cd}, indicated in Figure 1 can be estimated as $\alpha f_{ck}/\gamma$, where $\alpha = 0.67$ is the reduction factor which accounts for the reduction in concrete strength due to sustained load effects, size effects and also for the cube to cylinder strength conversion, and $\gamma = 1.5$ is the material safety factor. The expressions for ε_{c2}, ε_{cu2} and n (for $f_{ck} > 60$ MPa) are provided below.

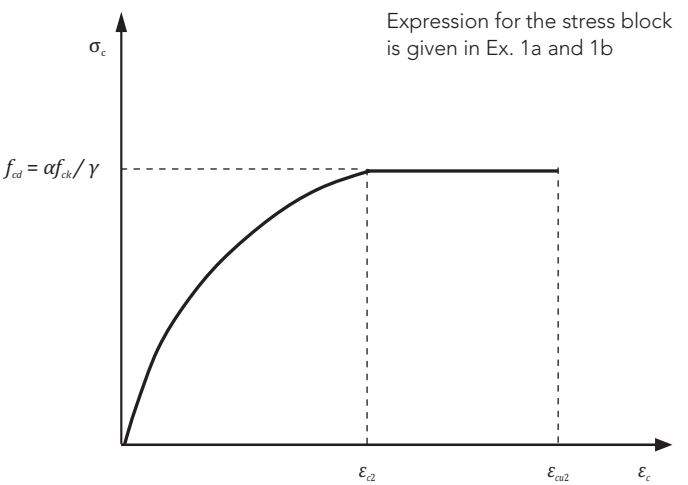

Figure 1: A schematic representation of the design stress-strain curve of concrete [12] with reduction factor α

$$\varepsilon_{c2}\,(^0/_{00}) = 2.0 + 0.085\,(0.8 f_{ck} - 50)^{0.53} \quad (2)$$

$$\varepsilon_{cu2}\,(^0/_{00}) = 2.6 + 35\left(\frac{90 - 0.8 f_{ck}}{100}\right)^4 \quad (3)$$

$$n = 1.4 + 23.4\left(\frac{90 - 0.8 f_{ck}}{100}\right)^4 \quad (4)$$

Since the Expressions 2, 3 and 4 are dimension bound, empirical relation, the value of f_{ck} in these Expressions has to be in MPa.

The design parameters for concrete with $f_{ck} \le 60$ MPa are to be taken as already given in the existing IS: 456 (2000). The stress-strain curves as suggested above for HSC (60 MPa – 90 MPa), without any reduction factors are plotted in Figure 2. Increases in the strain corresponding to peak stress and a reduction in ductility with increase in concrete strength are clearly demonstrated for concrete grade ranging from 60 MPa to 90 MPa.

3. EXPRESSIONS NEEDED FOR EVALUATING *P-M* INTERACTION CURVES FOR RECTANGULAR SECTIONS

The expressions to evaluate the load and moment values using IS: 456 (2000) are well known [13]. On the same lines generic expressions to evaluate the stress-block parameters for HSC using IRC: 112 (2019) are presented here. A schematic cross-section of a rectangular column having two layers of steel is shown in Figure 3.

At this stage it is also to be noted that the stress-block shown in Figure 1 for concrete compression zone is valid only for cases where the neutral axis lies within the cross-section. For cases where the neutral axis lies outside the section (see Figure 4), the stresses in concrete on both sides of the cross-section are compressive in nature. For such cases the failure strain ε_{u2} on the most compressed side is less than ε_{cu2} and is a function of the

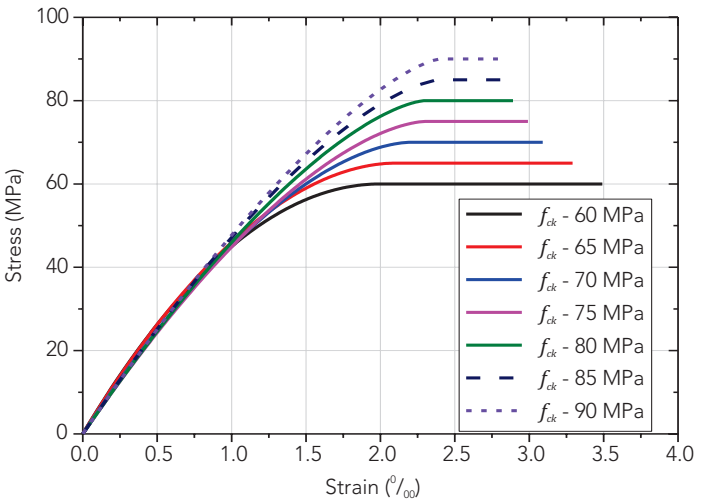

Figure 2: Stress-strain curves of high-strength concrete (without any reduction factors)

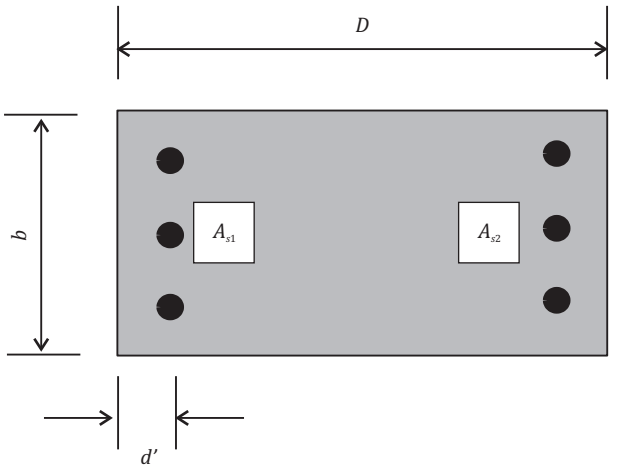

Figure 3: Cross-section of the column considered for the evaluation of P-M expressions

eccentricity of the load with the failure strain reaching a value of ε_{u2} uniform over the entire cross-section for the case of load with zero eccentricity (axial load). Furthermore there is a definite relationship between the strain ε_{u2} on the most compressed side and the strain ε_{u1} on the least compressed side at the time of failure under eccentric loading. The stipulation in the currently valid IS: 456 (2000) states the relationship as

$$\varepsilon_{u2} = (\varepsilon_{cu2} - 0.75\,\varepsilon_{u1}) \quad (5)$$

where ε_{u2} is the strain at the highly compressed edge, when the neutral axis lies outside the cross-section and ε_{u1} is the strain at the other face of the cross-section.

This recommendation is based on the experimental results reported in the literature [9, 10]. This can be shown to be mathematically equivalent to assuming that the strain distribution across the cross-section pivots on a point which is at a depth 3*D*/7 from the most compressed side.

Similar to the relationship (Expression 5) given above, the new recommendations given in EN 1992-1-1: 2004 + A1 : 2014 and also IRC: 112 (2019) give a relationship between ε_{u2} and ε_{u1} at the time of failure as the relationship that would be obtained by assuming the resultant strain diagram across the depth *D* to be pivoting about a point which is at a distance $\left(1-\frac{\varepsilon_{c2}}{\varepsilon_{cu2}}\right)D$ from the highly compressed edge. The recommendation is shown graphically in Figure 4.

In this connection it needs to be pointed out that for carrying out the calculations for the cases when the neutral axis lies outside the section, it is necessary to have an estimate of the load and the line of action of the load represented by the concrete stress block bounded by the mutually correlated values of ε_{u2} and ε_{u1}. Closed form expressions for these quantities for the parameters given in IRC: 112 (2019) are given below.

Considering the distance between the least compressed edge and the pivot as *y* (see Figure 4), and using the concept of similar triangles, we can calculate the value of *y* in terms of the strain at peak stress ε_{c2} and ultimate strain in concrete ε_{cu2} as:

$$y = D\left(\frac{\varepsilon_{c2}}{\varepsilon_{cu2}}\right) \quad (6)$$

The strain in the highly compressed edge ε_{u2} can be now determined as:

$$\varepsilon_{u2} = \varepsilon_{c2}\left(1 + \frac{D-y}{x_u - (D-y)}\right) \quad (7)$$

Similarly, the strain in the least compressed edge ε_{u1} can be determined as:

$$\varepsilon_{u1} = \varepsilon_{u2}\left(1 + \frac{x_u - D}{x_u}\right) \quad (8)$$

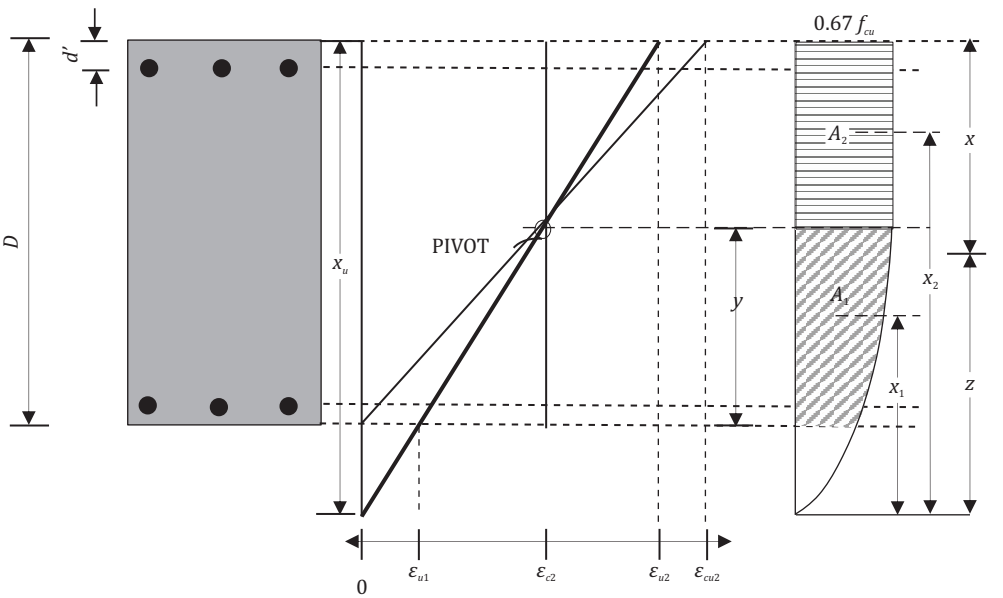

Figure 4: Stress block when neutral axis lies outside the cross-section

The expression of the stress block when $\varepsilon_c < \varepsilon_{c2}$ is given in Expression 1a.

The difference in the peak stress ($0.447f_{ck}$) and the concrete stress at least compressed edge can be calculated using Expression 9, which is the difference between Expressions 1a and 1b.

$$\Delta f = 0.447 f_{ck}\left(1 - \frac{\varepsilon_{u1}}{\varepsilon_{c2}}\right)^n \quad (9)$$

Writing ε_{u1} and ε_{c2} in terms of x_u and y using similar triangles, and substituting in Expression 9, we get

$$\Delta f = 0.447 f_{ck}\delta \quad (10)$$

where,

$$\delta = \left(\frac{y}{x_u - (D-y)}\right)^n \quad (11)$$

To find the area of the stress block, we integrate the stress-strain curve from ε_{u1} to ε_{u2}

$$A_c = \left[\int_{\varepsilon_{u1}}^{\varepsilon_{c2}} \sigma_{c1}\, d\varepsilon + \int_{\varepsilon_{c2}}^{\varepsilon_{u2}} \sigma_{c2}\, d\varepsilon\right]\frac{x_u}{\varepsilon_{u2}} \quad (12)$$

On solving and converting the strains in terms of geometrical cross-section parameters we get the area of the stress block as,

$$A_c = 0.447\, f_{ck}\, D\left(1 - \frac{\delta y}{(n+1)\,\mathrm{D}}\right) \quad (13)$$

In order to calculate the distance z between the centroid of the stress block and the neutral axis, the following formula is invoked:

$$Z = \frac{A_1 x_1 + A_2 x_2}{A_1 + A_2} \quad (14)$$

where, A_1 is the area of the stress block within the cross-section from ε_{u1} to ε_{c2} and A_2 is the area of stress block of the remaining cross-section from ε_{c2} to ε_{u2}

The expressions for x_1 and x_2 can be written as:

$$x_1 = \frac{\int_{\varepsilon_{u1}}^{\varepsilon_{c2}} \sigma_{c1}\varepsilon d\varepsilon}{\int_{\varepsilon_{u1}}^{\varepsilon_{c2}} \sigma_{c1} d\varepsilon}\left(\frac{x_u}{\varepsilon_{u2}}\right) \quad (15)$$

$$x_2 = \frac{\varepsilon_{c2} + \varepsilon_{u2}}{2}\left(1 - \frac{x_u}{\varepsilon_{u2}}\right) \quad (16)$$

Substituting Expressions 15 and 16 in 14, we get

$$z = \frac{\frac{(\varepsilon_{u2}+\varepsilon_{u1})(\varepsilon_{u2}-\varepsilon_{u1})}{2} - (\varepsilon_{c2}-\varepsilon_{u1})\frac{\delta(\varepsilon_{c2}+(n+1)\varepsilon_{u1})}{(n+1)(n+2)}}{(\varepsilon_{u2}-\varepsilon_{u1}) - \frac{\delta}{n+1}(\varepsilon_{c2}-\varepsilon_{u1})}\,\frac{x_u}{\varepsilon_{u2}} \quad (17)$$

The centroidal distance from the highly compressed edge is

$$\bar{x} = x_u - z \quad (18)$$

The load (P) can be calculated by applying force equilibrium by summing up the forces in concrete and steel. The force in the concrete can be evaluated using the expressions given above. The effective concrete area under compression is multiplied with the stress corresponding to the strain for the given eccentricity to evaluate the force in concrete. The contributions for steel (A_{s1} and A_{s2}) can be evaluated from the knowledge of corresponding strain at the location of the steel and the area of the steel provided. The moment (M) can be calculated by taking the moment of forces acting about the centroidal axis of the cross-section. The procedure for setting up the full range of a *P-M* interaction curve for a given section consists of, as given in several text books and also in SP 16 [13], choosing a number of pairs of mutually correlated strains ε_{u1} and ε_{u2} and evaluating the P and M values for each chosen pair. This procedure can also be extended to sections having reinforcement on all four sides or any other arbitrary reinforcement arrangement.

4. NUMERICAL EXAMPLES OF *P-M* INTERACTION CURVES FOR HSC RECTANGULAR SECTIONS WITH EQUAL REINFORCEMENT ON TWO SIDES

In order to carry out a comparative study of the sectional capacities derived from different stress blocks, a computer programme in MATLAB has been developed for generating non-dimensional *P-M* interaction curves for rectangular sections using the new design stress-strain curves [from IRC: 119 (2019)] as well as the existing stress-strain curve [from IS: 456 (2000)]. The schematic dimensions of the cross-section investigated in the numerical examples are shown in Figure 5. A material safety factor for steel of 1.15 and modulus of elasticity (E_s) of 2×10^5 MPa has been assumed. Steel having yield strength of 500 MPa has been considered for the analysis and it is assumed that the steel stress remains constant (at yield stress) for all strains beyond the yield strain.

The procedure discussed above has been used to develop non-dimensional *P-M* curves for the given cross-section with two different reinforcement percentages (with A_s/bD = 2% and 4%) with three different concrete groups: HSC 1 – M65, 67.5 and 70; HSC 2 – M75, 77.5 and 80; HSC 3 – M85, 87.5 and 90.

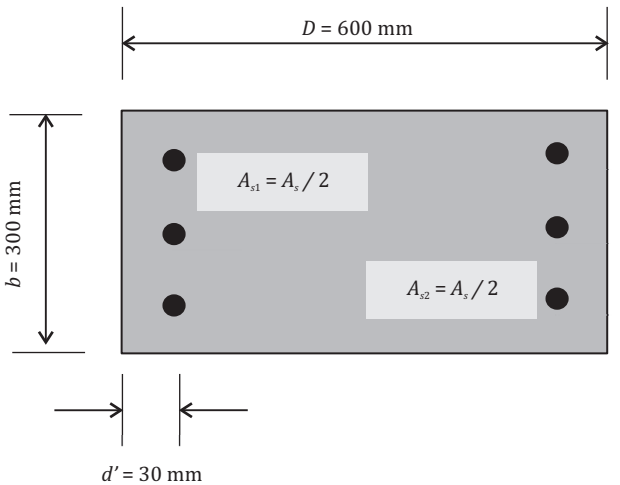

Figure 5: Cross-section of the column considered for the parametric study

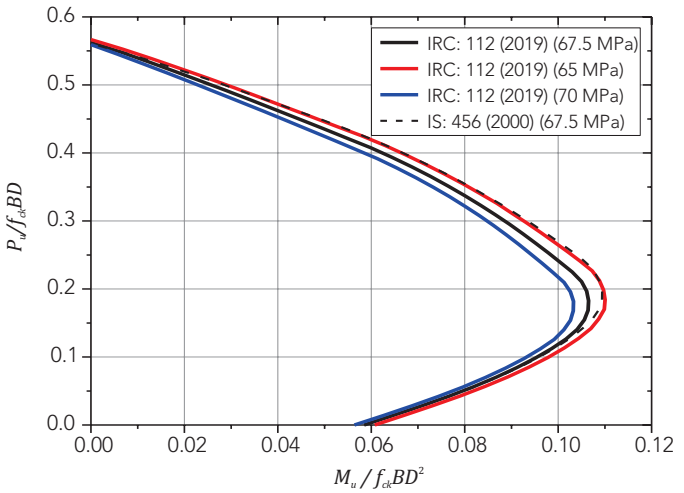

Figure 6: Comparison for *P-M* interaction curves for Group HSC-1 (2% reinforcement)

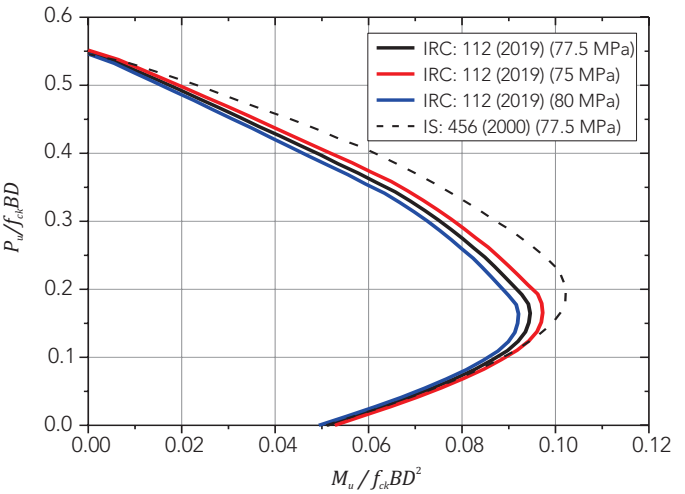

Figure 7: Comparison for *P-M* interaction curves for Group HSC-2 (2% reinforcement)

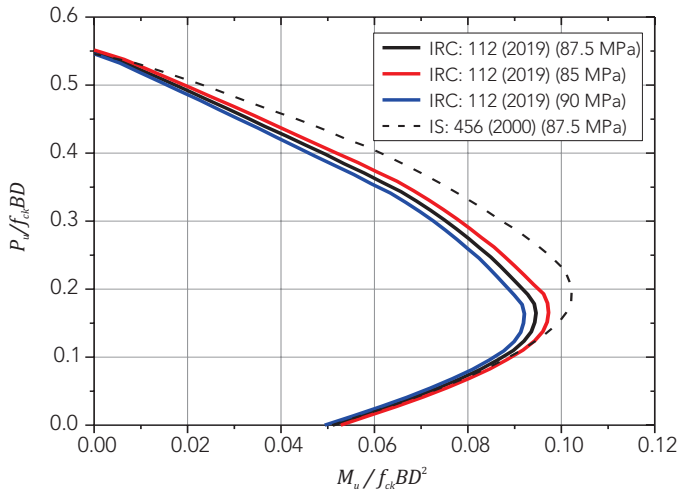

Figure 8: Comparison for *P-M* interaction curves for Group HSC-3 (2% reinforcement)

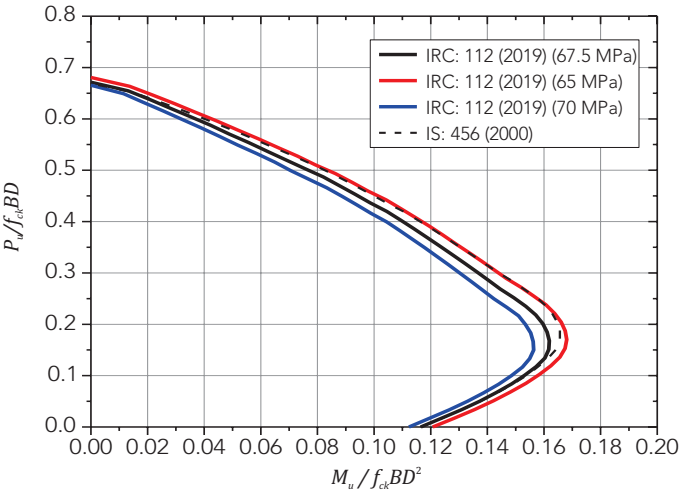

Figure 9: Comparison for *P-M* interaction curves for Group HSC-1 (4% reinforcement)

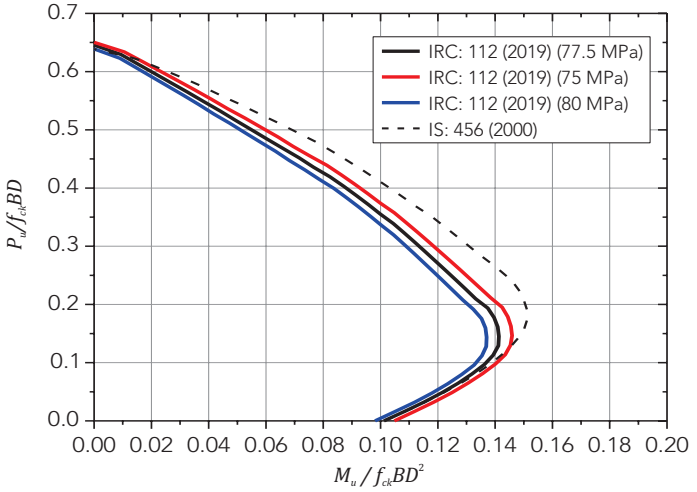

Figure 10: Comparison for *P-M* interaction curves for Group HSC-2 (4% reinforcement)

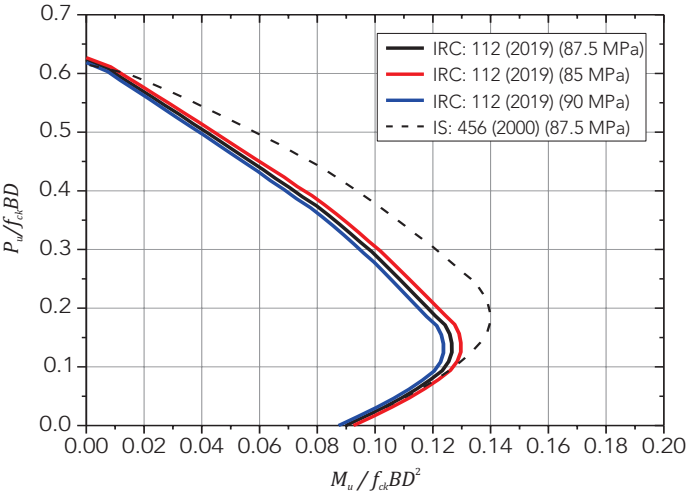

Figure 11: Comparison for *P-M* interaction curves for Group HSC-3 (4% reinforcement)

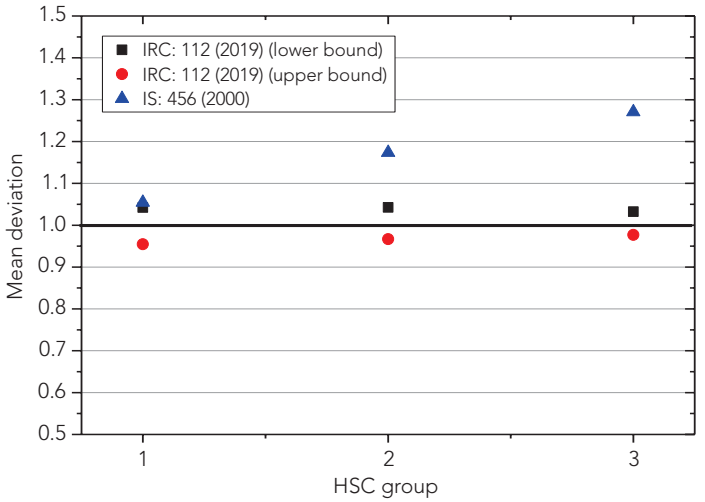

Figure 12: Mean deviation for 3 HSC groups (2% reinforcement)

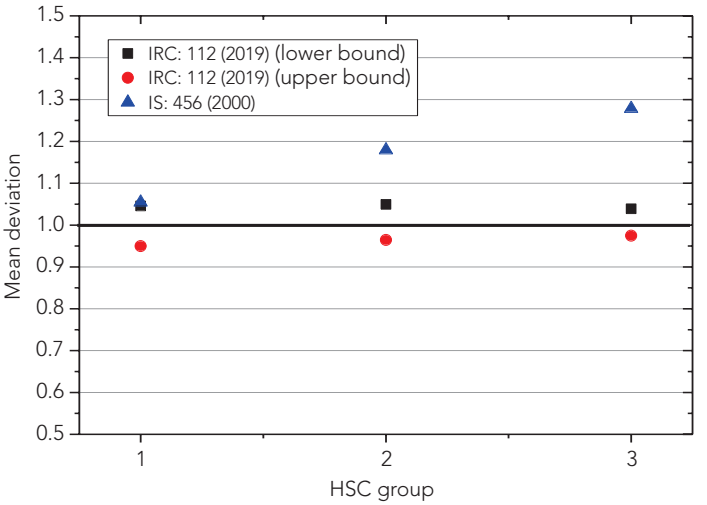

Figure 13: Mean deviation for 3 HSC groups (4% reinforcement)

5. RESULTS AND DISCUSSION

The *P - M* interaction diagrams obtained are shown in Figures 6 to 8 for a total reinforcement percentage of 2%. Figure 6 compares the *P-M* curves obtained using the parameters as given in IRC: 112 (2019) for M65 and M70 juxtaposed with the curve obtained using the expressions for a mean value of f_{ck} = 67.5 N/sq. mm. The *P-M* relationship obtained using the existing stress block given in IS: 456 (2000) for f_{ck} = 67.5 N/sq. mm is also shown in the Figure. Similar comparisons are shown in Figure 7 for the values of M75, M80 concretes and f_{ck} = 77.5 N/sq mm. Figure 8 shows the results obtained for M85, M90 and f_{ck} = 87.5 N/sq·mm. The Figures 9 to 11 show the same results as given above but with a total reinforcement percentage of 4%.

For quantifying the differences between any two chosen curves, differences in moment values have been calculated as percentages at 30 equally spaced values of *P* between zero and P_{max}. The mean of these 30 deviations has been termed as "mean deviation" between two chosen curves. The values of mean deviations have been plotted in Figure 12 (total reinforcement percentage of 2%) and in Figure 13 (total reinforcement percentage of 4%) as functions of the concrete groups HSC 1, HSC 2 and HSC 3. The pairs of curves chosen for comparison at a time were:

a. *P-M* interaction curves according to the properties valid for f_{ck} = 67.5, 77.5 and 87.5 N/sq mm as per IS: 456 (2000) and their corresponding curves evaluated as per the guidelines of IRC: 112 (2019).

b. *P-M* interaction curves for M65, M75 and M85 (called as lower bound values) compared with values for f_{ck} = 67.5 N/sq·mm, 77.5 N/sq·mm and 87.5 N/sq mm respectively, all as per IRC: 112 (2019) recommendations.

c. *P-M* interaction curves for M70, M80 and M90 (called as upper bound values) compared with values for f_{ck} = 67.5 N/sq·mm, 77.5 N/sq·mm and 87.5 N/sq·mm respectively, all as per IRC: 112 (2019) recommendations.

It can be seen from the Figures 6 to 13 that use of the concrete stress-block parameters of IS: 456 (2000) for high strength concrete results in over-estimation of the moment capacities of the section on an average by 7 to 28%, varying linearly from concrete of grades M65 to M100.

It can also be seen that the *P-M* interaction curves worked out according to the recommendation of IRC: 112 (2019) for any two adjacent concrete grades separated by 5 N/sq·mm, the curves for the two concrete grades are quite close to each other. When any two such curves are replaced by a mean curve the resulting mean deviations in moment capacities are less than ± 4% for all concrete grades and all percentage reinforcement.

6. CONCLUSIONS

Although the IS: 456 (2000) limits the applicability of the concrete design properties given therein only to concrete grades up to M55, the EN 1992-1-1: 2004 + A1 : 2014 and IRC: 112 have extended their applicability up to and including M60. Separate grade-specific recommendations have been specified only from M65 onwards up to grades of M110 and M90 respectively. The following conclusions can be drawn from the present study:

- A comparative study of sectional capacities of rectangular RC sections using the different stress-block properties recommended in the design standards considered in the present study reveals that use of existing recommendations of IS: 456 (2000) for concrete of grades between M65 to M90 leads to an over-estimation of capacities with mean deviations ranging from 5 to 28%.

The deviations at local points on the *P-M* curve may be even larger. This leads to un-conservative design and hence there is an urgent need to revise the corresponding specifications of IS: 456 (2000) for HSC.

- The IRC: 112 (2019) specifies grade-specific design parameters for high strength concretes for grades up to M90 at intervals of 5 MPa for f_{ck} whereas the EN 1992-1-1 : 2004 + A1 : 2014 specifies the values at intervals of 10 MPa up to M110. But as concrete grades are specified in our country at strength intervals of 5 N/sq·mm, it is better to specify the concrete properties at strength intervals equal to 5 N/sq·mm as already done in IRC: 112 (2019).
- When the concrete design properties are specified at strength intervals of 5 N/sq·mm, it is observed that the resultant *P-M* diagrams of any two adjacent concrete grades are quite close to each other. When the values of two such adjacent curves are compared with the values of a mean curve corresponding to a concrete strength equal to the mean strengths represented in the two curves, the resulting mean deviations in moment values between the mean curve and the individual curves are within ± 4 percent. Individual deviations are also of the same order. Hence, it is for discussion whether it is desirable to present the design concrete properties in a discrete form keeping them common for M65 and M70, M75 and M80, M85 and M90 and so on. This will reduce the number of design charts to be used in design offices.
- The suggestion made at above may seem to be a violation of the grade specific recommendation for design properties like ε_{c2}, ε_{cu2}, n etc. given in the closed-form expressions as functions of concrete strength IRC: 112 (2019) as well as in EN 1992-1-1: 2004 + A1 : 2014. But this has already been done in IRC: 112 (2019) as well as in EN 1992-1-1: 2004 + A1 : 2014 where the design properties for quite a few adjacent grades of concrete have been given to be the same in the respective design tables in spite of having given the expressions for them as a function of the concrete strength f_{ck}.
- The closed-form expressions given by the authors for determining the magnitude and line of action of the concrete compressive force when the entire section is under compressive stresses could be made either use of by designers for preparing their own design charts conforming to the recommendations of IRC: 112 (2019), by hand calculation or using a computer.

ACKNOWLEDGEMENTS

The authors wish to acknowledge the advice received from Prof. Devdas Menon and Prof. CVR Murty, Professors in the Department of Civil Engineering at IIT Madras, who contributed through technical discussions during the development of this manuscript.

REFERENCES

[1] IS: 456 (2000). "Indian standard code of practice for plain and reinforced concrete for general building construction", Bureau of Indian Standards, New Delhi.

[2] IS: 456 (1978). "Indian standard code of practice for plain and reinforced concrete for general building construction", Bureau of Indian Standards, New Delhi.

[3] CEB-FIP. (1970). "International Recommendations for the Design and Construction of Concrete Structures: Vol. 1 – Principles and Recommendations", Comite European Du Beton, Information Bulletin No 72.

[4] CP 110. (1972). "Code of Practice for the Structural Use of Concrete, British Standard", B.S.I., London.

[5] DIN 1045. (1972). "Concrete and Reinforced Concrete Structures: Design and Construction", Deutsches Institut fur Normung E.V. (DIN).

[6] EN 1992-1-1-1991. (1991). " Eurocode 2 – Design of Concrete Structures – European pre-standards".

[7] EN 1992. (2004). "Eurocode 2 – Design of Concrete Structures – Part 1-1: General rules and rules for buildings".

[8] EN 1992. (2013). "Eurocode 2 – Design of Concrete Structures – Part 1-1: General rules and rules for buildings", EN 1992 - 1 - 1 : 2004 + A1 : 2014.

[9] Ruesch, H., Grasser, E., Rao, P. S. (1961). "Grundlagen fuer die Bemessung bei einachsigen Spannungszustaenden im Betonbau", *Laboratory Report (69 pages), Lehrstuhl fuer Massivbau, Technical University Munich.*

[10] Ruesch, H., Grasser, E., Rao, P. S. (1962). "Principes du Calcul Beton Arme suos des Etats Constraintes Monoaxious", *Bulletin de Information No 36 (122 pages), CEB*, Paris.

[11] IRC: 112 (2011). "Code of practice for concrete road bridges", Indian Roads Congress, New Delhi.

[12] IRC: 112 (2019). "Code of practice for concrete road bridges", Indian Roads Congress, New Delhi.

[13] SP: 16 (1980). "Design aids for Reinforced Concrete to IS: 456 (1978)", Bureau of Indian Standards, New Delhi.

P. SRINIVASA RAO obtained his B.Tech. and M.Tech. Degrees in Civil Engineering from Indian Institute of Technology (IIT) Kharagpur and Dr Ing Degree from the Technical University Munich, Germany. He was formerly a Professor in the Department of Civil Engineering at Indian Institute of Technology (IIT) Madras and is currently Professor Emeritus and President of the educational society at Gayatri Vidya Parishad, Visakhapatnam. He is an FNAE and a recipient of ICI-L&T lifetime achievement award for the year 2008. His research interests are primarily in reinforced and prestressed concrete design, tall towers and concrete shells and folded plates. Email: spulugurta@hotmail.com

M. N. SHARIFF received his B.Tech. from Gayatri Vidya Parishad College of Engineering (Autonomous), Visakhapatnam and Master's and PhD degree from Indian Institute of Technology (IIT) Madras. He is currently working as a faculty in the Department of Civil Engineering at NIT Warangal. His research interests include behaviour of reinforced concrete structures, nonlinear analysis of structures, computational mechanics and structural evaluation. Email: mnshariff@alumni.iitm.ac.in

N. HARSHA is an undergraduate student in the Department of Civil Engineering at Indian Institute of Technology (IIT) Madras. His research interests include analysis and design of structures and finite element modelling. Email: harshaneduri9@gmail.com

Cite this article: Rao, P. S., Shariff, M. N., and Harsha, N. (2021). "Studies on *P-M* interaction curves for uniaxial bending of high strength concrete rectangular sections", *The Indian Concrete Journal*, Vol. 95, No. 7, pp. 41-48.

BIMODULAR DAMAGE-ELASTOPLASTICITY CONSTITUTIVE MODEL FOR CONCRETE

R. RAVEENDRA BABU,
ARBIND K. SINGH,
GURMAIL S. BENIPAL*

Abstract

The available constitutive models proposed for concrete generally aim at investigating its nonlinear inelastic mechanical behavior in all the aspects. Authors have recently proposed a new analytical bimodular elastic damage model with a restricted scope, viz., the identification of peculiar nonlinearity of damaged concrete. Isotropically-damaged bimodular concrete has been shown to belong to the class of homogeneous mechanical systems. Also, a new damage potential governing damage evolution is formulated. Authors have earlier proposed a standard stress-based purely elasto-plastic constitutive model based upon a new empirical unified loading function. In the present paper, a coupled damage-elastoplasticity constitutive model is proposed by coupling the authors' bimodular damage and elastoplastic constitutive models. Salient aspects of the predicted mechanical behavior of concrete are discussed. The contribution made by the proposed model to concrete mechanics is critically evaluated.

Keywords: Bimodular solids, Coupled constitutive model, Elastic damage model, Elastoplasticity model, Homogeneous mechanical systems.

1. INTRODUCTION

Analysis of reinforced concrete structures is very complex because of the difficulties of modelling concrete and concrete-reinforcement interface. Upon loading, hardened plain concrete suffers anisotropic stiffness degradation due to damage and undergoes irreversible plastic/viscoplastic deformations before failure/fracture under monotonic, cyclic or sustained loading. Like other quasi-brittle cohesive-frictional solids, it exhibits strain-softening in the post-peak response characterised by shear localisation and size effect. Over the last few decades, considerable research effort has been directed to construct coupled damage-elastoplasticity constitutive models to predict the nonlinear inelastic behavior of concrete till failure.

Most of such available constitutive models of concrete [1,2,3] are premised upon a theory of damage mechanics and a theory of elastoplasticity. Because of its importance, a number of sophisticated constitutive models dealing only with elastic damage have been proposed [4-10]. Scalar, vector or tensor variables have been adopted as damage measures. Different behavior in tension and compression has variously been considered as being based upon sense of volumetric strain [11] and uncoupling of material response in different principal stress directions [12].

For the purpose of thermodynamic consistency and material stability, the symmetry and the positive definitiveness of the secant operator has been maintained by employing energy equivalence. The observed decrease of Poisson's ratio with damage is also predicted by a recent proposed model [13]. Another anisotropic damage model is based upon the uncoupling of the principal stress-inelastic strain relations [14]. Attempts have also been made to incorporate the strain rate effects as well [15]. Thermodynamically-consistent models are generally required to satisfy Clausius-Duhem Ineqality [16,17]. Continuum-theoretic nonlocal or strain gradient type models of strain localisation and size effect define 'characteristic length' of the material. It is found that none of the available nonlocal models constitutes a universal coupled damage-elastoplasticity constitutive theory for concrete [18].

It can be observed that most of these constitutive models are based upon sound principles of solid mechanics and thermodynamics. However, being application-oriented, these models are constructed by following empirical-computational methodology. Of course, there exist no purely analytical loading functions and initial yield and failure criteria for concrete. Unilateral effect has been characterized as a difficult and open research field [4]. Even in the later investigations, there is no agreement on the proper approach for modelling the different behavior of damaged concrete in tension and compression. Such continuing diversity in approaches is symptomatic of the confusion in the basics.

*Corresponding author : Gurmail S. Benipal, Email: gurmail@civil.iitd.ac.in

In the present paper, a coupled damage-elastoplasticity constitutive model for concrete is proposed by coupling authors' damage and elastoplasticity models. The main point of departure here is the purely analytical bimodular elastic damage constitutive model. It is premised upon the understanding that damaged solids resemble bimodular elastic solids. Motivated by Green-Mkrtichian theory [19], new constitutive equations for isotropic bimodular solids have earlier been proposed by the authors [20]. A standard theory of hardening elastoplasticity of concrete has earlier been constructed in stress space based on a new empirical loading function valid for pre-peak stress regime [21]. The proposed model is validated using relevant available experimental data. Its most distinguishing aspects relative to the plethora of contending existing constitutive models are identified.

2. CONSTITUTIVE EQUATIONS FOR BIMODULAR SOLIDS

Bimodular materials possess different moduli of elasticity in tension and compression. Following Green and Mkrtichian [19], it is assumed here that it is the sense of the principal strain that decides which of the two possible values of Young's moduli of elasticity will be operative along the corresponding principal material axis. Depending upon the sense of the three principal strains, a material point can be in any of the four elastically-distinct states: When all the strains are tensile (or compressive), the material is isotropic with the elastic modulus as E_t (or E_c). In contrast, when the principal strains are of mixed sense, the material point is transversely isotropic. Such solids have same Young's modulus of elasticity in the plane of isotropy formed by the axes of the two principal strains of same sense. The orientation of the third principal strain of different sense constitutes the axis of rotation. It is well-known that conventional transversely isotropic hyperelastic solids with fixed material axes possess five independent elastic constants [22]. In contrast, the material or acoustical axes of the isotropic bimodular transversely isotropic solids always coincide with the principal strain/stress directions. The constitutive equations for such solids are presented below in reference to this principal coordinate system:

At any material point, the principal stresses σ_i as well as strain energy W can be stated in terms of the principal strains ϵ_j as $\sigma_i = C_{ij}\,\epsilon_j$ and $W = \frac{1}{2}\,C_{ij}\,\epsilon_i\,\epsilon_j$. Following Green and Mkrtichian [19], the stresses and the strain energy are assumed to be continuous functions of strains, even though the elastic constants experience discontinuous change with change in the sense of strain. For this hyperelastic material, the expressions for the strain energy for the four elastically distinct cases are stated.

The independent material constants are identified as $\lambda = \lambda_t = \lambda_c$, μ_1 and μ_c respectively. Here, λ and μ are Lame's constants and the subscripts c and t pertain to triaxial compression and tension cases respectively. The Poisson's ratios υ_c and υ_t are obtained from the fact that Lame's constant λ does not depend upon the bimodularity ratio (E_t/E_c). In contrast, the shear moduli are different for different elastic states of the material and depend upon bimodularity ratio. Thus, in contrast to the conventional transversely isotropic solids, the isotropic bimodular solid possesses only three independent elastic constants. The values of the elastic constants C_{ij} are known in terms of these three elastic constants for different cases.

Using the above constitutive equations stated in reference to the principal coordinate system, the constitutive equations are obtained below in reference to the general coordinate systems. Let complementary energy Ω be stated in terms of the principal stresses as primary variables as $\Omega = \frac{1}{2}\,D_{ij}\,\sigma_i\,\sigma_j$. The compliance tensor D_{ij} obtained as inverse of C_{ij} pertains only to the case when the chosen coordinate axes coincide with the principal stress/strain axes. The expressions for compliance tensor components D^e_{ijkl} in reference to any Cartesian coordinate system are stated here. The expression for principal stresses σ_r as function of stress invariants are as follows:

$$\sigma_r = \frac{I_1}{3} + \frac{2}{\sqrt{3}}\sqrt{J_2}\cos\theta_r \qquad r = 1,2,3. \tag{1}$$

Here, $\theta_1 = \cos\theta$; $\theta_2 = \cos\left(\theta - \frac{2\pi}{3}\right)$; $\theta_3 = \cos\left(\theta + \frac{2\pi}{3}\right)$.

Thus, like other isotropic solids, complementary energy function can be stated in terms of stress invariants as follows:

$$\Omega\left(I_1, J_2, \theta\right) = \frac{1}{9}\,D_1 I_1^2 + \frac{2}{3\sqrt{3}}\,D_2 I_1\sqrt{J_2} + \frac{4}{3}\,D_3 J_2 \tag{2}$$

Using Green's theorem for hyperelastic solids [23-25], the components of small strain tensor can be written as

$$\epsilon_{ij} = \frac{\partial\Omega}{\partial\sigma_{ij}} = \frac{\partial\Omega}{\partial I_1}\frac{\partial I_1}{\partial\sigma_{ij}} + \frac{\partial\Omega}{\partial J_2}\frac{\partial J_2}{\partial\sigma_{ij}} + \frac{\partial\Omega}{\partial\theta}\frac{\partial\theta}{\partial\sigma_{ij}}$$

$$= \alpha_1\,\delta_{ij} + \alpha_2\,S_{ij} + \alpha_0\,T_{ij} \tag{3}$$

$$\frac{\partial I_1}{\partial\sigma_{ij}} = \delta_{ij} \quad \frac{\partial J_2}{\partial\sigma_{ij}} = S_{ij} \quad \frac{\partial\theta}{\partial\sigma_{ij}} = T_{ij} \quad \alpha_1 = \frac{\partial\Omega}{\partial I_1} \quad \alpha_2 = \frac{\partial\Omega}{\partial J_2} \quad \alpha_0 = \frac{\partial\Omega}{\partial\theta}$$

The expressions for the required constants D_1, D_2 and D_3 are available in the cited publication [20]. The fourth rank tangent compliance tensor coefficients can easily be obtained as

$$D^e_{ijkl} = \frac{\partial\epsilon_{ij}}{\partial\sigma_{kl}} \tag{4}$$

It can be observed that the complementary energy function Ω, strain tensor components ϵ_{ij} and the compliance tensor components D^e_{ijkl} for such a solid are, in general, functions of the stress tensor components. To be specific, Ω, ϵ_{ij} and D^e_{ijkl} are functions positively homogeneous of order two, one and zero respectively of the stress tensor components. Obviously, the bimodular solids belong to the class of first order homogeneous mechanical (FOHM) systems. For such systems, the tangent compliance tensor D^e_{ijkl} is known to play the role of

secant compliance tensor as well. Thus, both the incremental and total constitutive equations, viz., $d\epsilon_{ij} = D^{e}_{ijkl}\, d\sigma_{kl}$ and $d\epsilon_{ij} = D^{e}_{ijkl}\, d\sigma_{kl}$, are valid.

The constitutive equations proposed above for bimodular solids resemble in form the well-known equation proposed by Rivlin for isotropic nonlinear elastic solids. Such elastic materials including the bimodular solids and isotropically damaged concrete are known to exhibit stress-induced anisotropy, normal stress effects as well as co-axiality of the principal stress axes, the principal strain axes and the material acoustic axes[20,25].

3. UNIFIED LOADING FUNCTION

As per the current practice, the following single general expression for the loading function has been proposed [21] in terms of first invariant I_1 of the stress tensor, the second invariant J_2 of the deviatoric stress tensor and Lode angle θ:

$$f(I_1,\ J_2,\ \theta) = A\frac{J_2}{(f_c')^2} + \alpha\frac{\sqrt{J_2}}{f_c'} + B\frac{I_1}{f_c'} + C\frac{(I_1)^2}{(f_c')^2} - 1 = 0 \qquad (5)$$

$$cos3\theta = \frac{3\sqrt{3}}{2}\frac{J_3}{J_2^{\frac{3}{2}}} \qquad \alpha = \left[X\,\kappa\, cos\theta + \left(1-\ \kappa\right) Y\right] \qquad C = C_0(1-\ \kappa)$$

The expression for the unified loading function is cast in the normalized form by using the uniaxial compressive strength f_c' of concrete so that the five empirical parameters *A, B, X, Y* and C_0 are valid for all grades of concrete. These constants are determined by calibration with experimental data on concrete undergoing both damage and plastic flow. The symbol κ denotes a hardening function of some hardening parameter. As shown in Figure 1 for different values of Lode angle, the evolution of the loading surfaces from initial yield to failure surface is governed by the increasing value of the hardening function . Its values at initial yield and failure surfaces are and respectively. There is considerable uncertainty about the initial

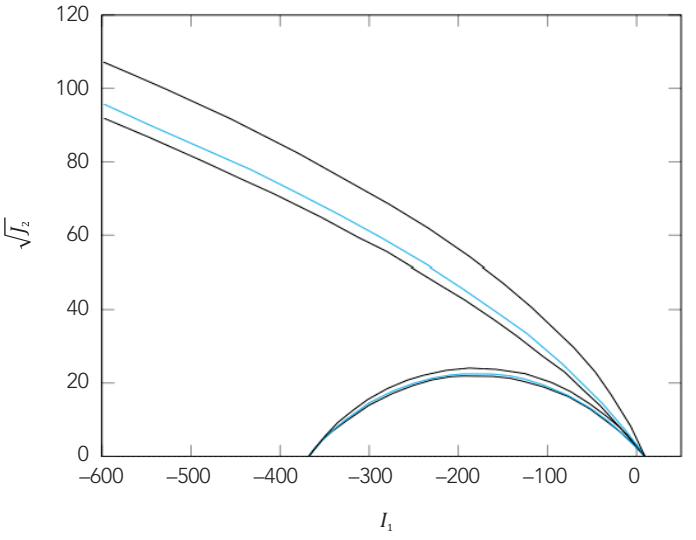

Figure 1: Unified loading surfaces

yield criterion. The following failure criterion resembling Ottosen criterion [26] can be deduced from the loading function as a special case (κ = 1.0):

$$f(I_1,J_2,\theta) = A\frac{J_2}{(f_c')^2} + \mathrm{X}\cos\theta\ \ \frac{\sqrt{J_2}}{f_c'} + B\frac{I_1}{f_c'} - 1 = 0 \qquad (6)$$

4. ELASTOPLASTICITY MODEL

Using the well-established classical theory of elastoplasticity and additional assumptions of associative flow rule and work hardening [26,27], the following incremental constitutive equation has been derived as $d\epsilon_{ij} = D^{ep}_{ijkl}d\sigma_{kl}$ where the fourth rank elastoplastic compliance tensor D^{ep}_{ijkl} can be determined from the following elastic and plastic compliance tensors:

$$D^{ep}_{ijkl} = D^{e}_{ijkl} + D^{p}_{ijkl} \qquad (7)$$

$$D^{e}_{ijkl} = \frac{-\upsilon}{E}\delta_{ij}\,\delta_{kl} + \frac{1+\upsilon}{E}\delta_{ik}\,\delta_{jl} \qquad D^{p}_{ijkl} = \frac{-1}{h}\frac{\partial f}{\partial\sigma_{ij}}\frac{\partial f}{\partial\sigma_{kl}}$$

$$h = \frac{\partial f}{\partial\kappa}H_p h_p; \quad \frac{\partial f}{\partial\kappa} = \frac{\sqrt{J_2}}{f_c'}(X\,cos\theta - Y) - \frac{C_0}{(f_c')^2}(I_1)^2$$

Here, the plastic work W_P has been assumed to play the role of the hardening parameter p which determines the instantaneous value of k such that $dp = dW_P = \sigma_{pq}\, d\varepsilon^{p}_{pq}$. The parameters H_P and h_P are defined [21] as follows: dk=$H_p\, dp$ and dp = $h_p d\lambda$. Also, positive and negative increments in k imply loading and unloading respectively, while the stress increments keeping κ constant imply neutral loading. During unloading, the material exhibits linear elastic response. During loading and neutral loading, the material response is elastoplastic. However, no plastic work is done in neutral loading and so no hardening occurs.

5. BIMODULAR ELASTIC DAMAGE MODEL

5.1 Constitutive Equations for Damaged Concrete

Upon loading, concrete suffers damage in the form of discrete microcracks of different lengths and oriented in different directions. Also, general stress history can inflict anisotropic damage on the initially isotropic elastic solid. In this constitutive model, the concrete has been assumed to suffer only isotropic damage. The proposed phenomenological model is based upon the continuum damage mechanics framework wherein the discrete cracks are smeared out in the material body. The extent of damage suffered at a material point is measured by a single scalar damage parameter which, in turn, depends upon the hardening function κ. The $\omega - \kappa$ relation controlling the damage evolution is mediated through another 'uniaxial stress' parameter σ. Within the initial loading surface, concrete is undamaged. Depending upon the stress history, the damage evolution occurs as for the following equations [20]:

$$0 \le \frac{\sigma}{f_c'} \le 0.3 \qquad 0 \le \kappa \le 0.3 \qquad \omega = 0$$

$$0.3 \le \frac{\sigma}{f_c'} \le 1 \qquad 0.3 \le \kappa \le 1 \qquad \omega = \omega_0 \left[\frac{\frac{\sigma}{f_c'} - 0.3}{0.7}\right]^2 \tag{8}$$

Here, ω_0 denotes the maximum value of the damage suffered by concrete at failure and has been assigned a value equal to unity.

A material point undergoing damage exhibits energy dissipation as well as stiffness degradation. However, within the current loading surface, the existing microcracks can be in the closed or the open state depending upon the current state of stress applied at that point. It is worth noting that these microcracks merely close under compression, but do not heal up. The extent of damage suffered by a material point subjected to any load history is measured by the maximum value of the damage parameter reached in the past. Damaged solids exhibit lesser stiffness under tension. However, partial stiffness recovery occurs upon crack closure or damage deactivation under compression. Based upon the above arguments, it is clear that an isotropically-damaged solid is a bimodular solid possessing different values of the moduli E_t and E_c of elasticity in tension and compression respectively. Depending upon the value of the damage parameter ω, the elastic moduli E_c and E_t are evaluated from the following equations[28]:

$$E_c = (1 - \alpha_c\, \omega)\, E_0 \qquad E_t = (1 - \alpha_t\, \omega)\, E_0 \tag{9}$$

Here, E_0 denotes the Young's modulus of elasticity of the undamaged concrete. Based upon the available experimental data, the parameters α_c and α_t are assigned values and respectively [20].

5.2 Evolution of damage surface

Application of stress increments on the concrete under a stress state on the current damage surface introduces incremental damage. The consequent incremental enhancement of the components of the compliance tensor results in strain increments. Here, it has been assumed that incremental damage suffered by concrete under stress increments does not result in any irreversible strain increments. The elastic strain increments as a direct effect of applied stress increments are obtained using the current tangent compliance tensor. In view of these facts, the incremental elastic strains caused by the applied stress increments are obtained as below:

$$d\epsilon_{ij} = d\epsilon_{ij}^e + d\epsilon_{ij}^d = D_{ijkl}^e\, d\sigma_{kl} + \sigma_{kl} dD_{ijkl}^e \tag{10}$$

Here, D_{ijkl}^e in this equation represents the elastic compliance tensor as obtained in equation (4) based upon elastic moduli E_c and E_t of the damaged nonlinear elastic concrete.

The component of the elastic strain increments associated with stiffness degradation or compliance enhancement can be quantified as follows: At any loading surface, the state of strain is determined by the state of stress and the extent of damage suffered by the concrete. Thus,

$$\epsilon_{ij} = \epsilon_{ij}\,(\sigma_{kl}, \omega) \qquad d\epsilon_{ij} = \frac{\partial \epsilon_{ij}}{\partial \sigma_{kl}} d\sigma_{kl} + \frac{\partial \epsilon_{ij}}{\partial \omega} d\omega \tag{11}$$

Here, $d\omega$ measures the additional damage caused by the applied stress increments. Using the equality $\left[\frac{\partial \epsilon_{ij}}{\partial \omega} d\omega = \frac{\partial}{\partial \omega}\frac{\partial \Omega}{\partial \sigma_{ij}} d\omega = \frac{\partial}{\partial \sigma_{ij}}\frac{\partial \Omega}{\partial \omega} d\omega = \frac{\partial Z_d}{\partial \sigma_{ij}} d\omega\right]$, the expressions for incremental strains are obtained as

$$d\epsilon_{ij} = D_{ijkl}^e d\sigma_{kl} + D_{ijkl}^d d\sigma_{kl} = \left[D_{ijkl}^e - \frac{1}{\frac{\partial f}{\partial D}} \frac{\partial Z_d}{\partial \sigma_{ij}} \frac{\partial f}{\partial \sigma_{kl}}\right] d\sigma_{kl} \tag{12}$$

$$D_{ijkl}^d = \frac{-1}{\frac{\partial f}{\partial \omega}} \frac{\partial Z_d}{\partial \sigma_{ij}} \frac{\partial f}{\partial \sigma_{kl}} \qquad Z_d = \frac{\partial \Omega}{\partial \omega} = Z_d\,(I_1, J_2, \theta, \omega)$$

Here, Z_d can be interpreted as the complimentary energy release rate which is the energy conjugate of damage parameter ω. As Z_d and f are different functions of σ_{ij} and ω, the tangent compliance tensor D_{ijkl}^e is asymmetric. Also, the above derivation yields the following expression for the strain increments $d\epsilon_{ij}$ associated with incremental damage.

$$d\epsilon_{ij}^d = D_{ijkl}^d d\sigma_{kl} = \frac{-1}{\frac{\partial f}{\partial \omega}} \frac{\partial Z_d}{\partial \sigma_{ij}} \frac{\partial f}{\partial \sigma_{kl}}\, d\sigma_{kl} = \left[\frac{-1}{\frac{\partial f}{\partial \omega}} \frac{\partial f}{\partial \sigma_{kl}} d\sigma_{kl}\right] \frac{\partial Z_d}{\partial \sigma_{ij}} \tag{13}$$

$$d\epsilon_{ij}^d = d\lambda_d \frac{\partial Z_d}{\partial \sigma_{ij}} \qquad d\lambda_d = \left[\frac{-1}{\frac{\partial f}{\partial \omega}} \frac{\partial f}{\partial \sigma_{kl}} d\sigma_{kl}\right] \tag{14}$$

This implies that the function Z_d plays the role of damage potential. Since the damage potential Z_d is distinct from the damage function $f(\sigma_{ij}, \omega)$, the equation (14) is the statement of non-associative damage flow rule[20].

6. BIMODULAR DAMAGE-ELASTOPLASTICITY CONSTITUTIVE MODEL

By coupling the elastoplasticity model and the elastic damage model, a unified bimodular damage-elastoplasticity constitutive model is proposed here. It is capable of predicting the irreversible plastic deformations and stiffness degradation exhibited by concrete in addition to the reversible elastic deformations. The constitutive equations for the incremental material behavior both within any loading surface and for loading beyond it till failure have been developed. Within the initial yield surface, the material is isotropic linear elastic. For stress variations within any current loading surface, the constitutive equations for the damaged bimodular nonlinear elastic concrete are valid even for the present case. For loading beyond the current loading surface, the material response includes elastic as well as plastic strain increments. The elastic strain increments include those caused by applied stress increments as well as those caused by incremental stiffness degradation. Thus, the total strain increments caused by the applied stress increments are obtained as

$$d\epsilon_{ij} = d\epsilon^e_{ij} + d\epsilon^d_{ij} + d\epsilon^p_{ij} = D^{epd}_{ijkl}\, d\sigma_{kl} \quad (15)$$

Here, D^{epd}_{ijkl} is the elastoplastic damage compliance tensor given by

$$D^{epd}_{ijkl} = D^e_{ijkl} + D^d_{ijkl} + D^p_{ijkl} = \left[D^e_{ijkl} - \frac{1}{\frac{\partial f}{\partial \omega}} \frac{\partial Z_d}{\partial \sigma_{ij}} \frac{\partial f}{\partial \sigma_{kl}} - \frac{1}{h} \frac{\partial f}{\partial \sigma_{ij}} \frac{\partial f}{\partial \sigma_{kl}} \right] \quad (16)$$

It must be emphasized that the compliance tensor components D^e_{ijkl} pertain to the damaged concrete. These are different from those of the undamaged concrete used in the pure elastoplasticity model given by the equation 7. These coefficients D^e_{ijkl} depend, apart from the state of stress and so extent of damage, upon the sense of the principal strains. Here, it must be emphasized that it is not the sense of the total principal strains but of only their elastic components which determines the relevant elasticity case. The relevant elastic reversible component of the total strain tensor is caused directly by applied stress increments and indirectly by compliance enhancement associated with incremental damage caused by the applied stress increment tensor. This is in contrast to the bimodular elastic damage model wherein it is the total strain tensor which determined the two elastic moduli of the damaged concrete as well as the damage potential Z_d. Thus, the irreversible part of the incremental strain tensor is contributed only by plastic flow as in the case of purely elastoplasticity model. However, the incremental energy dissipation is caused both by the incremental plastic flow and the incremental damage evolution. Because of this fact, the plastic work W_p chosen as hardening parameter differs from that for the purely elastoplastic model[21]. For the coupled damage-elastoplasticity model, the variation of plastic modulus H_p with hardening function is plotted in Figure 2.

The predicted response of concrete under some typical proportional stress histories is presented. Positive principal strains imply tensile strains. As shown in Figure 3, well-known

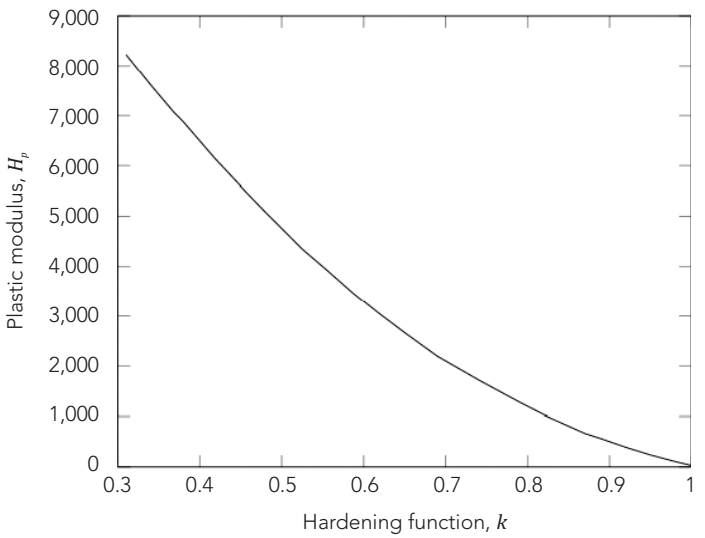

Figure 2: Variation of plastic modulus with hardening function

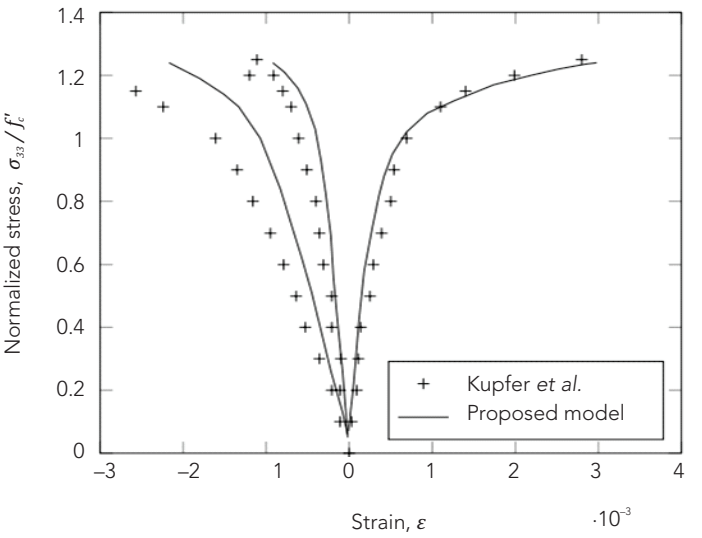

Figure 3: Response under unequal biaxial compression

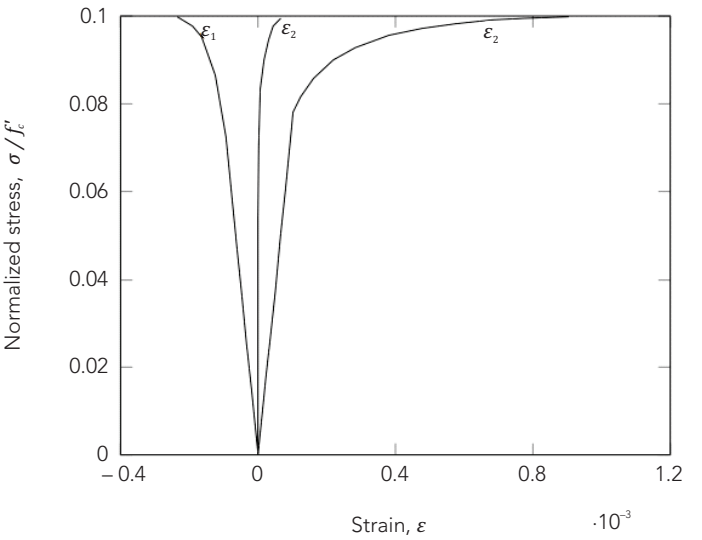

Figure 4: Response in pure shear

observed response of concrete in unequal biaxial compression[29] is predicted satisfactorily. Tensile strain in the third principal direction is predicted to dominate as the failure surface is reached. Response under monotonic pure shear is depicted in Figure 4. Within the initial yield surface, the state of pure shear stress introduces equal and opposite principal strains and the intermediate principal strain is predicted to vanish. For shear stresses exceeding initial yield value ($0.08f'_c$), the major and minor principal strains diverge and large tensile strain is introduced along the third principal direction. Like other cohesive-frictional materials, concrete is known to exhibit dilatancy under pure shear and the same is predicted here. This volumetric expansion is associated with the normal stress effect exhibited by concrete stressed into inelastic range. Of course, the failure is predicted to occur when the shear stress equals shear strength ($0.1f'_c$).

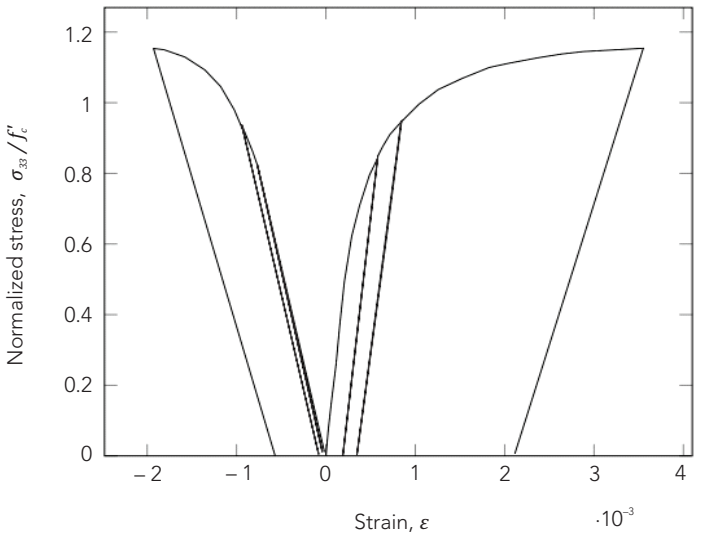

Figure 5: Coupled damage-elastoplastic response upon triaxial loading and unloading

Typical predicted coupled damage-elastoplastic response during loading, unloading and reloading in equal biaxial compression is presented in Figure 5. This plot apparently shows that, during unloading and reloading within the current loading surface, the concrete behavior is linear elastic. This is because of the chosen proportional stress-path. In fact, the damaged concrete is a nonlinear elastic bimodular solid. However, the strain tensor components are functions homogeneous of order unity of the stress tensor components. This implies that concrete behaves linearly under proportional stress variations and exhibits its peculiar nonlinearity only under non- proportional stress variations in the elastic region.

7. DISCUSSION

In this Paper, the authors have proposed a simple analytical model capable of predicting the nonlinear elastic response, stiffness degradation due to damage and plastic displacements of concrete in the pre-peak stress regime till its failure. Only the loading function and calibration for plastic modulus and damage with loading contain empirical constants. It should be noted that currently there exist in the available literature no purely analytical proposals for loading functions.

Proenka and Pituba [11] made the first attempt to model damage deactivation in concrete as a bimodular solid and used Cone-wise Linear Elastic Theory of bimodular solids [30]. As per this theory, the bimodular material is assumed to possess different elastic moduli at a point depending upon the sense of the volumetric strain at that point. As these elastic coefficients remain constant within a particular stress regime, the bimodular material is incapable of predicting the observed nonlinear response for damaged concrete. In contrast, following Green-Mkrtichian [19] approach, authors proposed a new model for bimodular materials and employed it to simulate damage deactivation in damaged concrete. Like the bimodular materials, the damaged concrete also turned out to be a nonlinear elastic solid. Here, the strains are shown to be functions homogeneous of order unity of the stresses. The tangent and secant compliance tensors for the damaged concrete are identical[20]. As is clear from the Introduction, even the latest models have not identified this characteristic nonlinearity of the damaged concrete.

A new damage potential is also proposed for simulating the damage evolution. Authors' bimodular elastic damage model has been identified [31] as one of the three different recent developments in damage mechanics, the others being those due to Chaboche [32] and Krajcinovic[33] and is employed for composite materials. This damage model is coupled with standard elastoplasticity model to construct the proposed constitutive model for concrete by these researchers.

The scope of the present paper is limited only to the isotropic damage suffered by concrete and measured by a scalar damage parameter. Of course, the stiffness degradation suffered by concrete differs in tension and compression. However, the applied stress histories are observed to introduce anisotropic damage in concrete requiring vector or tensor damage measures. Such an anisotropically-damaged concrete should more appropriately be modelled as an anisotropic bimodular material. The required anisotropic bimodular damage model could have demanded more complex damage evolution model as well. However, all is not lost. Of course, an anisotropically-damaged concrete would exhibit strongly anisotropic behavior even when all the principal strains are tensile. The present isotropic damage model is indeed incapable of predicting such a response. However, such a state of strain is rarely, if ever, encountered in concrete structures. Also, the material remains isotropic linear elastic within the initial yield surface which, for triaxial tension, lies just inside the failure surface. In the case of triaxial compressive states of strain, stiffness recovery upon crack-closure renders the concrete more or less isotropic quite easily predicted even by the present model as well. Similarly, even the isotropically-damaged concrete more commonly subjected to principal strains of mixed sense exhibits stress-induced anisotropy quite similar to the one exhibited by anisotropically-damaged concrete.

The elastic compliance tensor D^{e}_{ijkl} for the hyperelastic damaged concrete is symmetric. This implies the path-independence of the elastic strains, i. e., the state of elastic strain in damaged concrete introduced by a specified state of stress does not depend upon the manner in which this state of stress is reached. It also guarantees the existence of the complimentary elastic energy function whose partial derivative with respect to any

stress component gives the corresponding strain component. Assumption of associated flow rule ensures the symmetry of the plastic compliance tensor D^p_{ijkl} also. Thus, the irreversible plastic strains are bound to be stress path independent. In view of this fact, the equivalent deformation theory of pure elastoplasticity can be constructed from the above incremental constitutive equations. Also, the energy dissipated due to plastic flow alone depends only upon the current state of stress and not on stress history.

In contrast, the tangent damage compliance tensor D^d_{ijkl} derived here turns out to be asymmetric. Obviously, the reversible elastic strains caused by damage evolution are determined by the stress path followed to reach the current state of stress. The energy dissipated during damage evolution in taking the material from one state of stress to another during loading does not depend only upon these two states of stress but on the stress path followed while doing so. This component of energy spent during loading is not recovered upon unloading as the damage suffered by concrete does not heal up. In view of the above discussion, there is no cause for 'spurious energy generation' as predicted by some constitutive models [4,34].

Many constitutive models boast as being 'thermodynamically consistent' apart from claiming capability for predicting accurately the observed material response [16,17]. According to the contending approach, the thermodynamical consistency is not the intrinsic requirement for constitutive modelling [35]. In continuum mechanics, the existence of path-independent energy function is presumed only in hyperelastic or Green-elastic formulations implying symmetric constitutive tensors. Such is not the case for Cauchy-elastic formulations requiring no reference to existence of energy. The constitutive equations are stated in the form of incremental stress-strain relations without requiring the tangent compliance tensors to be symmetric. In this paper, the damaged concrete is indeed assumed to be hyperelastic. However, no additional restrictive condition of symmetry of damage compliance tensor D^d_{ijkl} is imposed. This Cauchy approach, though not thermodynamically consistent, is also admissible. According to Truesdell [35], mechanics is of more general scope than thermodynamics requiring symmetry of constitutive relations. After all, asymmetric stiffness matrices do arise in constitutive models and structural theory, e. g., due to non-associative flow rule for soils [27] and for structures subjected to follower forces [36].

In this stress-based formulation, the value of the hardening function k controlling the current loading function and the corresponding loading surface in the stress space is determined by the stress-history. The relevant value of the k is the maximum value reached in the entire past. In this paper, k is assumed to depend upon plastic work W_p chosen as the hardening parameter p and, in turn, it determines the scalar damage parameter ω. The applied stress increments resulting in positive increment dk cause incremental energy dissipation dW_p as well as damage increment $d\omega$ along with associated additional energy dissipation. Neither the dissipated energy is recoverable nor does the damage heal up upon unloading characterised by negative dk. Thus, hardening parameter p and scalar damage measure ω play the role of internal variables which can only increase in during the dissipative process. Thus, the proposed formulation of concrete inelasticity obeys the 'Internal Variable Thermodynamics'. To recapitulate, there exist three different formulations of second law of thermodynamics, viz., Generalized Thermodynamics, Rational Thermodynamics and Internal Variable Thermodynamics. In this last case, the internal variables play the role of one intrinsic time for each dissipative process. Because of their non-negative variation with real time, these internal variables constitute valid measures of entropy [37].

Generally, the experimental data on concrete is obtained by applying proportional loading which maintains the orientation of principal stress directions. Material behavior under non-proportional load histories resulting in rotation of principal stress directions relative to the material directions is termed 'vertex effect' [38]. It is claimed that the present model is capable of predicting vertex effect in the pre-peak range. Damaged concrete exhibits nonlinear response only under general non-proportional stress variations. Even otherwise, the proposed incremental constitutive equations can be used to simulate any stress-history including sudden changes from proportional path and predict the consequent damage-elastoplastic response.

The scope of the proposed model is restricted to size-independent pre-peak response. Here, the positive-definiteness of compliance tensor ensures stability of predicted material response. Of course, concrete does exhibit peculiar post-peak softening response: In place of stress-strain curves, stress-displacement curves are meaningful and the observed response is sensitive to size effect. This is attributed to the phenomenon of shear localisation involving large deformations occurring in very small region of the specimen and little deformation occurring outside it. Such body-theoretic behavior is not accessible to classical point-theoretic constitutive modelling. Of course, non-local constitutive models are capable of predicting shear localisation, size effect and post-peak response. In non-local formulations, the state of stress at a material point is determined by the state of strain at all points in a region surrounding that point. Alternatively, strain-gradient constitutive equations involving dependence of stress upon strains and strain gradients have also been proposed[18]. The constitutive model presented here is not equipped to predict these aspects of concrete inelasticity.

There are more fundamental problems with popular constitutive modelling. Generally, as in the present paper, the failure criterion of concrete for a material point is stated in terms of stress invariants. In contrast, fracture mechanics is based upon the unstable propagation of macrocracks resulting in the fracture of the material body into two parts. In linear elastic fracture mechanics (LEFM), the relevant material properties include, apart from elastic modulus, specific surface energy resembling surface tension. It is interesting to note that non-local constitutive models can predict the effects of surface tension of the solids. Other material models include micro-plane models wherein the behavior at a plane under specified traction vector is investigated[39]. Further, concrete structures under the simultaneous action of service loads and an aggressive ambient environment are known to exhibit time-dependent chemo-mechanical response resembling creep[40].

8. CONCLUSIONS

Concrete exhibits quite complex nonlinear inelastic time-dependent mechanical behavior. In this paper, a new damage elastoplastic constitutive model for predicting pre-peak time-independent behaviour of concrete is proposed. It is constructed by weakly coupling authors' earlier bimodular elastic damage model and pure elastoplasticity model. Reversible elastic strains are caused by stress increments as well as consequent damage evolution, while irreversible strains are associated only with plastic flow. It is claimed that damaged concrete is shown, for the first time, to be a bimodular nonlinear hyperelastic solid. Despite the restrictive assumption of only isotropic damage, the proposed model is capable of predicting, with some accuracy, the anisotropic response observed under general stress-histories. Admissibility of asymmetric tangent damage-elastoplastic compliance tensor is justified. The internal variable approach for satisfying the second law of thermodynamics has been followed in the proposed dissipative model. The theoretical predictions of pre-peak behavior of concrete subjected to some stress-histories are shown to be satisfactory. It is demonstrated here how authors' bimodular elastic damage model can be incorporated in the inelasticity models for concrete. It is hoped that this will motivate others to base their more general models upon authors' bimodular damage model.

REFERENCES

[1] Bielski J., Skrzypek, J. J., and Kuna-Ciskal, H. (2006). "Implementation of a model of coupled elasto-plastic unilateral damage material to finite element code", *International Journal of Damage Mechanics*, Vol. 15, No. 1, pp. 5-39.

[2] Wu, J. Y., Li, J., and Faria, R. (2006). "An energy release rate-based plastic-damage model for concrete", *International Journal of Solids and Structures*, Vol. 43, No. 3-4, pp. 583-612.

[3] Nguyen, G. D., and Houlsby, G. T. (2008). "A coupled damage-plasticity model for concrete based on thermodynamic principles: Part I: Model formulation and parameter identification", *International Journal of Numerical and Analytical Methods GeoMechanics*, Vol. 32, No. 4, pp. 353-389.

[4] Cormery, F., and Welmane, H. (2002). "A critical review of some damage models with unilateral effect", *Mechanics Research Communication*, Vol. 29, No. 5, pp. 391-395.

[5] Litewka, A., Bogucka, J., and Debinski, J. (2003). "Load induced oriented damage and anisotropy of rock-like materials", *International Journal of Plasticity*, Vol. 19, No. 12, pp. 2171-2191.

[6] Kuna-Ciskal, H., and Skrzypek, J. J. (2004). "CDM based modelling of damage and fracture mechanisms in concrete under tension and compression", *Engineering Fracture Mechanics*, Vol. 71, No. 4-6, pp. 681-698.

[7] Challamel, N., Lanos, C., and Casandjian C. (2005). "Strain-based anisotropic damage modeling and unilateral effects", *International Journal of Mechanical Sciences*, Vol. 47, No. 3, pp. 459-473.

[8] Badel, P., Godard, V., and Leblond, J. B. (2007). "Application of some anisotropic damage model to the prediction of the failure of some complex industrial concrete structures", *International Journal of Solids and Structures*, Vol. 44, No. 18-19, pp. 5848-5874.

[9] Kolari K. (2007). "Damage mechanics model for brittle failure of transversely isotropic solids: Finite element implementation", Ph.D. Thesis, Helsinki Univ. of Oxford.

[10] Desmorat, R., and Cantournet, S. (2008). "Modeling microdefects closure effect with isotropic/anisotropic damage", *International Journal of Damage Mechanics*, Vol. 17, No. 1, pp. 65-96.

[11] Proenca, S. P. B., and Pituba, J. J. C. (2003). "A damage constitutive model accounting for induced anisotropy and bimodular elastic response", *Latin American Journal of Solids and Structures*, Vol. 1, No. 1, pp. 101-117.

[12] Mollica, F., Ventre, M., Sarracino, F., Ambrosio, L., and Nicolais, L. (2007). "Implicit constitutive equations in the modelling of bimodular materials: An application

to biomaterials", *Computers and Mathematics with Applications*, Vol. 53, No. 2, pp. 209-218.

[13] Cervera, M., and Tesei, C. (2017) "An energy-equivalent d+/d- damage model for enhanced microcrack closure-reopening capabilities for cohesive-frictional materials", *Materials*, Vol. 10, No. 4, pp. 433-463.

[14] Long, Y. and He, Y. (2017). "An anisotropic damage model for concrete structures under cyclic loading - Uniaxial modelling", *Journal of Physics*: Conference Series, Vol. 842, No. 1.

[15] Mazars, J., Hamon, F., and Grange, S. (2015). "A New 3D damage model for concrete for monotonic cyclic and dynamic loadings", *Materials and Structures*, Vol. 48, No. 11, pp. 3779-3793.

[16] Liu, J., Lin, G., and Zhong, H. (2013). "An elastoplastic damage model for concrete", *China Ocean Engineering*, Vol. 27, No. 2, pp. 169-182.

[17] Zhang, J., and Li, J. (2014). "Elastoplastic damage model for concrete based on consistent free energy potential", *Science China Technological Sciences*, Vol. 47, No. 11, pp. 2278-2286.

[18] Marzec, I., and Tejchman, J. (2012), "Enhanced coupled elasto-plastic-damage models to describe concrete behaviour in cyclic laboratory tests: Comparison and improvement", *Archives of Mechanics*, Vol. 64, No. 3, pp. 227-259.

[19] Green, A.E., and Mkrtichian, J. Z. (1977). "Elastic solids with different moduli in tension and compression", *Journal of Elasticity*, Vol. 7, No. 4, pp. 369-386.

[20] Babu, R. R., Benipal, G. S., and Singh, A. K. (2010)., "Constitutive model for bimodular elastic damage of concrete", *Latin American Journal of Solids and Structures*, 7(2), Vol. 7, No. 2, pp. 143-166.

[21] Babu, R. R., Benipal, G. S., and Singh, A. K. (2006). "Plasticity-based constitutive model for concrete in stress space", *Latin American Journal of Solids and Structures*, Vol. 3, No. 4, pp. 417-441.

[22] Lekhnitskii, S.G. (1981). "Theory of elasticity of an anisotropic body", Mir Publishers, Moscow.

[23] Rivlin, R.S. (1948). "Large elastic deformations of isotropic materials I: Fundamental concepts", *Philosophical Transactions of the Royal Society of London*, Series A, Mathematical and Physical Sciences, Vol. 240, No. 822, pp. 459-490.

[24] Rivlin, R. S. (1997). "Collected papers of R.S. Rivlin, Vol. 1, G.I. Bareboat and D.D. Joseph (Ed.)", Springer-Verleg, New York.

[25] Truesdell, C., and Noll, W. (1965). "The nonlinear field theories of mechanics", In: Volume III/3, Editor: S. Flugge, Encyclopedia of Physics, Springer-Verlag.

[26] Chen, W. F., and Saleeb, A. F. (1994). "Constitutive equations for engineering materials, Vol. 1: Elasticity and modelling", Elsevier Publications.

[27] Chen, W. F. (1994). "Constitutive equations for engineering materials, Vol. 2: Plasticity and modelling", Elsevier Publications.

[28] Mazars, J., and Pijaudier-Cabot, G. (1989). "Continuum damage theory—application to concrete", *Journal of Engineering Mechanics*, Vol. 115, No. 2, pp. 345-365.

[29] Kupfer, H. B., Hilsdorf, H. D., and Rusch, H. (1969). "Behaviour of concrete under biaxial stresses", *ACI Journal*, Vol. 66, No. 8, pp. 656-666.

[30] Curnier A., Qi-Chang He., and Zysset, P. (1994). "Conewise linear elastic materials", *Journal of Elasticity*, Vol. 37, No. 1, pp. 1-38.

[31] Benzerga, D., Chouiter, A., Haddi, A., and Lavie, A. (2017). "Anisotropic Damage Modelling of Composite Plates and Shells", *Journal of Mechanical Engineering and Technology*, Vol. 9, No. 1, pp. 33-52.

[32] Chaboche, J. L. (1988). " Continuum damage mechanics, Part I: General concepts, Part II: Damage growth, crack initiation and crack growth", *ASME Journal of Applied Mechanics*, Vol. 55, No. 1, pp. 59-64 and 65-72

[33] Krajcinovic, D. (1984). "Continuum damage mechanics", *Applied Mathematics Reviews*, Vol. 37, No. 1.

[34] Carol, I., and Willam, K. (1996). "Spurious energy dissipation/generation in stiffness recovery models for elastic degradation and damage", *International Journal of Solids and Structures*, Vol. 33, No. 20-22, pp. 2939-2958.

[35] Truesdell, C. (1984). "Rational thermodynamics", Springer-Verlag, New York

[36] Benipal, G. S. (2015) "Contending schools of thought in engineering sciences:", Proceedings of the 17th ISME Conference, October 2015, IIT Delhi.

[37] Lavenda, B. H. (1978). "Thermodynamics of irreversible processes", MacMillan Press.

[38] Caner, C. C., Bazant, Z. P. and Cervenka, J. (2002). "Vertex effect in strain-softening concrete at rotating principal axes", *Journal of Engineering Mechanics*, Vol. 128, No. 1, pp. 24-33.

[39] Babu, R. R., Benipal, G. S., and Singh, A. K. (2005). "Constitutive modelling of concrete: An overview", *Asian Journal of Civil Engineering*, Vol. 6, No. 4, pp. 211-246.

[40] Suter M., and Benipal, G. S. (2006). "Time-dependent behaviour of reacting concrete I: Mechanism and theory", *Mechanics of Time-Dependent Materials*, Vol. 10, No. 1, pp. 51-62.

R. RAVEENDRA BABU is a consulting engineer involved in the analysis/design/project management of cryogenic storage tank projects. He hold a Ph.D. in civil/structural engineering from Indian Institute of Technology (IIT) Delhi. Email: rbraavi@iitdalumni.com

ARBIND KUMAR SINGH is a Professor of Civil Engineering at Indian Institute of Technology (IIT) Guwahati. He obtained his B.Tech. Degree in Civil Engineering in 1993 from Indian Institute of Technology (IIT) Delhi and M.E. and Ph.D. Degrees in 1995 and 2000 respectively from Indian Institute of Science, Bangalore. His research areas are continuum damage mechanics, plasticity, constitutive modeling of concrete, seismic analysis of structures and computation mechanics. Email: arvind@iitg.ac.in

GURMAIL S. BENIPAL is a Professor of Structural Engineering at Civil Engineering Department, Indian Institute of Technology (IIT) Delhi. His research interests include constitutive modelling and structural theory. Research students have worked on damage elasto-plasticity and thermo-chemo-viscoelasticity of concrete, nonlinear dynamic and stability analysis of cracked elastic concrete structures and nonlinear dynamics of cable structures. He has also written on foundations of and current trends in continuum mechanics and nonlinear dynamics. Email: gurmail@civil.iitd.ac.in

Cite this article: Babu, R. R., Singh, A. K., and Benipal, G. S. (2021). "Bimodular damage-elastoplasticity constitutive model for concrete", *The Indian Concrete Journal*, Vol. 95, No. 7, pp. 49-58.

ICJ

www.icjonline.com

THE INDIAN CONCRETE JOURNAL

TAKE A CONCRETE DECISION. SUBSCRIBE TO ICJ TODAY.

Write to us at info@icjonline.com and order your copy now!

SUBSCRIPTION FORM [For Indian Nationals]

☐ Collector's Edition ☐ New subscriber ☐ Renewal *(Please tick one)*

Name: _____
(Please fill in block letters)

Address: _____

_____

_____

_____

_____

City: _____

State / Province: _____

PIN Code: _____
(PIN code is compulsory)

Date of Birth: d d m m y y

Designation: _____
(Leave this blank if it is a residential address)

Company / Organisation: _____
(Leave this blank if it is a residential address)

_____

_____

Mobile No.: _____
(Mobile number is compulsory)

Email: _____
(Email is compulsory

Subscription Tariff, Rupees (Inclusive of Postage & Handling)	1 year
Collector's Edition	1000/-
Online E-Journal*	1200/-
Paper Edition	1800/-
Online E-Journal* & Paper Edition	2800/-

* In Online E-Journal, there will be no hard copy, subscribers can view the journal online at www.icjonline.com with username and password

Send this form or write to info@icjonline.com Website: www.icjonline.com

DETAILS OF OTHER PAYMENT OPTIONS AND GENERAL TERMS AND CONDITIONS

TERMS AND CONDITION:
1. Advance payment needed. 2. We are currently only accepting online payments. Details for the transfer are given below:
Account Name - ACC LIMITED **Account Number** - 57500000308512 **Branch Address** - Fort, Mumbai **IFSC Code** - HDFC0000060
3. After completion of each transaction, kindly inform us of the amount, transaction date, senders name, and senders bank account number by email. 4. Payment once received will not be refunded or adjusted. 5. Please note that the subscription will be started / renewed from the next month of the receipt of the payment. We do not offer backdated subscriptions. 6. For any extra hard copy of the past 10 years, write to us for applicable charges, subject to availability, until stocks last. 7. ICJ is ordinarily posted to all subscribers by ordinary post on the 1st of every month from the Mumbai post office. If you do not receive your copy by the end of the month, you can email us for a free replacement copy in the next month. A free replacement copy will not be entertained thereafter. For example, a free replacement copy for the March 2019 issue will be entertained only in April 2019, neither earlier, nor later. A free replacement copy for the March 2019 issue will not be entertained after April 2019. 8. Only one replacement copy will be entertained per year (12 months). 9. ICJ is posted to all subscribers by ordinary post. If you want to opt for courier service / registered post parcel, kindly add Rs. 2400 per year to the final amount.

(Please note that we have no branches)

Postal Registration Number: THC/125/2018-2020 | RNI Number: 13986/57 | Total Pages: 60
Published and posted on 1st of every month. Posted at Patrika Channel Sorting Office, Mumbai 400 001

ACC GOLD WATER SHIELD

पानी से करे SHIELD

Engineered with cutting-edge technology, ACC **GOLD WATER SHIELD** is an innovative water-repellent cement. Its unique formula offers your home a 360-degree shield against harmful effects of water seepage - making sure it remains strong and stylish, and continues to be admired, for years to come.

Strong & Durable

Scientifically Formulated

Innovative Technology

T&C Apply

ACC
करें कुछ कमाल